

Molecular signatures defining proprioceptor muscle-type identity

Inaugural-Dissertation
to obtain the academic degree
Doctor rerum naturalium (Dr. rer. nat.)

submitted to the Department of Biology, Chemistry, Pharmacy
of Freie Universität Berlin

by

STEPHAN DIETRICH

2022

The following work was carried out in the research group of Niccolò Zampieri between November 2016 and April 2022 at the Max-Delbrück Center for Molecular Medicine in the Helmholtz Association in Berlin.

1st reviewer: Niccolò Zampieri, PhD
Department of Disorders of the Nervous System
Max-Delbrück Center for Molecular Medicine Berlin

2nd reviewer: Prof. Dr. Ursula Koch
Institute of Biology, Neurophysiology
Freie Universität Berlin

Date of defense: 05.09.2022

Selbstständigkeitserklärung

Hierdurch versichere ich, dass ich meine Dissertation selbstständig verfasst und keine anderen als die von mir angegebenen Quellen und Hilfsmittel verwendet habe.

Acknowledgment

It all started with a scientific moment in the confocal room, two PhD students and the boss pointing to an unexpected double-labeled sensory neuron. Niccolò, thank you for the great scientific journey, thriving and lively discussions, critical and inspiring thinking, and always having an open door whenever problems needed to be solved. I am very grateful for the very instructive and exciting time. I learned a lot. Thank you!

I also would like to thank Prof. Dr. Ursula Koch for supervising and evaluating my PhD thesis.

Once, the boss said: “There is no I in a Team.” True words!

Sofia, thank you for providing the initial lucky section of the double-labeled sensory neuron and becoming a true friend during this PhD journey. Thank you for many great and sometimes even unrealistic scientific conversations during uncountable coffee breaks, always being honest and supportive when it was needed! Elisa, thank you for constantly listening to my monologues and having at the end always the right and sometimes amazing sarcastic comments and answers. We had good laughs. Your help is highly appreciated! Katrin, thank you for always being very supportive, helpful, and purely honest. Elijah, thank you for your technical help on the cDNA libraries, many scientific discussions, ridiculous bets, challenges and becoming an excellent friend. Carlos, I am grateful for your help with the bioinformatical analysis and for always having the patience to explain to me how UMAP, tSNE, ggplot, and even basic R functions work. I also would like to thank our lab technician Liana and former secretary Jasmin for their constant help, Matthias from the microscope facility for sharing his expertise in imaging related questions and Sophie for the many rolling eyes when I was looking for something obvious in the lab and could not find it. In addition, I would like to thank Dimitra and Lena for fantastic lunch conversations and moral support when it was needed.

Last, I would like to express my gratitude to my sister Josephine and parents Frank and Annett for their constant support beyond of my PhD work. My final gratitude goes to my partner Helena, who is by now almost an expert in proprioception. ¡Muchas gracias!

Table of Contents

List of Figures	VII
List of Supplemental Figures.....	IX
List of Tables.....	X
Abbreviations.....	XI
Summary	1
Zusammenfassung	2
1. Introduction	3
1.1 Generic proprioceptor development	4
1.2 Proprioceptor specification	6
1.2.1 <i>Functional properties of muscle spindles and Golgi-tendon organs</i>	6
1.2.2 <i>Molecular distinction of group Ia, II, and Ib proprioceptors</i>	9
1.3 Sensory-motor circuits	10
1.3.1 <i>The stretch reflex arc</i>	10
1.3.2 <i>Sensory-motor connectivity</i>	11
1.4 Peripheral muscle target connectivity	14
2. Aims of the study	17
3. Materials.....	18
3.1 Primary antibodies	18
3.2 Secondary antibodies	18
3.3 RNAscope probes	19
3.4 Fluorescent dyes.....	19
3.5 Neuronal tracers	19
3.6 Genotyping primers	20
3.7 Mouse lines	21

3.8 Software	21
3.9 Devices.....	22
3.10 Chemicals and kits	23
4. Methods	25
4.1 Animal experiments	25
4.2 Genotyping.....	25
4.3 Dissection and tissue processing.....	25
4.4 Single-cell isolation	26
4.5 Preparation of cDNA libraries	26
4.5 Sequencing of cDNA libraries	28
4.6 Single-cell sequencing analysis	28
4.7 Immunohistochemistry and multiplex fluorescent <i>in situ</i> hybridization	29
4.8 Tissue clearing and light sheet microscopy	29
4.9 Retrograde labeling of proprioceptors and motor neurons	30
4.10 Density analysis	30
4.11 Quantification and statistical analysis.....	31
5. Results.....	32
5.1 Single-cell-RNA sequencing of embryonic proprioceptors.....	32
5.2 Genetic labeling of <i>Trpv1</i> defines proprioceptors of back muscles.....	35
5.3 Molecular signatures of muscle-type specific proprioceptors	38
5.4 Proprioceptor muscle-type identities emerge early in development.....	42
5.5 The presence of muscle spindle and Golgi-tendon organ signature genes	43
5.5 Distinct expression of ephrin/EphA in back and limb proprioceptors.....	44
5.6 Expression of <i>Efna5</i> in the lumbar spinal cord.....	47
5.7 Expression of <i>Gabrg1</i> and <i>Efna5</i> in lumbar proprioceptors.....	48
6. Discussion	50

6.1 Early expression of <i>Trpv1</i> labels a subset of back proprioceptors.....	50
6.2 Molecular signatures defining proprioceptor muscle-type identities.....	52
6.3 Developmental emergence of proprioceptor subtypes.....	55
6.4 Ephrin-A signaling controls muscle-target specificity of proprioceptors.....	56
7. Relevance and outlook	58
8. References	59
9. Appendix	71
9.1. Supplemental figures	71
9.2 List of publications	77

List of Figures

Figure 1. Proprioceptor neurogenesis.	5
Figure 2. Proprioceptive sensory neuron receptors - muscle spindle and Golgi-tendon organ.	7
Figure 3. Sensory-motor circuits.....	11
Figure 4. Hierarchical organization of motor neurons.	12
Figure 5. Strategies to establish sensory-motor connectivity.	14
Figure 6. Eph/ephrin signaling in motor axon guidance.	15
Figure 7. Single-cell transcriptome analysis of thoracic and lumbar parvalbumin ⁺ sensory neurons at e15.5.	33
Figure 8. Transcriptome analysis of e15.5 proprioceptors.	34
Figure 9. Genetic labeling of back proprioceptors.....	35
Figure 10. Central and peripheral labeling of back proprioceptors.	36
Figure 11. Genetic labeling of back proprioceptor afferents in <i>Trpv1^{Cre}; tdT</i> mice.	37
Figure 12. Transcriptomic approach reveals molecular signatures for back, abdominal, and limb proprioceptors.	39
Figure 13. Expression of marker genes for back, abdominal, and limb proprioceptors.	40
Figure 14. Rostro-caudal expression of marker genes for back, abdominal, and limb proprioceptors.	41
Figure 15. <i>Tox</i> and <i>Gabrg1</i> are specific for back and limb proprioceptors.	42
Figure 16. Signature genes of p1back, abdominal, and limb proprioceptors are present at e15.5.	43
Figure 17. Presence of signature genes for group Ia, Ib, II proprioceptor subtypes at e15.5 and p1.....	44
Figure 18. Distinct expression of EphA/ephrin-A in back and limb proprioceptors.	45

Figure 19. The absence of ephrin-A5 affects the targeting specificity of *Tibialis anterior* Proprioceptors.....46

Figure 20. Density analysis of central parvalbumin⁺ afferents in *Efna5*^{+/+} and *Efna5*^{-/-} mice.....47

Figure 21. Expression of *Efna5* in lumbar motor neurons.....48

Figure 22. Combined expression of *Gabrg1* and *Efna5* in lumbar proprioceptors.....49

List of Supplemental Figures

Figure S1. <i>Hoxc10</i> expression of thoracic and lumbar parvalbumin ⁺ sensory neurons at e15.5.....	71
Figure S2. Muscle spindles in back muscles.....	72
Figure S3. Genetic labeling of back-pSN afferents.	73
Figure S4. Expression of marker genes for back, limb, and abdominal proprioceptors in <i>Pv</i> ⁺ sensory neurons.	74
Figure S5. Retrograde labeling of back and hindlimb innervating motor neurons.....	75
Figure S6. Expression of <i>Efna5</i> in DRG of <i>Efna5</i> ^{+/+} and <i>Efna5</i> ^{-/-} mice.....	76

List of Tables

Table 1. Primary antibodies used for immunohistochemistry.....	18
Table 2. Secondary antibodies used for immunohistochemistry.....	18
Table 3. Antisense probes used for fluorescent in situ hybridization (RNAscope).	19
Table 4. Fluorescent dyes used for in situ hybridization and immunohistochemistry.	19
Table 5. Non-viral tracers used for retrograde labeling experiments.....	19
Table 6. Primers used to perform genotyping of mouse lines.....	20
Table 7. Mouse lines used for in vivo experiments.....	21
Table 8. Software used for data processing and analysis.	21
Table 9. Equipment used to perform experiments.	22
Table 10. Chemicals used to perform experiments.....	23

Abbreviations

Ab	Abdominal
Ba	Back
C1qI2	Complement component 1, q subcomponent-like 2
Cdh	Cadherin
Ce	Cervical
CEL-Seq	Cell Expression by Linear amplification and Sequencing
ChAT	Choline-Acetyl-Transferase
CM	Cutaneous Maximus
CNS	Central Nervous System
CTB	Cholera Toxin B subunit
Cy	Cyanin
DNA	Deoxyribonucleic acid
DRG	Dorsal Root Ganglia
FACS	Fluorescence-Activated Cell Sorting
FDR	False Detection Rate
FHS	Fetal Horse Serum
FSF	Frt-Stop-Frt
Gabrg1	Gamma-aminobutyric acid (GABA) A receptor, subunit gamma 1
GO	Gene Ontology
GPI	Glycosyl-Phosphatidyl-Inositol
GTO	Golgi-Tendon Organ
H	Hamstring
HMC	Abdominal Motor Column
HRP	Horseradish peroxidase
KO	Knock Out
Li	Limb
LMC	Lateral Motor Column
LogFC	Logarithmic Fold Changes
LSL	Lox-Stop-Lox
Lu	Lumbar
MMC	Medial Motor Column

MN	Motor Neuron
MS	Muscle Spindle
NCC	Neural Crest Cells
Ngn	Neurogenin
NT3	Neurotrophin-3
PCR	Polymerase Chain Reaction
PDZ	Postsynaptic Density Protein
PSN	Proprioceptive Sensory Neurons
Pv	Parvalbumin
R	Rectus femoris
RA	Retinoic Acid
RFP	Red Fluorescent Protein
RhD	Rhodamine-Dextran
RNA	Ribonucleic acid
RT	Room Temperature
Runx3	Runt related transcription factor 3
SEM	Standard Error of Mean
SN	Sensory Neurons
tdT	tdTomato
Th	Thoracic
Tm	Primer melting temperature
Tox	Thymocyte selection associated high mobility group box
Trk	Tyrosine kinase receptor
Trpv1	Transient receptor potential cation channel subfamily V member 1
UMAP	Uniform Manifold Approximation and Projection
V	Vasti
vGluT1	Vesicular Glutamate Transporter 1

Summary

Proprioception, the sense of body position in space, is critical for generating coordinated movements and reflexive actions. Proprioceptive sensory neurons (pSN) reside in the dorsal root ganglia and constantly monitor muscle stretch and tension with their mechanoreceptive organs (muscle spindles and Golgi-tendon organs) and relay this information to central circuits that generate coordinated motor actions. In particular, group Ia pSN afferents (muscle spindle) provide direct sensory feedback to motor neurons controlling the activity of the same muscle while avoiding motor neurons of antagonistic muscle groups. This precise connectivity pattern represents the basis of the stretch reflex arc and suggests the existence of proprioceptor subtypes defined by the muscle they innervate. However, molecular programs controlling critical aspects of pSN subtype identities, such as the central and peripheral connectivity, are mainly unknown.

In this study, we devised a single-cell transcriptomic approach that takes advantage of the topographic organization of the pSN system to reveal molecular features of cardinal proprioceptor subtypes defined by their connectivity to limb, back, and abdominal muscles. First, we identified and validated molecular signatures for each pSN muscle-type population. Second, we found that molecular programs defining these identities are acquired early in development and maintained until early postnatal stages. Last, we discovered distinct expression patterns of axon guidance molecules of the ephrin-A/EphA family that distinguish axial- and limb-pSN. In particular, we found that the absence of ephrin-A5 affects the peripheral connectivity of limb-pSN with specific hindlimb muscles, thus implying an important role for ephrin-A signaling in controlling the assembly of sensorimotor circuits. Altogether, this work reveals the molecular foundation of pSN muscle-type identity and paves the way for studying the development and function of muscle-specific sensory feedback circuits.

Zusammenfassung

Propriozeption ist die Wahrnehmung des eigenen Körpers im Raum und ist essenziell für die Koordinierung von Bewegungen. Propriozeptive sensorische Neurone (pSN) befinden sich in den Spinalganglien und innervieren mit ihren mechanorezeptiven Organen (Muskelspindeln (MS) und Golgi-Sehnenorgan (GTO)) die Skelettmuskulatur, um deren Kontraktionen und Spannungen zu detektieren. Informationen zum Muskelstatus werden kontinuierlich über die propriozeptiven Nervenfasern an das zentrale Nervensystem weitergeleitet. Im zentralen Nervensystem werden diese Informationen verarbeitet und benutzt, um die Aktivität von Motorneuronen zu kontrollieren, sodass koordinierte Bewegungen generiert werden können. Eine Grundvoraussetzung dafür ist, dass individuelle Muskeln mit unterschiedlichen biomechanischen Aufgaben von diskreten pSN innerviert werden. Molekulare Programme, welche diese präzise Konnektivität gewährleisten und die Identität von muskelspezifischen pSN definieren, sind weitestgehend unbekannt.

Folglich wurde in der vorliegenden Dissertation unter Berücksichtigung der topografischen Organisation von pSN und der damit einhergehenden pSN-Muskelkonnektivität das Transkriptom von einzelnen thorakalen und lumbalen pSN analysiert. Wir konnten distinkte molekulare Marker für pSN der Rücken-, Abdominal- und Hintergliedmaßen-Muskulatur identifizieren. Diese pSN-Subtypen spezifischen molekularen Profile sind bereits während der embryonalen Entwicklung vorhanden und werden mindestens bis ins frühe postnatale Entwicklungsstadium aufrechterhalten. Des Weiteren konnten wir in den genetischen Profilen von unterschiedlichen muskelspezifischen-pSN Gene identifizieren, die zur Familie der Ephrine und Ephrin-Rezeptoren gehören und an axonalen Wachstumsprozessen beteiligt sind. Schlussendlich konnten wir zeigen, dass in Ephrin-A5 defizienten Mäusen die Muskelkonnektivität von pSN der Hintergliedmaßen beeinträchtigt ist. Die in dieser Arbeit identifizierten pSN Marker können in zukünftigen Studien genutzt werden, um die Entwicklung und Funktion von individuellen Muskel-spezifischen sensorischen Netzwerken zu untersuchen.

1. Introduction

The nervous system comprises networks of specialized neurons, the somatosensory system, able to perceive and encode distinct sensory stimuli. Upon transmitting this information to circuits of the central nervous system (CNS, brain and spinal cord), specific actions and motor behaviors are generated to react to environmental changes. In general, the somatosensory system distinguishes between three major functions, interoception (perception of internal/visceral stimuli), exteroception (perception of external/outside stimuli), and proprioception (sense of self) (1, 2).

Interoceptive afferents are either chemoreceptors, monitoring organ functions through indicators such as blood gases and pH, or visceral mechanoreceptors sensing the stretch and tension of smooth muscles of internal organs. Although most visceral events do not evoke a conscious sensation, they are crucial for controlling autonomic functions in the cardiovascular, respiratory, digestive, and renal system.

In contrast, exteroceptive afferents reside in the skin and respond to immediate external innocuous, noxious, and pruriceptive stimuli. The ability to sense touch stimuli such as pressure, stroking, and vibration allows us, among others, to recognize objects and discriminate textures (2, 4, 5). Perception of additional stimuli such as heat, cold, and pain is used to prevent tissue damage and adjust ongoing motor behaviors (1).

Last, proprioception allows us to move our bodies seemingly without any conscious effort in space and to react rapidly to changes in our surroundings. This ability relies on specialized primary somatosensory neurons, so-called proprioceptors residing in dorsal root ganglia (DRG). With their mechanoreceptive organs located in skeletal muscles (muscle spindles) and associated myotendinous junction (Golgi-tendon organs), they are constantly monitoring muscle stretch and tension, thus contributing to the sense of limb and body position. Upon conveying this information to the CNS, brain circuits use this sensory feedback for motor planning, online corrections, and sensorimotor adaption (6). At spinal levels, descending supraspinal commands merge with proprioceptive feedback and generate coordinated motor responses by activating spinal motor neurons. Sensory feedback from proprioceptors contributes to both unconscious sensations such as the classical knee jerk reflex and conscious sensations, for example, when walking in the dark. Among all sensory neurons in dorsal root ganglia, proprioceptors represent approximately 10 %. They are generally classified on the basis of their physiological afferent properties and end-organs that they innervate. Although proprioceptors possess a key role in posture and coordinated movements, little is known about

the precise molecular mechanisms controlling their distinct subtype identity, formation, and upkeep of central and peripheral connectivity and function.

1.1 Generic proprioceptor development

Proprioceptive sensory neurons derive from trunk neural crest cells (NCC), a population migrating from dorsal aspects of the neural tube ventrally to form dorsal root ganglia (Figure 1) (7). During migration and when NCC start to coalesce into definite DRG, the expression of the transcription factors Neurogenin1 (Ngn1) and Neurogenin2 (Ngn2) orchestrate neuronal differentiation. In two successive waves, early sensory neuron subtypes are born with a characteristic expression of neurotrophic tyrosine receptor kinases (TrkA, TrkB, TrkC), which are important for further survival and maturation. Early proprioceptive/mechanoreceptive (TrkB⁺ and/or TrkC⁺) and few large diameter nociceptors (TrkA⁺) derive from the first neurogenic wave (e9.5 - e11.5) controlled by Ngn2. Slightly later (e10.5 - e13.5), the Ngn1 dependent, second wave produces mainly small diameter thermosensitive/nociceptive (TrkA⁺) and few proprioceptive/mechanoreceptive neurons (TrkB⁺ and/or TrkC⁺) (5, 8–10). The expression of the Runt related transcription factor 3 (Runx3) shortly after cell cycle exit is needed to maintain TrkC expression and to drive bipotent TrkB⁺/TrkC⁺ progenitors toward proprioceptive fate by repressing Shox2, which is required for TrkB expression and cutaneous mechanoreceptor fate (11, 12). Early Runx3 expression and activation of TrkC by the growth factor neurotrophin-3 (NT3) are essential for proprioceptive sensory neurons survival and axonal outgrowth. A recent study confirms that the early presence of Runx3 is positively correlated with proprioceptor survival; however, its expression was shown to be controlled by retinoic acid (RA) from the paraxial mesoderm and not by NT3 signaling as previously reported (12, 13). The final commitment of TrkC⁺/Runx3⁺ neurons to the proprioceptor lineage is subsequently marked by the expression of parvalbumin (Pv) at ~e14.5 (14–16). Altogether, the generic proprioceptor identity is defined by the expression of TrkC, Runx3, and Pv.

In addition, a complex interplay of intrinsic determinants and extrinsic signals is necessary to establish central connectivity with motor neurons and interneurons, as well as specific muscle targets in the periphery. Proprioceptors first project an axon to their peripheral muscle target and extend delayed collaterals to their central spinal targets. The peripheral connectivity is achieved at ~e14.5, while central axons enter the dorsal spinal cord from e13.5 to e15.5 and reach ventrally located motor neurons at ~e17.5 (17–20). A key molecule in proprioceptor axon targeting and extension is NT3, expressed by skeletal muscles,

mesenchyme, and motor neurons in the spinal cord, inducing the expression of the transcription factor Etv1 upon NT3-mediated TrkC signaling.

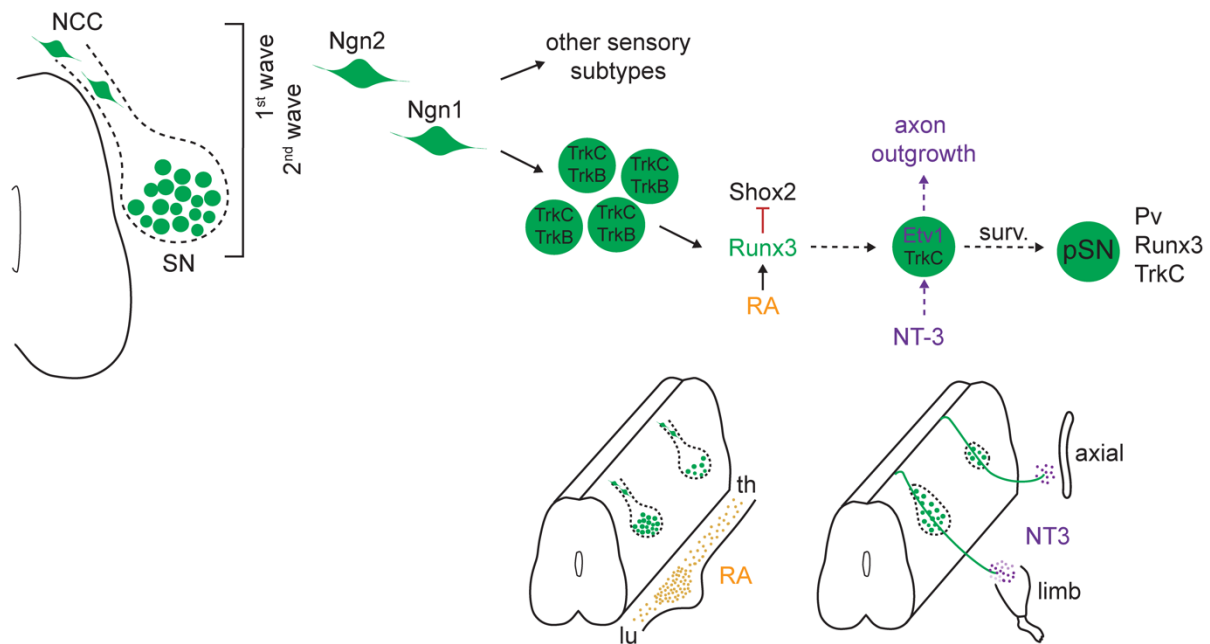


Figure 1. Proprioceptor neurogenesis. The expression of the transcription factors neurogenin 1 and 2 in neural crest cells (NCC) generates early proprioceptive progenitors (TrkC^+ , $\text{TrkC}^+/\text{TrkB}^+$). The exposure to retinoic acid (RA) from the paraxial mesoderm induces Runx3 expression, leading to proprioceptive sensory neuron fate commitment by maintaining TrkC expression. The positive correlation of Runx3 expression and proprioceptor survival suggests further that different RA concentrations along the rostro-caudal axis may influence different proprioceptor numbers at thoracic and lumbar levels. Further exposure of NT3 from surrounding tissues and activation of TrkC signaling lead to Etv1 expression promoting proprioceptor survival and peripheral axon outgrowth. Thereby, different levels of NT3 expressed by single muscles can predict the Etv1-dependent proprioceptor survival. The final generic proprioceptive sensory neuron identity is defined by the expression of Pv, Runx3, and TrkC. The figure was adapted from Zampieri and de Nooij, 2021 (21) and Shadrach et al., 2021 (22).

Manipulations of TrkC-NT3 signaling or genetic inactivation of Etv1 causes defects in central and peripheral projecting proprioceptive sensory neuron axons (23–26). Although the underlying molecular mechanisms are still unknown, a recent study suggests that proprioceptor connectivity/subtype differentiation depends on the strength of NT3 expression and signaling from every single muscle. Proprioceptors innervating axial muscles show an almost complete dependence on Etv1 for survival, while those innervating hindlimb muscles exhibit a muscle-by-muscle sensitivity or resistance to Etv1 (27). Another study demonstrates that also Runx3

acts as an afferent regulator directing the peripheral growth of proprioceptive sensory neuron axons (28). Although the underlying signaling pathways are still unknown, the transcriptional activities of *Etv1* and *Runx3* could serve to fine-tune various proprioceptor subtypes with respect to their peripheral muscle and central neuronal targets during development (27).

1.2 Proprioceptor specification

1.2.1 Functional properties of muscle spindles and Golgi-tendon organs

After acquiring their generic identity and initial muscle contact, proprioceptors differentiate simultaneously along two distinct trajectories corresponding to their receptor organ and the muscle they innervate. With respect to their receptor organ in the periphery, proprioceptors can be distinguished by muscle spindles (MS) and Golgi-tendon organs (GTO). Both receptor organs are encapsulated, specialized mechanoreceptive structures in skeletal muscles or their myotendinous junctions, respectively.

Muscle spindles are located in the belly of skeletal muscles. They are typically innervated by one primary afferent (group Ia) and a variable number of secondary afferents (group II) of proprioceptive sensory neurons (Figure 2). Group Ia afferents innervate the central region of the muscle spindle, surrounding nuclear bag1, bag2, and intrafusal chain fibers forming the characteristic annulospiral MS morphology (29, 30). Group II afferents are located lateral of group Ia afferents, and they are associated with chain fibers, sometimes with bag2 fibers, but rarely with bag1 fibers (Figures 2B and 2C) (21). Essential for the development of muscle spindles is the transcription factor *Egr3* (early growth response protein). Mice lacking *Egr3* show an abnormal spindle morphology impairing the innervation by proprioceptive afferents and exhibit gait ataxia and scoliosis (15, 31). Interestingly, a recent study shows that targeted deletion of *Egr3* in sensory neurons does not cause any muscle spindle defects, suggesting intrafusal muscle fibers as a key contributor of *Egr3* to normal muscle spindle development (32). Likewise, a splice variant of Neuregulin1 (Ig-Nrg1) selectively expressed in proprioceptors and its ErbB2 receptor in intrafusal muscle fibers are required for correct spindle differentiation. Mice in which Ig-Nrg1 or ErbB2 were eliminated showed reduced numbers of muscle spindles and had deficits in motor coordination (ataxia) (14, 33, 34). Although both muscle spindle afferents are myelinated, they can be further distinguished by their physiological properties that allow the detection of qualitatively different information about muscle stretch. While both transmit changes in the static length of the muscle

(contribution to the sense of position), the high dynamic sensitivity of group Ia afferents allows them also to sense the velocity of changes in muscle length (contribution to the sense of movement) (35, 36). Furthermore, group Ia afferents exhibit a lower activation threshold and a higher conduction velocity (Ia: 80-120 m/s, II: 30-75 m/s) compared to group II afferents (36, 37).

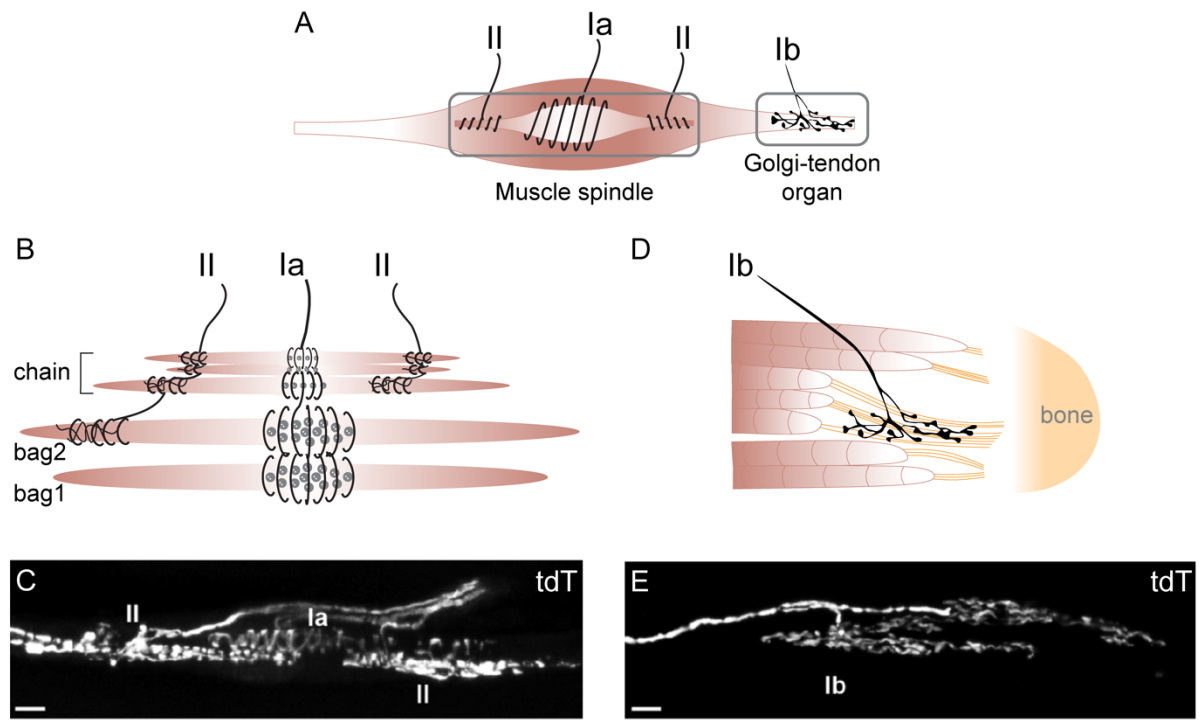


Figure 2. Proprioceptive sensory neuron receptors - muscle spindle and Golgi-tendon organ. (A) The illustration shows the location and afferent innervation of muscle spindles (intrafusal muscle fiber, group Ia, II) and Golgi-tendon organs (myotendinous junction, group Ib) in skeletal muscle. (B) Typical composition of a muscle spindle with group Ia afferents innervating the equatorial region of the intrafusal muscle fiber. Group II afferents are positioned at the polar ends of the intrafusal muscle fiber. (C) Genetically labeled (tdTomato) muscle spindle with group Ia and II afferents in an adductor muscle of an adult *Pv^{Cre}; Runx3^{Flp}; Ai65* mouse (38). Scale bar: 20 μ m. (D) Illustration of group Ib afferent innervating collagen fibers between extrafusal muscle fibers and tendon or aponeurosis. (E) Golgi-tendon organ of an adductor muscle labeled using an adult *Pv^{Cre}; Runx3^{Flp}; Ai65* mouse (38). Scale bar: 20 μ m. The figure was modified from Zampieri and de Nooij, 2021 (21).

In contrast to MS, Golgi-tendon organs intertwine between collagen fibers connecting the extrafusal muscle fibers with their tendon or aponeurosis and respond to changes in muscle load or applied forces. Group Ib afferents have activation thresholds and conduction velocities similar to those of group Ia afferents but show very little activation to muscle stretch. Nevertheless, group Ib afferents are highly sensitive to contractions of motor units in close

proximity, display a dynamic sensitivity, and relay rapid changes in contractile forces (39, 40). As a consequence of their physiological similarities to group Ia afferents, it remains challenging to selectively activate group Ib afferents and study their central pathways, as well as their role in motor control.

Not much is known about the underlying mechanisms converting the mechanical deformations of proprioceptive organs into sensory signals. Yet physiological studies revealed that Na⁺ ions mainly carry out the receptor potential with small contributions from Ca²⁺ ions. The initial discharge activity depends on the velocity of muscle stretch and contraction, whereby the primary endings of muscle spindles show an increased conductance to Na⁺, resulting in depolarization of sensory endings. Additionally, due to stretch, the membrane becomes more permeable to Ca²⁺, which can partially generate the receptor potential in the absence of Na⁺. Under normal conditions, variations in external Ca²⁺ ion concentrations do not affect the receptor potential amplitude (41). Interestingly, a recent study (42) shows that the internal increase of Ca²⁺ ions enhances the rate of exocytosis of synaptic-like vesicles releasing glutamate within the confines of the spindle capsule. This leads to an increased afferent excitability (sensitivity) to stretch upon activation of PLD-mGLuR (Phospholipase D - metabotropic glutamate receptor) and allows maintained discharges during stretch (43). The general physiological properties of proprioceptors correspond to those of slow-adapting low-threshold mechanoreceptors (44, 45).

Studies have revealed molecules with potential roles in proprioceptive mechanotransduction, such as sodium channels of the degenerin/epithelial family (DEG/ENaC, ASIC3), Piezo2, or the PDZ-scaffold protein Whirlin (46–48). The latter has been shown to facilitate stretch-evoked activity in proprioceptive mechanosensory endings to ensure high sensitivity to muscle stretch. Whirlin mutant mice show decreased stretch-evoked firing frequencies and reduced fidelity in response to repeated stretch (46). In contrast, a more prominent role in proprioceptive mechanotransduction plays the mechanosensitive ion channel Piezo2 (47, 49). Conditional elimination of Piezo2 in proprioceptors (Piezo2^{ckO}) leads to severe problems in limb and body coordination, while it does not affect the number and morphology of muscle spindles and Golgi-tendon organs. These behavioral phenotypes were consistent with the loss of low-threshold mechanical responses demonstrated in *in vitro* experiments. In addition, the lack of Piezo2^{ckO} results in dramatically reduced stretch-evoked firing in proprioceptive muscle afferents, implying that Piezo2 plays a major role in mechanotransduction in proprioceptors (47). By now also human Piezo2 mutations are known, displaying complex phenotypes including proprioceptive defects (uncoordinated movements,

loss of postural control), skeletal abnormalities (scoliosis, hip dysplasia), congenital contractures of multiple joints, and muscle weakness (43, 49–51). Interestingly, the elimination of Piezo2 from proprioceptive sensory neurons in mice could recapitulate several human skeletal abnormalities, suggesting that proprioceptive sensory neurons are essential for spinal alignment and hip joint integrity. This implies that the proprioceptive system also plays a central role in skeletal integrity, and further research could help expand treatments for orthopaedic pathologies (52).

1.2.2 Molecular distinction of group Ia, II, and Ib proprioceptors

Despite the current information about the generic development, physiological properties, anatomy, and connectivity of group Ia, II, and Ib proprioceptors, their molecular identities remain largely unknown. Only recently, two independent studies used single-cell transcriptomic approaches to reveal molecular signatures of adult proprioceptors and assigned them to group Ia, II, and Ib afferents (38, 53). Oliver et al., 2021 (38) identified the transmembrane protein *Heg1* as a marker for muscle spindle innervating proprioceptors and the transcription factor *Pou4f3* and *Pcdh8* for proprioceptors associated with Golgi-tendon organs. Interestingly, proprioceptors expressing *Heg1* were comprised of four distinct molecular subsets. While one cluster was marked by the expression of *Calb2*, the remaining three clusters exhibited the expression of the synaptic molecule *Nxph1*. Based on morphological properties, *Calb2*⁺ proprioceptors could be assigned to group Ia afferents, while by exclusion, *Nxph1*⁺ clusters were suggested to be group II afferents. Additionally, Wu et al., 2021 (53) revealed partially similar markers and defined group Ia proprioceptors mainly by *Lmcd1*, comprising three subgroups marked by *Runx1* (Ia₁), *Calb1* (Ia₂), and *Calb1/Calb2* (Ia₃). Group II MS afferents were mainly defined by the expression of *Fxyd7* and further subclusters by *Cartpt* (II₁), *Tox* (II₂), *Aldh1a3* (II₃), and *Chodl* (II₄). Lastly, a single cluster expressing *Chad* and *Pou4f3* was defined as group Ib proprioceptors. In agreement with an earlier bulk RNA transcriptome analysis, both studies imply that proprioceptive subtypes are characterized by the combinatorial expression of marker genes rather than single ones (45).

Further transcriptional analyzes of different embryonic and early postnatal stages suggest that molecular signatures of muscle spindles and Golgi-tendon organs emerge later in development when muscle target innervation is already achieved. In particular, Wu et al. 2021 could provide some evidence that *Tnfrsf8l3* might label group Ia and *Doc2b* group Ib afferents at embryonic stage e16.5. Despite this, both studies show that adult molecular differences

between group Ia and II muscle spindles as well as Golgi-tendon organs appear at early postnatal stages, followed by a molecular maturation for at least two weeks after birth (21, 38, 53). This is in agreement with a recently suggested model of neurogenesis and transcriptional maturation of somatosensory neurons, where sensory neuron subclasses undergo a transition from a transcriptionally unspecialized state to transcriptionally distinct subtypes influenced by temporal or spatial signaling cues from intermediate or final peripheral targets (54, 55). Although definitive molecular determinants for all three functionally distinct proprioceptive subtypes still need to be established, these novel molecular insights into muscle spindles and Golgi-tendon organs offer not only advancements in understanding their developmental emergence, but also allow genetic access to sensory feedback circuits enabling to study their distinct function in sensory motor-circuits (21).

1.3 Sensory-motor circuits

1.3.1 The stretch reflex arc

Muscle spindles and Golgi-tendon organs are necessary to collect information about muscle contraction and tension. To use this information for controlling movements and posture, group Ia, Ib, and II afferents engage with spinal reflex circuits and projecting neurons tasked to orchestrate the activity of relevant muscles. In mammals, sensory-motor circuits in the spinal cord are constructed with exquisite specificity, where proprioceptors convey continuous sensory feedback from distinct limb muscles to appropriate motor neurons generating coordinated movements, such as walking (6, 56). Proprioceptive afferents form direct and indirect connections with alpha-motor neurons, which innervate the neuromuscular junction in extrafusal muscle fibers and initiate muscle contractions. In particular, group Ia afferents form direct strong monosynaptic connections with alpha-motor neurons innervating the same muscle (homonymous) and weaker connections with synergistic muscle groups (heteronymous) promoting muscle contraction, while avoiding motor neurons of antagonistic muscles or non-related functions. This monosynaptic circuit represents the anatomical basis of the stretch reflex arc (Figure 3A). In addition, group Ia afferents can also synapse onto interneurons inhibiting motor neurons of antagonistic muscles (non-homonymous), thus controlling flexor-extensor muscle activity required for coordinated movements. In contrast to group Ia afferents, Golgi-tendon organ group Ib afferents synapse onto interneurons that inhibit homonymous alpha-motor neurons and excite those of antagonistic muscles (Figure 3B). Due to their relatively

simple structure, well-characterized physiological properties, as well as anatomical and genetic accessibility, spinal sensory-reflex circuits have been used as a model system to understand the fundamental principles of neural circuit assembly, connectivity, and function for the last several decades (57–59).

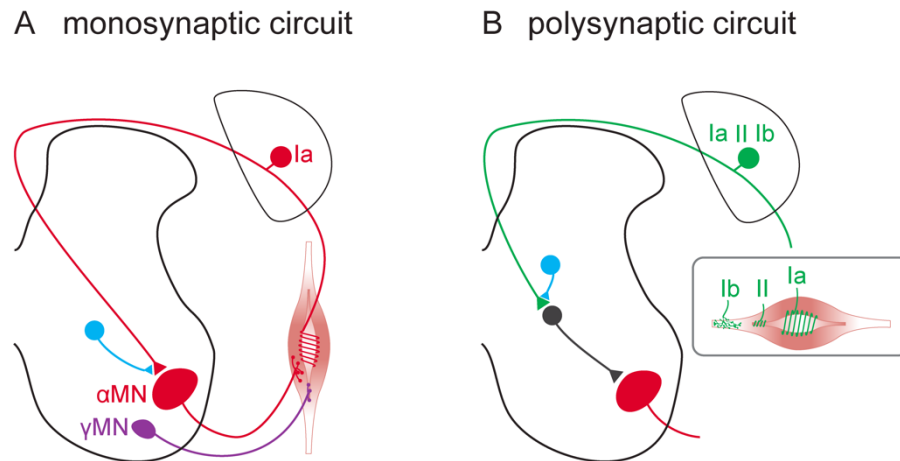


Figure 3. Sensory-motor circuits. (A) The monosynaptic stretch reflex circuit (labeled in red) is based on a group Ia afferent (MS) sensing muscle stretch at the intrafusal muscle fiber and conveying this information through direct synaptic contacts to synergistic alpha motor neurons (α MN), promoting muscle contraction. Monosynaptic proprioceptive feedback from group Ia afferents can be presynaptically inhibited by GABApre interneurons (blue). Gamma-motor neurons (γ MN, violet) innervate intrafusal muscle fibers to control the stretch sensitivity of muscle spindles. (B) All three proprioceptive afferents are also engaged in more complex polysynaptic circuits with motor neurons, whereby afferents synapse to inhibitory and excitatory interneurons (dark gray) in the intermediate spinal cord. The figure was adapted from Shadrach et al., 2021 (22).

1.3.2. Sensory-motor connectivity

In limbed vertebrates, spinal sensory-motor reflex circuits are fundamentally conserved and established at late embryonic stages in an activity-independent manner (17, 58–62). Although a recent study shows that the distribution of sensory connections with heteronymous motor neurons is regulated in an activity-dependent manner, the overall evidence is limited that sensory-motor connectivity is controlled by neural activity (63, 64). Proprioceptors face the challenge of forming selective connections with distinct individual muscles and their homonymous motor neurons (65).

A possible strategy to increase the probability of correct sensory-motor connectivity relies on the stereotyped organization of motor neurons. During development, single motor neurons that share the same transcriptional identity and muscle connectivity are hierarchically

organized into distinct groups occupying discrete positions in the ventral horn of the spinal cord (Figure 4). Depending on the selective expression of Hox genes (Homeobox family proteins), motor neurons segregate along the rostro-caudal axis into segmentally restricted longitudinal motor columns with distinct peripheral targets. Motor neurons of the medial motor column (MMC) are located at all spinal levels innervating the dorsal axial musculature (back muscles). In contrast, motor neurons innervating abdominal and intercostal muscles are exclusively found at thoracic levels and belong to the hypaxial motor column (HMC).

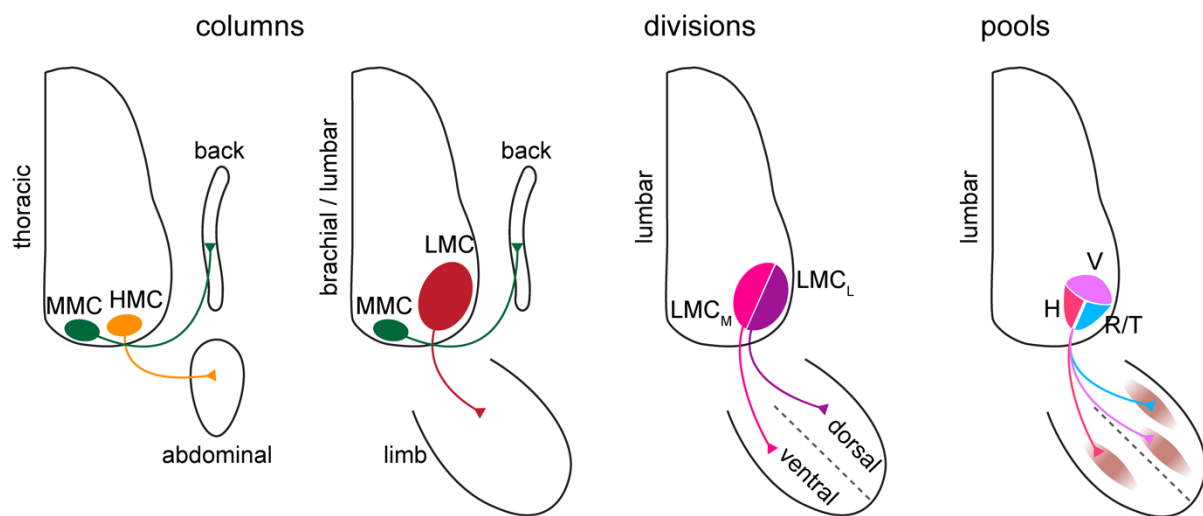


Figure 4. Hierarchical organization of motor neurons. During development, distinct transcriptional programs define motor neurons, which segregate at distinct topographic locations in the spinal cord and innervate defined muscle targets. Motor neurons of the medial motor column (MMC, back muscles) are defined by the expression of Hb9, Isl1/2, and Lhx3, motor neurons of the hypaxial motor column (HMC, abdominal muscles) express Hb9, Isl1, Isl2^{low}, and Etv1. Motor neurons of the lateral motor column (LMC) exhibit expression of Foxp1 and Raldh2. At limb level, LMC motor neurons are further subdivided into two divisions, the lateral and medial LMC defined by Foxp1, Lhx1, and Isl2 (LMC_L) or Foxp1 and Isl1/2 (LMC_M), respectively. At the highest level, single muscle pools innervate single muscles, for example, *Hamstring* motor neurons (Nkx6.1), *Vasti* motor neurons (Er81), and *Rectus femoris* and *fasciae latae* motor neurons (Nkx6.2). The figure was adapted from Dasen and Jessell, 2009 (66).

At limb levels, the lateral motor column (LMC) comprises motor neurons that exclusively innervate limb muscles. LMC motor neurons are further subdivided into the medial (LMC_M) and the lateral (LMC_L) division, innervating the ventral and dorsal part of the limb, respectively. Lastly, at the highest level of organization, clusters of motor neurons of one LMC division innervating a single muscle are termed motor pools and have a stereotypic dorsoventral

and mediolateral position in the ventral spinal cord, determined by the transcription factor FoxP1 (67–72).

Conditional elimination of Foxp1 in motor neurons causes a profound scrambling of LMC motor neurons, disrupting the stereotypic motor pool organization due to the loss of putative pool-specific cell-cell recognition tags (72, 73). Despite the perturbation of specific sensory-motor connections, proprioceptive sensory neuron axons that innervate each muscle still maintain the same dorsoventral tier projection in the spinal cord as in wild-type mice (Figure 5A) (73). Consequently, the exact positional organization of motor pools is critical for motor neurons to receive the appropriate sensory feedback. Nevertheless, it is unlikely that only the precise positioning of motor neuron cell bodies is sufficient to establish exquisite sensory-motor connectivity since they do not represent the overall neuronal territory.

Proprioceptive axons are primarily located along motor neuron dendrites, which are extensive and cover a large spinal cord surface area, reasoning their role in establishing sensory-motor connectivity. In support of this, it was shown that dendrites of motor pools exhibit stereotyped morphologies and orientations, suggesting that the positional features of axo-dendritic interactions are crucial for establishing selective sensory-motor connectivity (74). Indeed, spinal proprioceptive trajectories of distinct hindlimb muscles are topographically organized according to the proximal-distal axis of the limb, matching with dendritic arborization patterns (angles) of homonymous motor pools (75). In agreement with classical physiological studies (58), motor neuron dendrites receive mainly direct sensory input from homonymous proprioceptive afferents and only a few, if any, from non-homonymous afferents. A current study (75) takes spatial axo-dendritic constraints into account and shows that a small angle of axo-dendritic approach together with a high degree of axo-dendritic overlap is important in achieving selective proprioceptive-motor neuron connectivity. Thereby the axo-dendritic overlap affects the number of synaptic connections, while the axo-dendritic angle influences the formation of synaptic clusters when proprioceptive afferents cross dendrites of different motor pools (Figure 5B). (57)

The specificity of sensory-motor connectivity is also influenced by cell-cell recognition programs (76, 77). For example, group Ia afferents of the *cutaneous maximus* muscle (Cm) generally do not form monosynaptic connections with Cm innervating motor neurons expressing Sema3E. However, elimination of Sema3E from motor neurons or PlexD1 from proprioceptors results in monosynaptic connections between Cm-motor neurons and Cm innervating group Ia afferents. This led to the conclusion that a repellent Sema3E-PlexD1 signaling mechanism plays a role in preventing atypical monosynaptic connections between

PlexD1⁺ proprioceptive afferents and Sema3E⁺ motor neurons (Figure 5C) (76). However, it is unknown whether other repulsive or adhesive cell recognition mechanisms are involved in establishing sensory-motor connectivity. Despite their fine controlled monosynaptic connectivity, both proprioceptors and motor neurons are required to innervate homonymous muscle targets in the periphery.

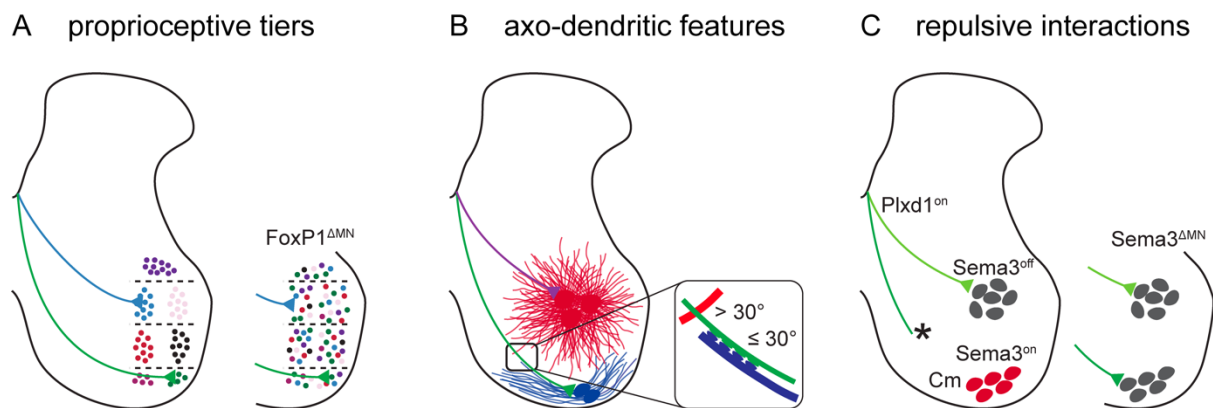


Figure 5. Strategies to establish sensory-motor connectivity. (A) Proprioceptive afferents target dorso-ventral tiers in the spinal cord independently of motor neuron identity and position. (B) Axo-dendritic interactions account for sensory-motor connectivity and synaptic organization. (C) Repulsive mechanisms prevent inappropriate connections between Sema3a⁺ *cutaneous maximus* (Cm) motor neurons and Plexd1⁺ proprioceptive afferents. The figure was adapted from Balaskas et al., 2019 and 2020 (57, 75).

1.4 Peripheral muscle target connectivity

Motor neurons are well defined by their transcriptional programs and downstream effectors that permit motor neuron axons to respond to guidance cues expressed by the limb mesenchyme and to innervate distinct muscle targets. Among many other guiding cues, studies have shown that Eph/ephrin-mediated signaling plays an important role in these processes. Classical membrane bound Eph tyrosine kinases interact with membrane-tethered ephrin ligands, which lead to the activation of signaling pathways responsible mainly for cell repulsion and, in some cases, for cell adhesion. Eph receptors are classified into EphA (EphaA1-9) and EphB (EphB1-5), depending on binding either to the membrane anchored ephrin-As (GPI-linked, EfnA1-5) or transmembrane ephrin-Bs (PDZ domains, EfnB1-3), respectively. Notable exceptions are binding interactions of Epha4 with ephrin-Bs and EphB2 with EfnA5.

Despite being involved in many different developmental processes, Eph/ephrin signaling plays a prominent role in navigating the LMC_L and LMC_M motor neuron axons

toward the dorsal or ventral hindlimb mesenchyme. The expression of *Epha4* (dependent on *Lhx1*) by LMC_L motor neurons causes repulsion in the receptor-expressing cell from the ventral limb mesenchyme expressing ephrin-As, defined as forward signaling. In turn, EphAs in the dorsal limb and the additional expression of ephrin-As in LMC_L lead to reverse signaling in the ligand-expressing cell mediating attraction, enhanced by GDNF-*Ret*- α GFR, of LMC_L axons towards the dorsal limb mesenchyme (Figure 6A). In contrast, LMC_M motor neurons express *EphB1* (*Isl1* dependent) and their axons are repelled from the dorsal limb expressing ephrin-Bs. At the same time, ephrin-A expression in LMC_M motor neurons attenuates residual EphA function (*cis*-interaction), which enables LMC_M axons to innervate the ephrin-A expressing ventral limb mesenchyme (Figure 6B) (78–80). These complex and tight controlled mechanisms lead to exquisite motor neuron-muscle connectivity.

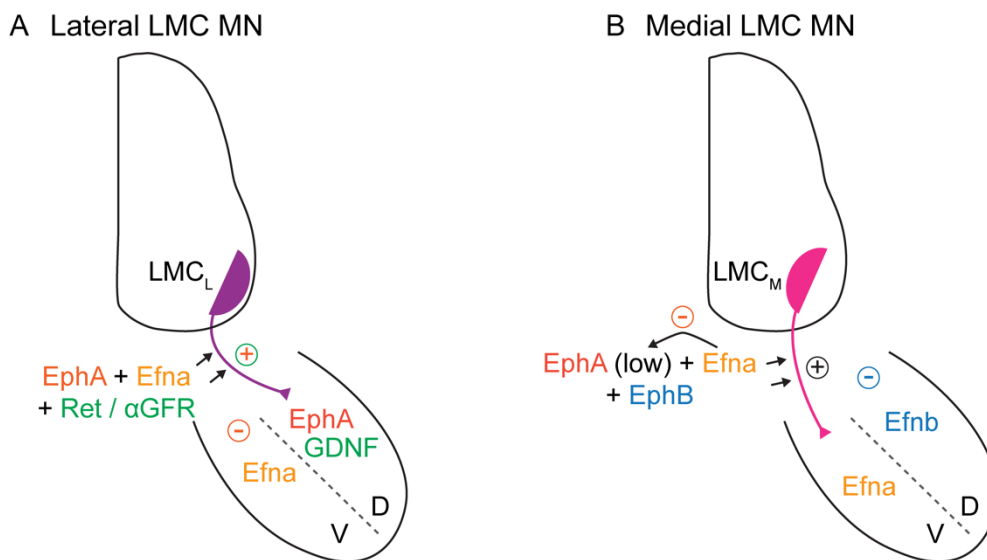


Figure 6. Eph/ephrin signaling in motor axon guidance. (A) Lateral LMC motor neuron axons are directed by EphA/ephrin-A signaling toward the dorsal (D) limb mesenchyme. LMC_L axons express EphA4 and are repelled from the ventral (V) limb mesenchyme expressing ephrin-As (forward signaling), but attracted by the EphA⁺ dorsal limb mesenchyme (reverse signaling). GDNF expressed by the dorsal limb mesenchyme guides *Ret*/ α GFR positive LMC_L axons further to the dorsal pathway. (B) In medial LMC motor neuron axons EphA repulsion is attenuated by *cis*-interactions with ephrin-As, allowing them to enter the ventral limb mesenchyme upon EphB/ephrin-B mediated repulsion from the dorsal mesenchyme. The figure was adapted from Kania and Klein, 2016 (78).

However, in stretch reflex circuits, motor neurons rely on direct monosynaptic input from proprioceptors supplying the same muscle, which raises the question of how proprioceptor identities are assigned in a manner that matches their muscle targets. A current study (81) addressed this question and performed a molecular screen of retrogradely labeled

proprioceptors from two different muscles with antagonistic function at the ankle joint, the *Tibialis anterior* muscle (TA) and the *Gastrocnemius* muscle (GS). Both muscles are located at the proximal-distal end of the limb, with the TA position dorsally and the GS ventrally. Among other genes, Cadherin 13 (Cdh13) and Semaphorin 5a (Sema5a) were identified as marker genes for proprioceptors innervating the dorsal-distal hindlimb muscles and the cartilage acidic protein 1 (Crtac1) for proprioceptors targeting ventral-distal hindlimb muscles. Interestingly, genetic manipulations of the dorsoventral limb identity, transforming the ventral mesenchyme into the dorsal mesenchyme or vice versa, revealed changes in the proprioceptor gene expression. For example, upon changing the ventral limb mesenchyme identity into a dorsal one, Cdh13⁺ afferents were also detected in the “ventral” part. Furthermore, changing the dorsal limb mesenchyme identity into a ventral one showed an almost complete absence of Cdh13⁺ afferents in both parts. For the first time, this study identified molecular markers for proprioceptors according to their muscle target and suggested that these molecular markers depend on instructive cues from the limb mesenchyme (81). These and the described observations (see 1.2.1) indicate that proprioceptor muscle-type identities are dependent on extrinsic molecular programs derived from a distinct muscle target. Nevertheless, proprioceptors endow the capability to terminate in defined dorsal-ventral spinal domains independently from the position and presence of motor neurons, implying the involvement of intrinsic programs controlling the spatial targeting with exquisite specificity. To fully resolve proprioceptors muscle-type identity, it is necessary to acquire more molecular information based on their peripheral target connectivity.

2. Aims of the study

Proprioceptors provide direct sensory feedback to motor neurons innervating homonymous muscles, suggesting the existence of proprioceptor subtypes defined by the muscle they innervate. Thus, in this study, we aimed to reveal the molecular signatures of proprioceptors innervating back, abdominal, and hindlimb muscles.

Aim 1: To uncover molecular determinants for proprioceptors of distinct muscle groups.

Aim 2: To characterize back proprioceptors using an intersectional mouse line that allows their labelling.

Aim 3: To identify and validate molecular markers for back, abdominal and limb proprioceptors.

Aim 4: To functionally evaluate Ephrin-A5 as a limb proprioceptor marker.

3. Materials

3.1 Primary antibodies

Table 1. Primary antibodies used for immunohistochemistry.

Target	Host	Source	Dilution
ChAT	Goat	Millipore (AB144P)	1:200
Pv	Chicken	Jessell lab (CU1664)	1:8000
vGluT1	Guinea-Pig	Jessell lab (CU1328)	1:5000
dsRed	Rabbit	Takara (632496)	1:1000
tdTomato	Rabbit	Rockland (600-401-379)	1:500

3.2 Secondary antibodies

Table 2. Secondary antibodies used for immunohistochemistry.

Target	Host	Source	Conjugate	Dilution
Goat	Donkey	Jackson ImmunoResearch	Alexa-Fluor488	1:800
			Cyanin3 (Cy3)	1:1000
			Cyanin5 (Cy5)	1:250
Chicken	Donkey	Jackson ImmunoResearch	Alexa-Fluor488	1:800
			Cy3	1:1000
			Cy5	1:250
Guinea-Pig	Donkey	Jackson ImmunoResearch	Alexa-Fluor488	1:800
			Cy3	1:1000
			Cy5	1:250
Rabbit	Donkey	Jackson ImmunoResearch	Cy3	1:1000
Rabbit	Donkey	Jackson ImmunoResearch	Cy3	1:1000

3.3 RNAscope probes

Table 3. Antisense probes used for fluorescent *in situ* hybridization (RNAscope).

Target	Channel	Source	Dilution
<i>Mm - Epha3</i>	C1	ACDBio (409251)	1:50
<i>Mm - Tox</i>	C1	ACDBio (484781)	1:50
<i>Mm - Clql2</i>	C1	ACDBio (480871)	1:50
<i>Mm - Efna5</i>	C2	ACDBio (316641-C2)	1:50
<i>Mm - Pvalb</i>	C2	ACDBio (421931-C2)	1:50
<i>Mm - Trpv1</i>	C2	ACDBio (313331-C2)	1:50
<i>Mm - Gabrg1</i>	C3	ACDBio (501401-C3)	1:50
<i>Mm - Pvalb</i>	C3	ACDBio (421931-C3)	1:50
<i>Mm - Runx3</i>	C3	ACDBio (451271-C3)	1:50

3.4 Fluorescent dyes

Table 4. Fluorescent dyes used for *in situ* hybridization and immunohistochemistry.

Dye	Source	Dilution
<i>Opal 690</i>	Akoya Bioscience (FP1497001KT)	1:1500
<i>Opal 520</i>	Akoya Bioscience (FP1487001KT)	1:1000
<i>Opal 570</i>	Akoya Bioscience (FP1488001KT)	1:1000
NeuroTrace™ 435/455	ACDBio (316641-C2)	1:250

3.5 Neuronal tracers

Table 5. Non-viral tracers used for retrograde labeling experiments.

Tracer	Source	Solution
Cholera Toxin Subunit B - Alexa Fluor™ 555	Invitrogen™ (C34776)	10 % w/v
Rhodamine-Dextran	Invitrogen™ (D1824)	20 % w/v

3.6 Genotyping primers

Table 6. Primers used to perform genotyping of mouse lines.

Mouse line	Primer	Sequence	Fragment
Trpv1-Cre	WT-Fwd	TTCAGGGAGAAACTGGAAGAA	490 bp
	WT-Rev	TAGTCCCAGCCATCCAAAAG	
	MUT -Fwd	GCGGTCTGGCAGTAAAAACTATC	102 bp
	MUT -Rev	GTGAAACAGCATTGCTGTCACTT	
Pv-Cre	WT-Fwd	CAGAGCAGGCATGGTGACTA	500 bp
	WT-Rev	AGTACCAAGCAGGCAGGAGA	
	MUT -Fwd	GCGGTCTGGCAGTAAAAACTATC	100 bp
	MUT -Rev	GTGAAACAGCATTGCTGTCACTT	
Pv-Flpo	Co-Rev	TGTTTCTCCAGCATTTCAG	
	WT-Fwd	GGATGCTTGCCGAAGATAAG	238 bp
	MUT-Fwd	CTGAGCAGCTACATCAACAGG	196 bp
Pv-tdT	MUT-Fwd	ACTGCAGCGCTGGTCATATGAGC	130 bp
	MUT -Rev	ACTCTTTGATGACCTCCTCG	
Ai14 (tdT), Ai65 (ds- tdT)	WT-Fwd	AAGGGAGCTGCAGTGGAGTA	297 bp
	WT-Rev	CCGAAAATCTGTGGGAAGTC	
	MUT-Fwd	CTGTTCCTGTACGGCATGG	196 bp
	MUT -Rev	GGCATTAAAGCAGCGTATCC	
Efna5; Efna2	E5-Co-Fwd	TCCAGCTGTGCAGTTCTCCAAAACA	
	E5-WT-Rev	ATTCCAGAGGGGTGACTACCACATT	397 bp
	E5-MUT-Rev	AGCCCAGAAAGCGAAGGAGCAAAGC	513 bp
	E2-Co-Fwd	CCGCTTCCTCGTGCTTTACGGTATC	
	E2-WT-Rev	GGCTATACCGTGGAGGTG	110 bp
	E2-MUT-Rev	CTGCCGGTGGTCACAGGA	650 bp

3.7 Mouse lines

Table 7. Mouse lines used for *in vivo* experiments.

Mouse line	Source	Identifier
C57BL/6J	Jackson Laboratory	Stock No: 664
B6.129- <i>Trpv1</i> ^{tm1(cre)Bbm/J}	Jackson Laboratory	Stock No: 017769
<i>Tg</i> ^{(<i>Trpv1-cre</i>)1} Hoon	Hoon Lab	MGI: 4942415
B6.Cg- <i>Pvalb</i> ^{tm4.1(flpo)Hze/J}	Jackson Laboratory	Stock No: 022730
B6.129P2- <i>Pvalb</i> ^{tm1(cre)Arbr/J}	Jackson Laboratory	Stock No: 017320
C57BL/6- <i>Tg</i> ^{(<i>Pvalb-tdTomato</i>)15Gfng/J}	Jackson Laboratory	Stock No: 027395
B6;129S6- <i>Gt(ROSA)26Sor</i> ^{tm14(CAG-tdTomato)Hze/J}	Jackson Laboratory	Stock No: 007908
B6;129S- <i>Gt(ROSA)26Sor</i> ^{tm65.1(CAG-tdTomato)Hze/J}	Jackson Laboratory	Stock No: 021875
<i>Efna2</i> ^{tm1Jgf} <i>Efna5</i> ^{tm1Ddmo/J}	Jackson Laboratory	Stock No: 005992

3.8 Software

Table 8. Software used for data processing and analysis.

Mouse line	Version	Source
Adobe Illustrator	v 22.4.3	Adobe
Adobe Photoshop	v 25.4.1	Adobe
Arivis Vision4D	v 3.5.1	Arivis AG
ImageJ2	v 2.3.0/153f	NIH
Imaris	v 9.8.0	Oxford Instruments
Microsoft Office	v 16.56	Microsoft
Prism - GraphPad	v 9.3.1	GraphPad Software
R	v R4.1.1 GUI 1.77	The R project
ZENblue	v 3.4	Zeiss

3.9 Devices

Table 9. Equipment used to perform experiments.

Device	Model	Source
Bioanalyzer	2100 Bioanalyzer	Agilent
Centrifuge	Sorvali RC6	Thermo Scientific
Centrifuge	5804	Eppendorf
Centrifuge	PerfectSpin Mini	Peqlab
Confocal microscope	LSM 800	Zeiss
Cryostat	CM1860	Leica
Electrophoresis system	Owl Easycast B1/B2	Thermo Scientific
Fluorescence lamp	HXP 120V	Zeiss
Fluorescence microscope	DFC3000G	Leica
Gel imager	C150	Azure Biosystems
Hot plate stirrer	VMS-C7 advanced	VWR
Hybridization system	HybEZTM II	ACDBio
Incubator	Series CB	Binder
Infrared lamp	SIL06	Sanitas
Inverted microscope	Eclipse TS100	Nikon
Light sheet microscope	Zeiss Z1	Zeiss
Light source for Binocular	KL1500LCD	Leica
Micropipette puller	P97	Sutter instruments
Nanodrop	ND-1000	Peqlab
Orbital shaker	Sky Line	ELMI
PCR cycler	Mastercycler nexus GX2	Eppendorf
Pipettes	Research plus	eppendorf
Platform Shaker	Polymax 1040	Heidolph Instruments
Power/Voltage supply	Power Pac 200	Bio-Rad
Scale	PF	Shinko Denish
Thermomixer	Thermomixer comfort	Eppendorf
UV table	TFX-35	Vilber Lourmat
Vortex mixer	Vortex-Genie2	Specific Industries
Water bath	Alpha A6	Lauda

3.10 Chemicals and kits

Table 10. Chemicals used to perform experiments.

Component	Source
Agarose	Roth
AMPure XP beads	Beckman
Calcium chloride dihydrate	Roth
Collagenase	Sigma
D (+) Saccharose	Roth
D (+)-Glucose	Roth
DAPI, 4',6-Diamidino-2-phenylindole	Sigma
Di-sodium hydrogen phosphate heptahydrate	Roth
Dithiothreitol	Thermo Fisher Scientific
DMEM	Gibco
DNA polymerase	Thermo Fisher Scientific
dNTPs, deoxynucleotides	Promega
DPBS without calcium and magnesium	Thermo Fisher Scientific
EasyIndex	LifeCanvas Technologies
EDTA 0.5 MpH 8.0	Ambion
Ethanol	Roth
Ethidium bromide	Roth
F12 medium	Gibco
Fetal horse serum	Thermo Fisher Scientific
Gene-ruler 1kb plus	Thermo Fisher Scientific
Glucose	Roth
Green GoTaq reaction buffer 85x)	Promega
HBSS	Life Technology
HBSS (Hanks Balanced Salt Solution9	Gibco
Heat-inactivated horse serum	Life Technology
Hydrochloric acid (1N)	Roth
Ketamine (ketamidor)	WDT
Ligase	Thermo Fisher Scientific
Magnesium chloride hexahydrate	Roth

Methanol	Roth
N,N,N',N'-tetrakis(2-hydroxypropyl) ethylenediamine (Quadrol)	Sigma
Optimum cutting temperature compound	Tissue-Tek
OptiPrep™	Sigma
Paraformaldehyde	Roth
PBS liquid concentrate (10x)	Merck Millipore
Potassium chloride	Roth
ProLong™ Gold Antifade Mountant	Life Technology
RNAscope® Multiplex Fluorescent Kit v2	ACDBio
Sodium carbinatate monohydrate	Roth
Sodium chloride	Roth
Sodium dihydrogen phosphate dihydrate	Roth
Sodium hydrogen carbonate	Roth
Sodium hydroxide solution (1N)	Roth
Sylgard 184	Dow corning
Tissue glue	Vetbond
Tris	Roth
Triton X-100	Roth
Trypsin (0.25 %), phenol red (1x)	Gibco
Urea	Sigma
Vectashield	Vector
Xylazine (Rompun 2%)	Bayer

4. Methods

4.1 Animal experiments

All experiments were carried out in accordance with the German Animal Welfare Act and approved by the Regional Office of Health and Social Affairs of Berlin (LAGeSo) under the license numbers G0148/17 and G0191/18. Mice were housed in standardized cages on a 12 h light-dark cycle with food and water *ad libitum*.

4.2 Genotyping

To extract DNA for genotyping, the ear biopsies were lysed in 200 μ l of 0.05 % NaOH at 95°C for 1 h. Subsequently, 20 μ l of 1 M Tris/HCl pH 7.5 were added to neutralize the DNA solution. For one PCR reaction 2 μ l of DNA solution was used and mixed with a master mix containing 12.5 μ l KAPA2G Fast Ready Mix, 0.5 μ l of each primer (10 mM) and Milli-Q H₂O (filled up to 25 μ l). PCR was performed using the following program:

Step	Temperature	Duration	Repeats
1	94°C	3 min	
2	94°C	15 sec	
3	T _m - 2°C	30 sec	35x
4	72°C	1 min/ kb	
5	72°C	10 min	
6	4°C	forever	

Lastly, 25 μ l of each PCR product was loaded onto a 2% agarose gel containing ethidium bromide. Electrophoresis was performed at 100 V for 1 h and the gel was imaged using a UV light documentation system.

4.3 Dissection and tissue processing

Postnatal mice were anesthetized by intraperitoneal injection of 120 mg/kg ketamine and 10 mg/kg xylazine and transcardially perfused with PBS and 4 % PFA in 0,1 M phosphate buffer. For embryonic tissue, pregnant females were sacrificed by cervical dislocation and

embryos dissected and pinned down into a petri dish containing ice cold PBS. To expose the spinal cord and DRG of embryonic and postnatal mice, a ventral laminectomy was performed and tissue postfixed O/N in 4 % PFA at 4°C. The next day, the tissue was washed three times with ice-cold PBS and transferred to 30 % sucrose in PBS for cryoprotection at 4°C O/N. The tissue was embedded in Tissue-Tek OCT embedding compound and stored at -80°C until further processing.

4.4 Single-cell isolation

The dorsal root ganglia were dissected separately from the thoracic (T1-T12) and lumbar (L1-L5) segments and collected in F12 medium with 10 % Fetal horse serum (FHS) on ice. Next, DRG were incubated in F12/FHS with 0.125 % collagenase (Sigma C0130) for 1 h (p1) or 30 min (e15.5) at 37°C. After three washes with PBS DRG were transferred to 0.25 % trypsin solution (Gibco 15050-065) and incubated for 15 min at 37°C. Afterwards, DRG were mechanically triturated using a fire polished Pasteur pipette until a homogenized solution was visible followed by a centrifugation step at 200xg for 10 min. The final cell pellet was resuspended in HBSS (plus 10 mM HEPES, 10 mM Glucose) and the resulting cell suspension was applied to fluorescence-activated cell sorting (FACS) (e15.5) or manual cell selection under an inverted fluorescent microscope (p1). Single tdT⁺ cells were sorted into individual wells containing 1.2 µl scRNA sequencing lysis buffer (10 % Triton X-100, 25 mM dNTPs, barcoded primer 25 ng/µl) and stored at -80°C until further processing.

4.5 Preparation of cDNA libraries

For the preparation of the cDNA libraries, the CEL-Seq2 protocol was used as previously described by Hashimshony et al., 2016 (82). Frozen plates with sorted single neurons were incubated for 5 min at 65°C to break cells open and centrifuged afterwards at maximum speed for a few seconds. Next, 0.8 µl of reverse transcription buffer (0.4 µl first strand buffer, 0.2µl DTT 0.1 M, 0.1 µl RNase inhibitor, 0.1 µl Superscript II) was added to each well and plates were incubated for 1 h at 42°C followed by 10 min of heat inactivation at 70°C. After reverse transcription, second strand synthesis was carried out by adding 10 µl of second strand buffer mix (7 µl ddH₂O, 2.31 µl second strand buffer, 2.31 µl dNTP, 0.08 µl ligase, 0.3 µl E. coli DNA polymerase, 0.08 µl RNaseH) to every well and incubated for 2 h at 16°C. At this point, all single samples were barcoded and the cDNA of each well from one plate was pooled. The

pooled cDNAs were then purified using AMPure XP beads. To each 100 µl of the pooled sample, 20 µl beads and 100 µl bead buffer were added. After 15 min of incubation at room temperature (RT), magnetic beads were separated by magnetic forces and the supernatant removed. The beads were washed twice with 200 µl of 80 % EtOH and cDNA was resuspended in 6.4 µl ddH₂O. For the next step, the *in vitro* transcription, amplified RNA (aRNA) and 9.6 µl of transcription buffer mix (1.6 µl of each dNTP (A, G, C, U), 1.6 µl 10x T7 buffer, 1.6 µl T7 enzyme) were added to resuspended cDNA, incubated for 13 h at 37°C, and treated with EXO-SAP (6 µl enzyme, 15 min at 37°C) to remove primers. Afterwards, the fragmentation of aRNA was performed by adding 5.5 µl fragmentation buffer to 22 µl of aRNA and incubated for 3 min at 94°C. Immediately after, 2.75 µl of fragmentation stop buffer was added on ice, aRNA fragments were purified using the AMPure XP beads, and resuspended in 7 µl ddH₂O. Before starting the actual library preparation, the quantity and quality of aRNA fragments were acquired using the Bioanalyzer platform with a Bioanalyzer RNA pico chip. A fragment size peak at ~500 bp and 500-1000 pg/µl were used as threshold parameters to continue library preparations. First, 1 µl of random reverse transcription primers and 0.5 µl of dNTPs were added to 5 µl of purified aRNA fragment solution and incubated for 5 min at 65°C for primer annealing. For further reverse transcription, 4 µl of the reverse transcription buffer mix (2 µl first-strand buffer, 1 µl 0.1 M DTT, 0.5 µl RNaseOUT, 0.5 µl Superscript II) were added and incubated for 10 min at 25 °C and an additional hour at 42°C. Next, to amplify the cDNA, 40 µl of a PCR master mix (24.5 µl ddH₂O, 10 µl 5X Phusion HF buffer, 1 µl 10 mM dNTPs, 2 µl PCR primer RPI1, 2 µl PCR primer RPI X (individual for each original plate), and 0.5 µl Phusion DNA polymerase) were added to the reverse transcription solution and the following PCR performed:

Step	Temperature	Duration	Repeats
1	98°C	30 sec	
2	98°C	10 sec	
3	60°C	30 sec	11 - 15x
4	72°C	30 sec	
5	72°C	10 min	
6	4°C	forever	

Afterwards, the PCR products were purified using the above described AMPure XP beads procedure twice and resuspended in 10 μ l ddH₂O. Lastly, the quality and quantity of amplified cDNA libraries were analyzed using a high-sensitivity DNA chip on the Bioanalyzer platform. A minimum of \sim 1 ng/ μ l DNA and a fragment distribution of 200-400 bp were applied as threshold parameters before proceeding with library sequencing.

4.5 Sequencing of cDNA libraries

For sequencing 1.6 pM of library were used on an Illumina NextSeq500 platform with high-output flow cells at the Next Generation Sequencing Core Facility of the Max-Delbrück Center for Molecular Medicine. Libraries were sequenced in read one 15+1bp; Index 6+2 bp and in read two 50+1 bp. We sequenced 960 neurons (480 from T1-T12 and 480 from L1-L5) from e15.5 P_V^{tdTomato} DRG and 576 neurons (96 thoracic and 96 lumbar from P_V^{Cre}; *tdT*; 96 thoracic and 96 lumbar from *Trpv1*^{Cre-Basbaum}; P_V^{Flp}; *tdT*; 96 thoracic and 96 lumbar from *Trpv1*^{Cre-Hoon}; P_V^{Flp}; *tdT*) from early postnatal DRG (p1).

4.6 Single-cell sequencing analysis

Initial demultiplexing was performed as a standard procedure by the Next Generation Sequencing Core Facility of the Max-Delbrück Center for Molecular Medicine. For both data sets (e15.5 and p1) we used the scruff package v1.4.0 (R package version 1.12.0) to further demultiplex, map and generate count matrices. Then we evaluated the statistics of each data set using Scater v1.14.6 R package. To increase the quality of the experiments, we individually removed low-quality cells based on low total gene counts ($>$ quantile 0.3), low gene abundance ($>$ quantile 0.3), and high mitochondrial gene values per cells ($<$ quantile 0.75). 519 of 960 e15.5 cells and 244 of 576 p1 cells passed the quality control criteria. After log-normalization, we used the scran v1.14.1 buildKNNGraph and cluster_walktrap functions with default parameters to define each data set cell populations and subclusters. Finally, we assigned gene markers to each population using the findMarkers function from the scran with default parameters. For single-cell analysis, R v3.6.2 environment was used to generate the results, statistical analysis and graphical evaluation of the datasets.

4.7 Immunohistochemistry and multiplex fluorescent *in situ* hybridization

For both methods tissue sections of 16 μm were acquired on a cryostat, dried for 1 h and directly used or frozen at -80°C . For immunohistochemistry, dry tissue sections were washed for 10 min with PBS followed by another 10 min incubation of 0.1 % Triton-X-100 in PBS (0.1 % PBX) for permeabilization. Primary antibodies were diluted in 0.1 % PBX and incubated O/N at 4°C . The next day, slides were washed three times for 5 minutes with 0.1% PBX followed by secondary antibody/NeuroTrace incubation for 1 h at RT. After staining with secondary antibodies, slides were washed three times with 0.1 % PBX and subsequently mounted with Vectashield antifade mounting medium.

For multiplex fluorescent *in situ* hybridization, the RNAscope Multiplex Fluorescent Kit v2 was used with a modified manufactures protocol. Tissue sections were dried, fixed with ice-cold 4 % PFA in PBS for 15 min and dehydrated in a series of 50 %, 70 %, 100 % ethanol for 5 min each. Afterwards, sections were treated with a hydrogen peroxide solution for 15 min at RT to block endogenous peroxidase activity followed by another wash with 100% ethanol for 5 min. Next, either Protease IV (postnatal tissue) or Protease III (embryonic tissue and sections from CTB/RhD tracing experiments) was applied for 30 min at RT. After three washes with PBS, probes were applied and hybridization was carried out in a humidified oven at 40°C for 2 h. Following hybridization, amplification was performed using Amp1, Amp2, and Amp3 each for 30 min at 40°C . For detection, each section was treated sequentially with channel-specific HRP (HRP-C1, HRP-C1, HRP-C3) for 15 min, followed by TSA-mediated fluorophore binding for 30 min and final HRP blocking for 15 min (all steps at 40°C). When necessary, additional immunostaining was performed as described above. Images were acquired with a Zeiss LSM800 confocal microscope (20x objective for RNAscope experiments). For quantification of RNAscope experiments, neurons (evaluated by Nissl staining) with ≥ 5 puncta/neuron were considered as positive.

4.8 Tissue clearing and light sheet microscopy

Mice were anesthetized and transcardially perfused as described above. Afterwards, spinal cords and/or DRG were extracted after ventral laminectomy and postfixed in 4 % PFA for two days at 4°C . DRG were kept separately and embedded in 1 % low-melt agarose in OptiPrepTM after post fixation. Tissue clearing was performed as previously described with modifications (83). In short, tissue was transferred to CUBIC1 (25 wt % Urea, 25 wt % N,N,N',N'-tetrakis(2-

hydroxypropyl) ethylenediamine, 15 wt % Triton X-100) and incubated (shaking) at 37°C. Every other day, CUBIC1 solution was exchanged until tissue appeared transparent (spinal cord ~4 d, DRG ~1-2 d). Afterwards, samples were washed for one day with PBS at RT, the refractive index matched with EasyIndex at 37°C for one day and imaged with the ZEISS Light sheet microscope Z.1.

4.9 Retrograde labeling of proprioceptors and motor neurons

For retrograde labeling of p1 proprioceptors and motor neurons, mice were anesthetized with isoflurane and a small incision was made in the skin to expose the muscle of interest. Alexa555-conjugated CTB (50 nl) was pressure injected into the desired muscles using a glass capillary. Afterwards, the skin incision was closed using tissue glue (Vetbond) and the animal was moved back into its home cage after anesthesia recovery. Three days after surgery, animals were perfused and tissue (DRG and spinal cord) collected for further histological analysis.

For retrograde labeling of e15.5 proprioceptors, embryos were dissected in ice-cold artificial cerebrospinal fluid (ACSF: 125 mM NaCl, 3 mM KCl, 1.25 mM NaH₂PO₄ * 2 H₂O, 26 mM NaHCO₃, 10 mM D-glucose, 2 mM CaCl₂, 1 mM MgCl₂) and pinned down. The skin from limb or back muscles was removed and Rhodamine-Dextran (RhD, 50 nl) pressure injected into the desired muscle using a pulled glass capillary. Afterwards, embryos were incubated in circulating oxygenated artificial cerebrospinal fluid (5 % CO₂, 95 % O₂) for 6 h at 27°C and fixed with 4 % PFA overnight.

4.10 Density analysis

For the detection of Pv⁺ afferents in lumbar spinal cord sections, the 'spot' detection function of the Imaris imaging software was used. Spots with an average diameter of 2 µm were detected based on their fluorescence intensity. Subsequently, reference points were assigned for later positional normalization of all spinal cord sections analyzed. After extraction of spots coordinates, data sets were normalized using a custom R script. Heatmaps were generated using the ggplot function in R Studio.

4.11 Quantification and statistical analysis

Details for statistical analysis and number of samples are indicated in figure legends. The significance of the t-tests was defined as * $p < 0.05$; ** $p < 0.01$; *** $p < 0.001$. Statistical analyzes were performed using Prism - GraphPad v9.2.

5. Results

5.1 Single-cell-RNA sequencing of embryonic proprioceptors

During development, proprioceptive sensory afferents first reach their muscle targets and later progress toward their synaptic partners in the spinal cord. Based on their segmental location, thoracic proprioceptors are predicted to collect information from dorsal (back) and ventral (abdominal) trunk muscle groups, while lumbar proprioceptors innervate lower back/tail (back) and hindlimb muscles (illustration in Figures 7A and 7B).

To reveal molecular signatures of proprioceptive sensory neurons (pSN) targeting specific muscles, we performed a single-cell sequencing experiment of pSN isolated separately from thoracic and lumbar DRG on embryonic day (e) 15.5 when primary muscle connectivity is achieved (18, 19). At this stage, pSN express their generic marker parvalbumin (Pv), which can be used to genetically label proprioceptors. We isolated in total 960 single parvalbumin⁺ neurons (480 thoracic and 480 lumbar), from a mouse line expressing tdTomato under control of the parvalbumin promoter (BAC mouse line, Pv^{tdTomato}; (84)) by fluorescence-activated cell sorting (FACS) (Figure 7C). Afterwards, cDNA libraries of single neurons were prepared using the CEL-Seq2 protocol (82) and sequenced. After initial analysis, 519 of 960 neurons (235 thoracic and 284 lumbar) passed the applied quality controls (see method section 4.6). On average 7830 genes/cell were detected and further transcriptome analysis revealed five distinct molecular clusters (Figure 7D). Differential gene expression analysis (Figure 7E) suggests that clusters (C) 1 and C5 represent pSN due to the presence of the generic pSN markers *Pvalb*, *Runx*, *Ntrk3*, and *Etv1*, while transcripts indicating a contamination with Satellite/Schwann cells (*ApoE*, *Mpz*) are present in C5. Genes known to be characteristic of mechanoreceptors (*Maf*, *Ntrk2*) are present in C2-C4. Furthermore, C2 and C4 also show proliferation markers (*Mki67*, *Mcm2*, *Pcna*), while neurons expressing postmitotic genes (*Avil*, *Isl1*) are present mainly in C1, C3 and C5. Next, to identify differences within the identified pSN cluster, we performed a subcluster analysis of C1 (192 neurons) and obtained seven distinct subsets of pSN (pC1-pC7) (Figure 8A). To further test whether these clusters can reflect the regional muscle-pSN identities, we assigned the thoracic and lumbar origin to each cell (Figure 8B). Neurons of pC2, pC4, pC5, and pC7 originate mainly from lumbar DRG and therefore could represent hindlimb-pSN (li-pSN) and a subset of lower back muscle pSN (ba-pSN). In contrast, neurons of mainly thoracic origin were present in pC1 and pC3 recapitulating dorsal (ba-pSN) and ventral (ab-pSN) trunk muscle proprioceptors (Figures 8B and 8C). Cluster pC6 was

comprised almost equally of thoracic and lumbar neurons implying a ba-pSN identity. We could confirm the lumbar and thoracic identity of neurons on a transcriptional level by evaluating the expression of *Hoxc10* (Figure S1), a gene that defines the identity of the lumbar spinal segment (85). In agreement, neurons from thoracic DRG did not express *Hoxc10*.

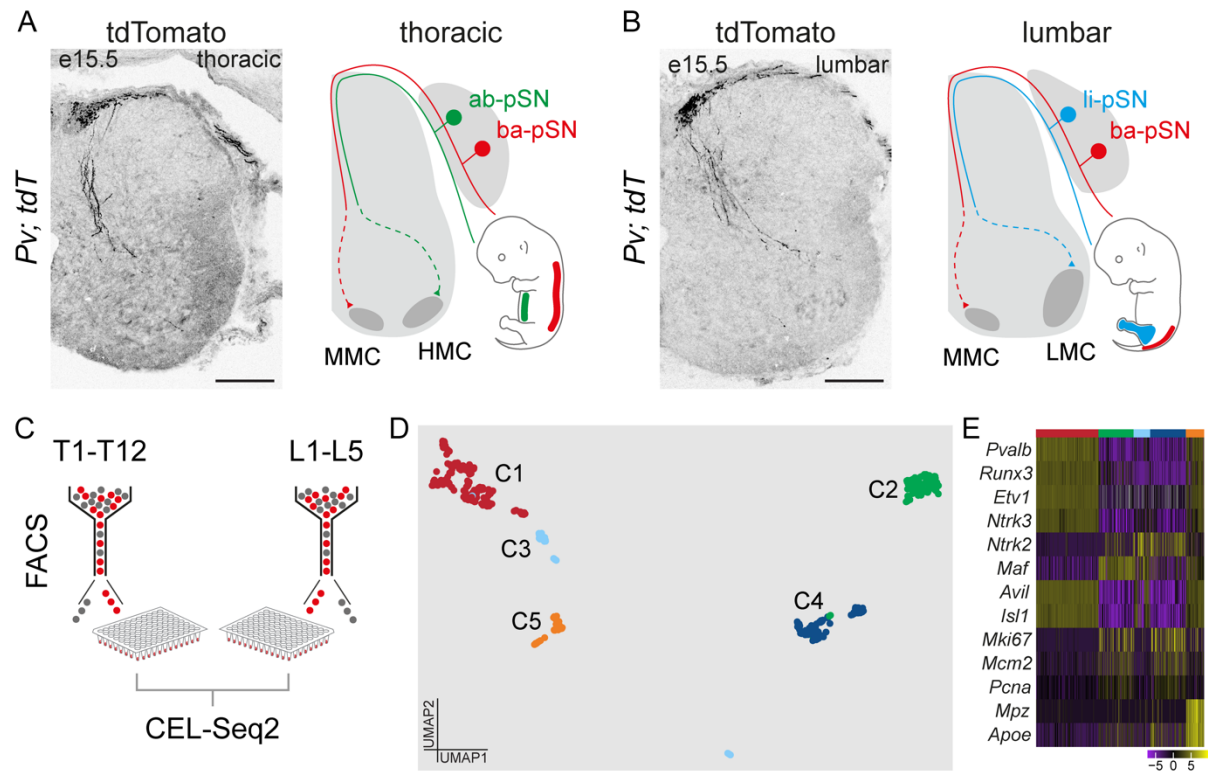
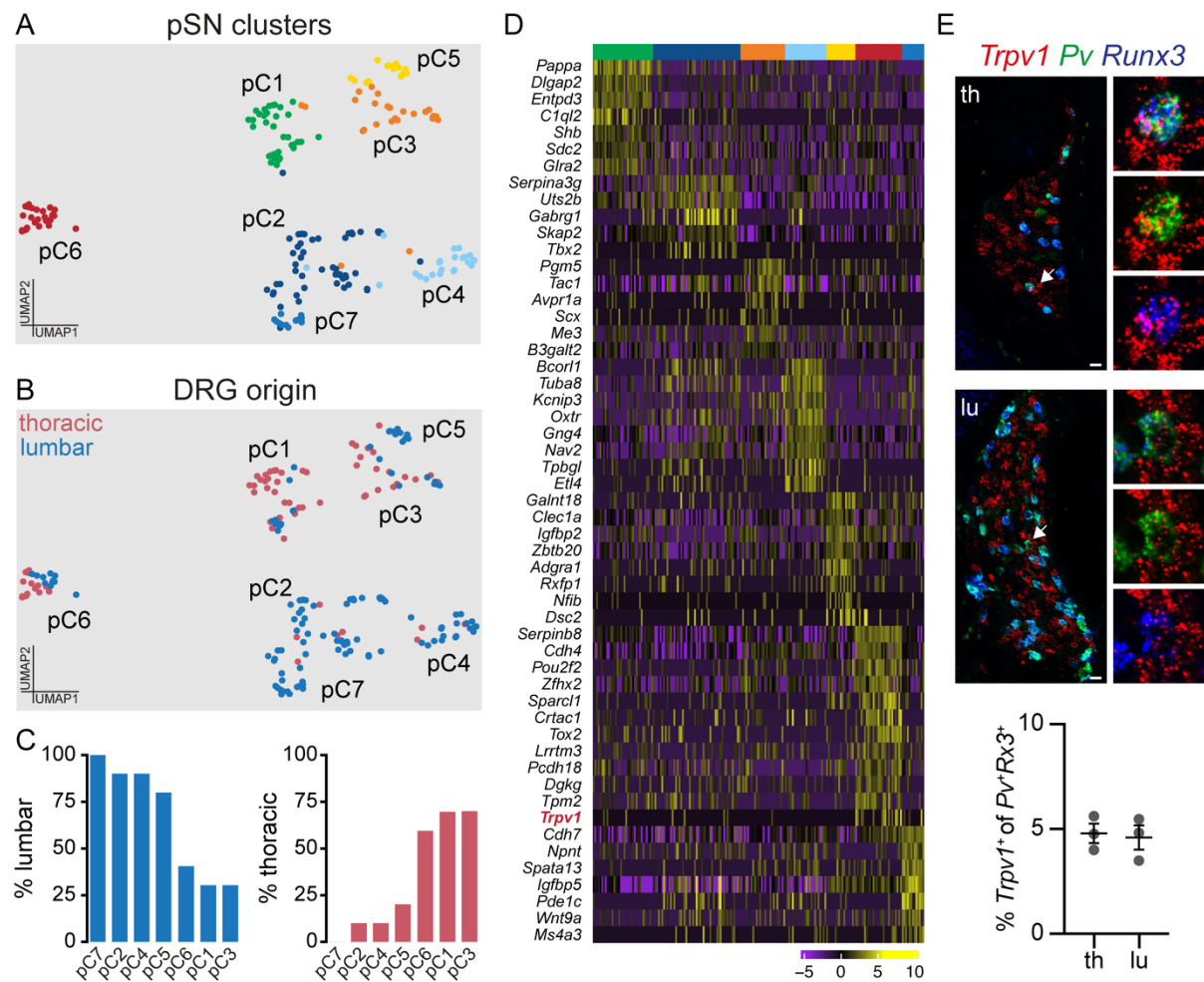


Figure 7. Single-cell transcriptome analysis of thoracic and lumbar parvalbumin⁺ sensory neurons at e15.5. (A and B) Representative images of central tdT⁺ afferents in a thoracic and lumbar spinal cord section from a *Pv^{Cre}; tdT* mouse at e15.5. Schematics illustrate the central and peripheral connectivity of pSN at thoracic and lumbar spinal levels at e.15.5. At thoracic levels, pSN innervate abdominal (green) and back (red) muscles, while lumbar pSN project to limb (blue) and lower back muscles (red). Dashed lines indicate central afferent projections to motor neuron columns (HMC - hypaxial motor column; MMC - medial motor column; LMC - lateral motor column). Scale bar: 100 μ m. (C) Illustration visualizes the single-cell sorting strategy of tdT⁺ sensory neurons dissociated from thoracic and lumbar DRG of e15.5 *Pv^{tdTomato}* mice. The CEL-Seq2 protocol (82) was used to generate cDNA libraries. (D) UMAP of tdT⁺ sensory neurons after transcriptome analysis. (E) Heatmap of cardinal markers for proprioceptors (*Pvalb*, *Runx3*, *Ntrk3*, *Etv1*), mechanoreceptors (*Maf*, *Ntrk2*), postmitotic neurons (*Avil*, *Isl1*), cycling cells (*Mki67*, *Mcm2*, *Pcna*) and Satellite/Schwann cells (*ApoE*, *Mpz*) among clusters. Scale: log-counts.

Differential gene expression analysis revealed several potential marker genes for each cluster (Figure 8D). In particular, cluster pC6 showed a selective enrichment of *Trpv1* (transient receptor potential cation channel subfamily V member 1) (Figure 8D, highlighted in red).

Trpv1 is a well-known marker of nociceptive and thermosensitive sensory neurons and was not expected to be expressed in proprioceptors (86). Further *in situ* hybridization of *Trpv1* in combination with cardinal proprioceptive sensory neuron markers (*Pv* and *Runx3*) confirmed the presence of *Trpv1* in ~5% of thoracic and lumbar proprioceptors at e15.5 (Figure 8E). Taken together these data show that proprioceptors at e15.5 can be divided into molecular distinct clusters, whose anatomical origin suggests their back, abdominal, and hindlimb pSN identity. In addition, the expression of *Trpv1* defines a cluster of thoracic and lumbar proprioceptors, suggesting them as ba-pSN.



5.2 Genetic labeling of *Trpv1* defines proprioceptors of back muscles

To verify the observation that embryonic *Trpv1* expression labels a discrete subset of proprioceptors, we generated a mouse line expressing the recombinases Cre and Flp under the control of *Trpv1* (*Trpv1^{Cre}*, (87)) and *Pv* (*Pv^{Flp}*, (88)) promoters, which allowed to label neurons with an intersectional tdTomato reporter allele (*Trpv1^{Cre}; Pv^{Flp}; tdT* (*Ai65*) (89)). In the cells expressing both recombinases the double-stop cassette (LSL-FSF-tdT) is removed, allowing the expression of tdT. Histological analysis of early postnatal day (p) 7 *Trpv1^{Cre}; Pv^{Flp}; tdT* mice revealed labeling of a defined subset of proprioceptive sensory neurons (Figures 9-11). In thoracic and lumbar spinal cord sections, central tdT⁺ afferents were detected that project mainly to immunostained ChAT⁺ motor neurons of the medial motor column (MMC), known to specifically innervate back muscles (Figure 9A) (79).

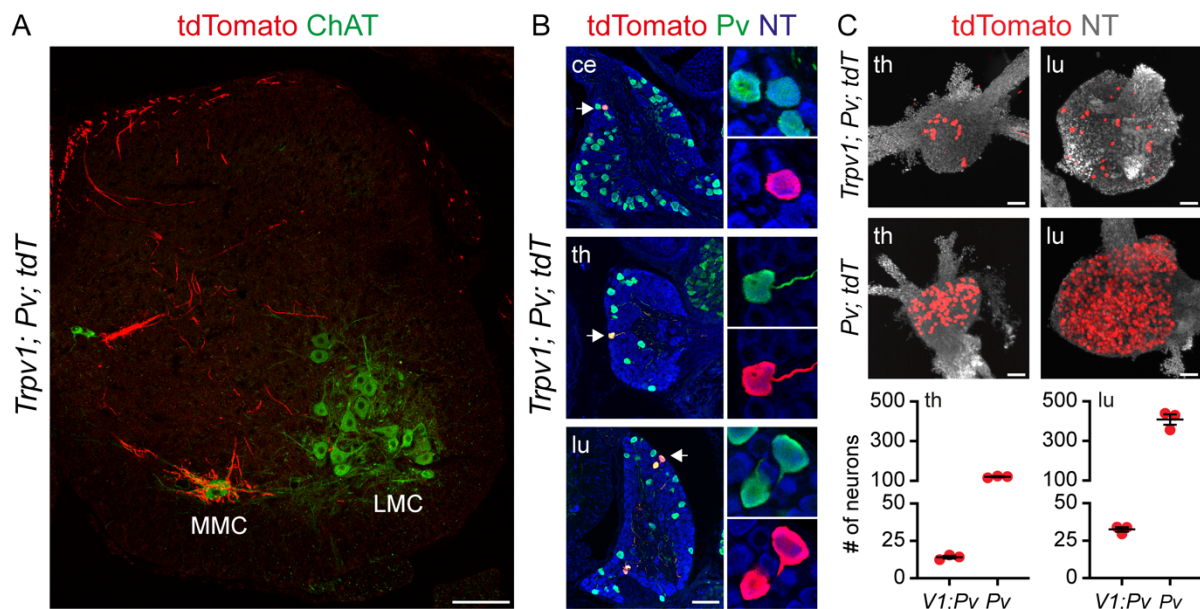


Figure 9. Genetic labeling of back proprioceptors. (A) Representative image of immunostained tdT⁺ afferents and ChAT⁺ motor neurons in a lumbar spinal cord section from a p7 *Trpv1^{Cre}; Pv^{Flp}; tdT* mouse. Labeled tdT⁺ afferents project to MMC motor neurons. Scale bar: 100 μ m. (B) Representative images of a cervical, thoracic and lumbar DRG section with tdT⁺, Pv⁺ sensory neurons (immunostaining) from p7 *Trpv1^{Cre}; Pv^{Flp}; tdT* mice. Scale bar: 100 μ m. (C) Maximum projection (Light sheet microscope acquisitions) of thoracic and lumbar whole mount DRG preparations (top) as well as quantification of T1-T12 DRG (left) and L1-L5 (right) tdT⁺ sensory neurons from p1 *Trpv1^{Cre}; Pv^{Flp}; tdT* and *Pv^{Cre}; tdT* mice (each point represents one animal, mean \pm SEM). Scale bar: 100 μ m.

Next, we evaluated the synaptic connectivity of these proprioceptive afferents and performed immunostainings for vGluT1 and tdT to label pSN synapses in close proximity to motor

neurons. The labeled tdT⁺ afferents showed presynaptic vGluT1⁺ contacts with MMC motor neurons (~11 puncta/MN), but rarely with limb innervating motor neurons (~0.3 puncta/MN) of the lateral motor column (LMC) at lumbar level (Figures 10A and 10B). Furthermore, among all vGluT1⁺ puncta in close proximity to MMC motor neurons ~70 % were tdT⁺ (Figure 10C). In accordance with the specificity of central afferents to MMC, which is the only motor column present on the entire rostro-caudal axis, we detected the labeling of a subset of parvalbumin⁺ neurons expressing tdT in cervical, thoracic, and lumbar DRG (Figure 9B). Evaluation of neuron numbers from thoracic (T1-T12) and lumbar (L1-L5) DRG of *Trpv1^{Cre}; Pv^{Flp}; tdT* and *Pv^{Cre}; tdT* mice revealed that the identified pSN subset represents ~10 % (thoracic 11,6 %; lumbar 8,0 %) of genetically labeled parvalbumin⁺ neurons (Figure 9C). Furthermore, in the periphery, we were able to detect all three types of receptors (Ia, Ib, and II) of proprioceptors in back muscles labeled with vGluT1 and tdT (Figures 10D and S2).

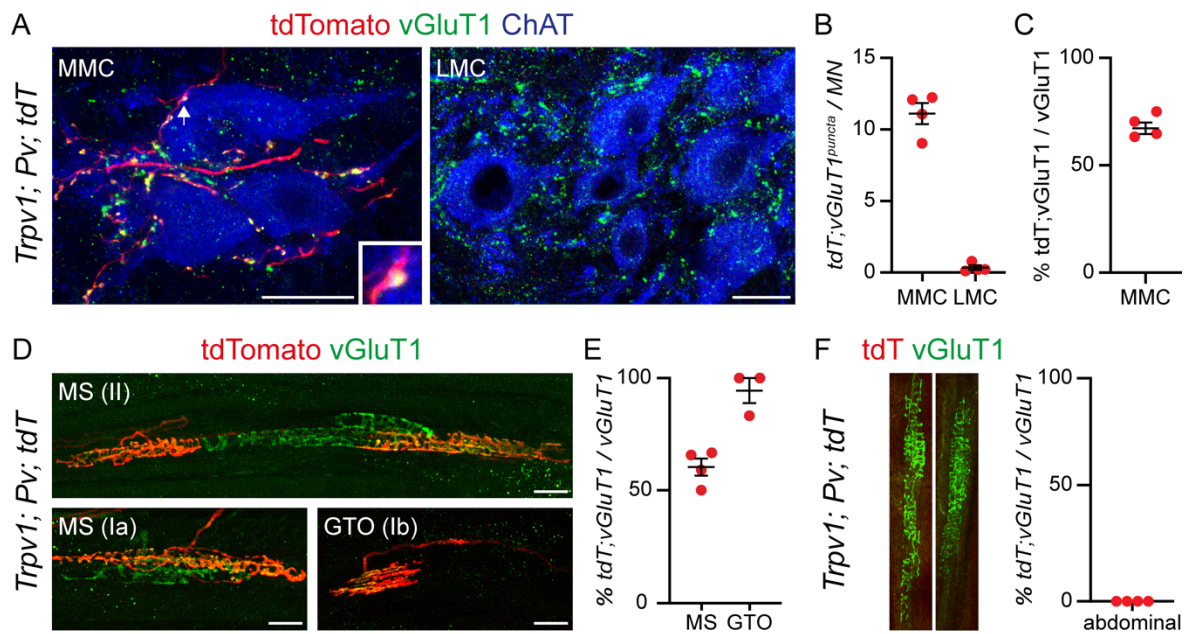


Figure 10. Central and peripheral labeling of back proprioceptors. (A) Images show tdT⁺, vGluT1⁺ presynaptic puncta in close proximity to MMC motor neurons (left), but rarely, if ever, co-labeled puncta around LMC motor neurons (right) in p7 *Trpv1^{Cre}; Pv^{Flp}; tdT* mice. Scale bar: 25 μ m. (B) Quantification of tdT⁺, vGluT1⁺ presynaptic puncta per MMC and LMC motor neuron and (C) percentage of tdT⁺ among all vGluT1⁺ presynaptic MMC motor neuron puncta in p7 *Trpv1^{Cre}; Pv^{Flp}; tdT* mice (each point represents one animal, mean \pm SEM). (D) Expression of vGluT1⁺, tdT⁺ in group Ia, II MS and Ib GTO of back muscles from *Trpv1^{Cre}; Pv^{Flp}; tdT* mice. Scale bar: 25 μ m. (E) Percentage of tdT⁺ MS and GTO in back muscles (73/128 MS and 7/8 GTO, each point represents one animal, mean \pm SEM). (F) Representative images and percentage of tdT⁺ MS in abdominal muscles from p7 *Trpv1^{Cre}; Pv^{Flp}; tdT* mice (0/70 MS, each point represents one animal, mean \pm SEM).

Muscle spindles showed incomplete labeling with tdT in some cases, while GTO were always completely labeled with tdT. We observed that ~60 % of vGluT1⁺ muscle spindles expressed tdT, while ~94 % of vGluT1⁺ GTO were labeled with tdT (Figure 10E). In abdominal muscles (control), no co-labeling of group Ia, Ib, and II receptors could be found in *Trpv1^{Cre}; Pv^{Flp}; tdT* mice (Figure 10F). All these data indicate that the mouse line *Trpv1^{Cre}; Pv^{Flp}; tdT* labels proprioceptors connected to back muscles at all spinal levels. To analyze the overall labeling specificity of the *Trpv1^{Cre}; Pv^{Flp}; tdT* mouse line, we evaluated the tdT expression in brain sections. We could only find labeling of axons projecting to the dorsal column nuclei of the brainstem, which receive direct innervation of proprioceptive sensory neurons ((90), Figure S3). Finally, we used the *Trpv1^{Cre}; tdT* mouse line (*Ail4*, (88)) to analyze whether lineage tracing under the control of Trpv1 would also capture the same subset of proprioceptors. We could observe labeling of immunostained Pv⁺, tdT⁺ neurons in cervical, thoracic, and lumbar DRG and central afferents projecting to MMC motor neurons (Figures 11A and 11B). Taken together, these data show that early expression of *Trpv1* labels a subset of proprioceptors whose central and peripheral afferents are consistent with proprioceptors of the back muscles.

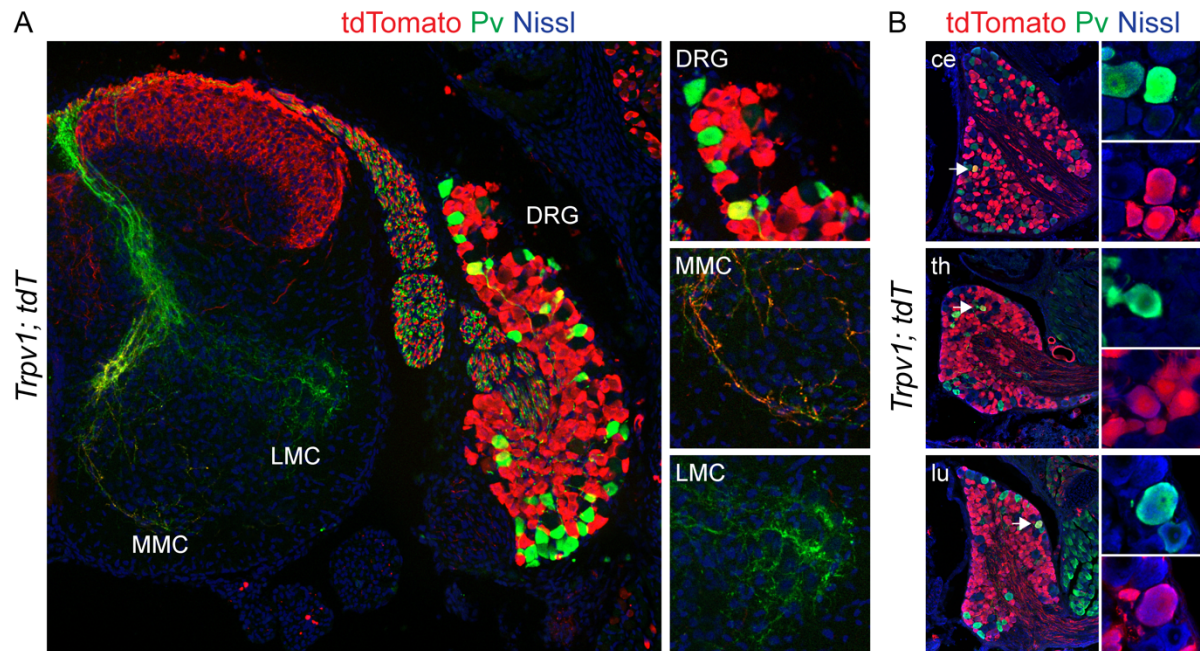


Figure 11. Genetic labeling of back proprioceptor afferents in *Trpv1^{Cre}; tdT* mice. (A) Lumbar spinal cord/DRG section showing co-labeling (immunostaining) of tdT⁺, Pv⁺ sensory neurons in DRG and afferents to motor neurons of the MMC area of p7 *Trpv1^{Cre}; tdT* mice. Only Pv⁺ labelled afferents are projecting to the LMC motor neuron area (B) Co-labeling of tdT⁺, Pv⁺ sensory neurons (arrows) in cervical, thoracic, and lumbar DRG sections of p7 *Trpv1^{Cre}; tdT* mice. Scale bar: 25 μ m.

5.3 Molecular signatures of muscle-type specific proprioceptors

The ability to genetically label a subset of back proprioceptors prompted us to devise a single-cell transcriptomic experiment that takes advantage of the topographic organization of the proprioceptive system to reveal features of postnatal pSN muscle-type identities defined by the connectivity to hindlimb, back, and abdominal muscles. We analyzed the single-cell transcriptome of 576 manually picked tdT⁺ neurons from thoracic and lumbar DRG of *Pv^{Cre}; tdT* mice labeling all proprioceptors (96 th, 96 lu) and *Trpv1^{Cre}; Pv^{Flp}; tdT* (192 th, 192 lu) labeling proprioceptors connected to back muscles at p1 (Figures 12A and 12B). In total 244 sequenced neurons passed the applied quality control parameters and were divided into four distinct clusters (Figure 12C). Generic proprioceptor genes (*Pv*, *Runx3*, *Ntrk3*, and *Etv1*) were highly expressed in all clusters. Additionally, C1 included genes of Satellite/Schwann cells (*ApoE*, *Mpz*) and was consequently excluded from further analysis (Figures 12D and 12E). Next, to identify the putative pSN muscle-type identity, we assigned the mouse line and segmental level to each neuron of the remaining clusters (Figures 12F - 12I). We confirmed the lumbar and thoracic identity on a transcriptional level by evaluating the *Hoxc10* expression. In agreement with our assignment, *Hoxc10* was expressed in lumbar neurons, but not in thoracic neurons (Figure 12H). Furthermore, we quantified the composition of each cluster considering the mouse line origin of each neuron (Figure 12I). The majority of neurons picked from *Trpv1^{Cre}; Pv^{Flp}; tdT* mice (~90 %) were found in C2 suggesting its ba-pSN identity (Figure 12I). In contrast, the majority of lumbar neurons from *Pv^{Cre}; tdT* mice were assigned to C3, presumably li-pSN. C4 neurons were exclusively from thoracic DRG of *Pv^{Cre}; tdT* mice and consequently putative ab-pSN (Figures 12F and 12G). To reveal the molecular signatures of each individual assigned cluster, we performed a differential gene expression analysis (Figure 12J). To further validate each cluster, we conducted fluorescent *in situ* hybridization experiments using the following differentially expressed marker genes: *Tox* (ba-pSN; C2), *Gabrg1* (li-pSN; C3), and *Clql2* (ab-pSN; C4). First, the gene expression of representative markers was analyzed in DRG of *Trpv1^{Cre}; Pv^{Flp}; tdT* mice labeling ba-pSN at p1. *Tox* as potential ba-pSN was expressed in almost all thoracic (100 %) and lumbar (~93 %) tdT⁺ neurons, while *Gabrg1* (thoracic 0.8 %, lumbar 1.4 %) and *Clql2* (thoracic 0 %, lumbar 3 %) were not (Figure 13A).

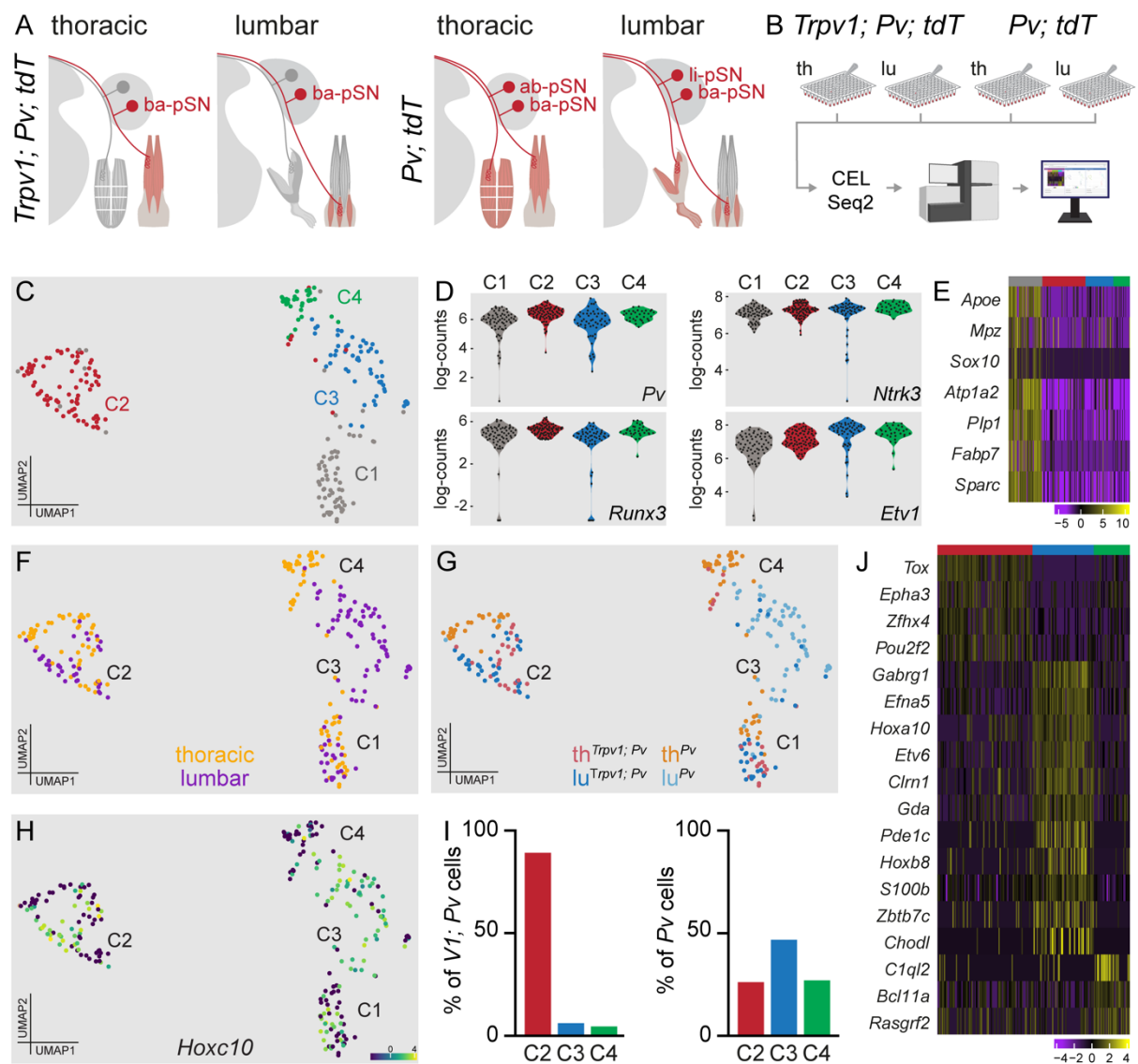


Figure 12. Transcriptomic approach reveals molecular signatures for back, abdominal, and limb proprioceptors. (A) Schematics illustrate the labeling of back proprioceptors by *Trpv1^{Cre}; Pv^{Flp}; tdT* and all pSN by *Pv^{Cre}; tdT* at thoracic and lumbar levels. (B) Single-cell sorting and sequencing strategy of pSN from *Trpv1^{Cre}; Pv^{Flp}; tdT* and *Pv^{Cre}; tdT* mice. (C) UMAP visualization after transcriptome analysis of *tdT⁺* neurons sorted from *Trpv1^{Cre}; Pv^{Flp}; tdT* and *Pv^{Cre}; tdT* mice. (D) Violin plots showing the expression of generic pSN markers (*Pv*, *Ntrk3*, *Runx3*, *Etv1*) in all clusters. (E) Heatmap of characteristic genes expressed by Satellite/Schwann cells (*ApoE*, *Mpz*). Scale: log-counts. (F) UMAP visualization with assigned thoracic (yellow) and lumbar (purple) origin of neurons. (G) UMAP representation of clusters color coded by the thoracic and lumbar origin of cells manually picked from *Trpv1^{Cre}; Pv^{Flp}; tdT* and *Pv^{Cre}; tdT* mice. (H) Expression of the lumbar marker gene *Hoxc10* among clusters (UMAP). Scale: log-counts. (I) Bar graph showing the distribution of *Trpv1^{Cre}; Pv^{Flp}; tdT* (left) and *Pv^{Cre}; tdT* (right) neurons in clusters C2 (red), C3 (blue) and C4 (green). (J) Heatmap of the main differential expressed genes (FDR ≤ 0.05 , logFC > 2) of C2, C3, and C4. Scale: log-counts.

Second, we analyzed the expression of candidate genes within the entire proprioceptor population labeled by *Pv^{Cre}; tdT* mice at p1. At thoracic levels where the back and abdominal muscle groups are innervated by pSN, we determined the expression of *Tox* in ~60 % and *C1ql2* in ~28 % of tdT⁺ neurons. In contrast, proprioceptors innervate predominantly hindlimb over back muscles at lumbar levels, where expression of *Gabrg1* in ~46 % and *Tox* in ~10 % of tdT⁺ labeled neurons was observed (Figure 13B). To evaluate whether our results were influenced by lineage tracing using *Pv^{Cre}; tdT* mice, we analyzed the co-expression of each pSN subtype marker (*Tox*, *C1ql2*, and *Gabrg1*) with endogenous *Pv* expression in DRG neurons of wild-type p1 mice and could detect similar expression frequencies (Figure S4).

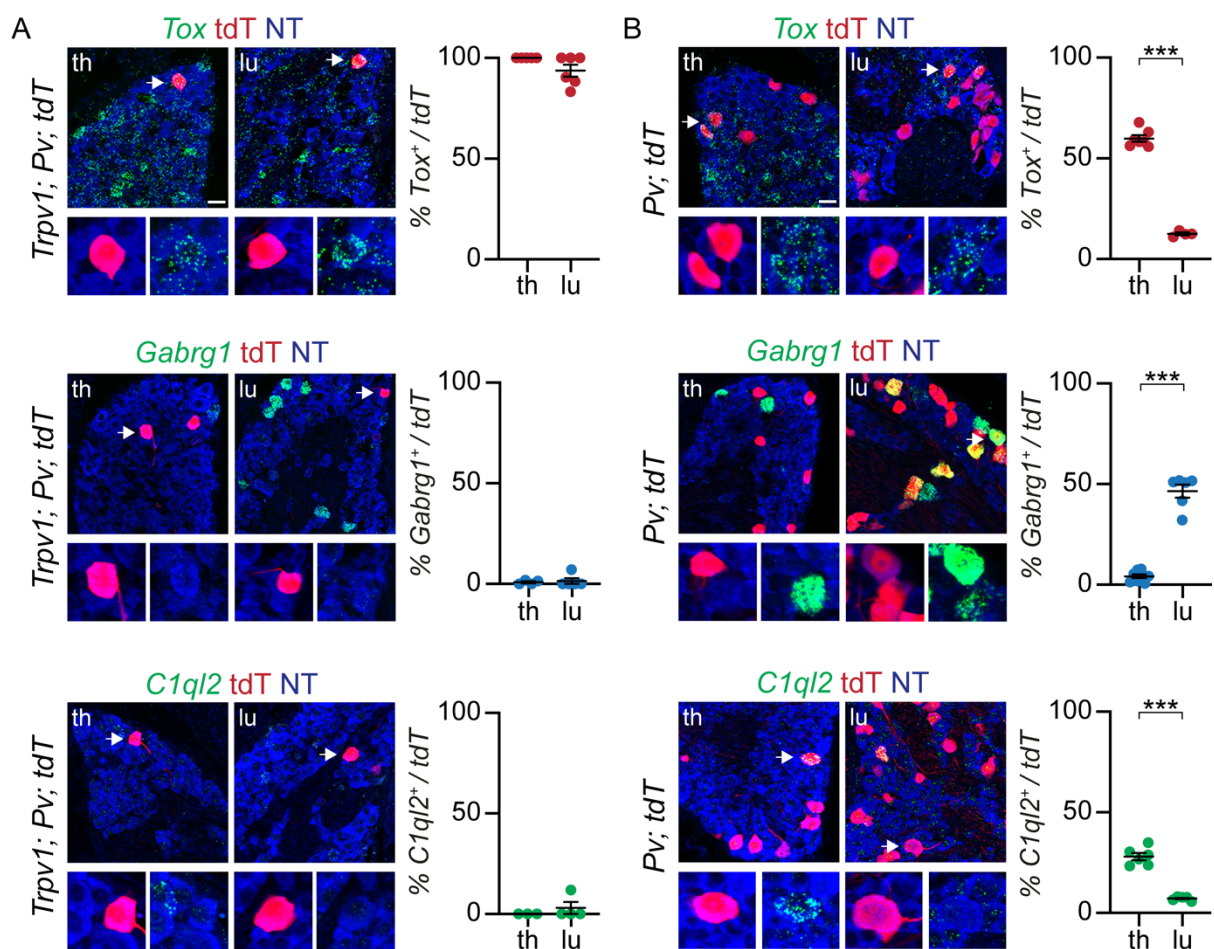


Figure 13. Expression of marker genes for back, abdominal, and limb proprioceptors. (A) Representative images and quantification of *in situ* hybridization of marker genes for ba-pSN (*Tox*), li-pSN (*Gabrg1*) and ab-pSN (*C1ql2*) in immunostained tdT⁺ thoracic (T6-T9) and lumbar (L3, L4) DRG neurons from p1 *Trpv1^{Cre}; Pv^{Flp}; tdT* and (B) *Pv^{Cre}; tdT* mice (each point represents one animal, mean \pm SEM, t-test, *** $p < 0.001$). Scale bar: 25 μ m.

Next, we analyzed the rostro-caudal distribution of *Tox*, *C1ql2*, and *Gabrg1* in single thoracic and lumbar DRG of *Pv^{Cre}; tdT* to evaluate segmental differences in marker expression. As already described, *Tox* and *C1ql2* were found predominantly at thoracic and *Gabrg1* at lumbar levels. Interestingly, we found the opposite in lumbar L2 DRG where *Tox* (ba-pSN) and *C1ql2* (ab-pSN) were expressed at higher frequencies compared to the li-pSN marker *Gabrg1* (Figures 14B-C). Altogether, these data confirm the existence of molecular markers, whose expression frequencies recapitulate ba-pSN, ab-pSN, and li-pSN.

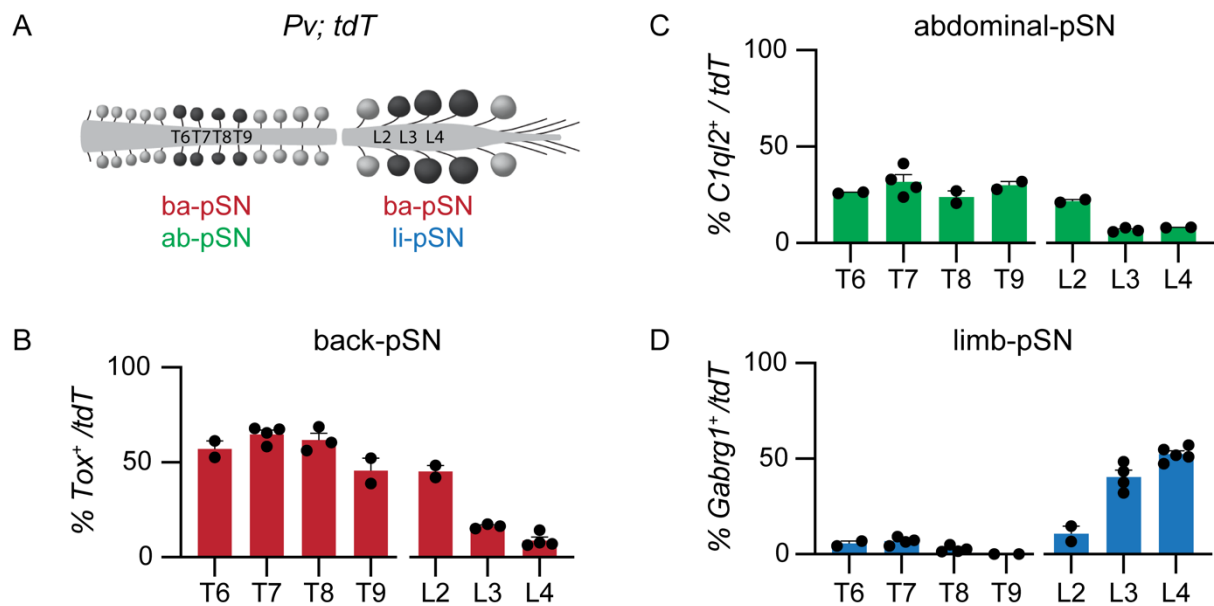


Figure 14. Rostro-caudal expression of marker genes for back, abdominal, and limb proprioceptors. (A) Illustration showing the main presence of muscle group specific proprioceptors at thoracic (back- and abdominal-pSN) and lumbar (back- and mainly limb-pSN) spinal levels. (B) Expression of *Tox* (ba-pSN), (C) *C1ql2* (ab-pSN), and (D) *Gabrg1* (li-pSN) in proprioceptors of single thoracic and lumbar DRG from p1 *Pv^{Cre}; tdT* mice (each point represents one animal, mean \pm SEM).

To directly link these molecular identities with muscle connectivity, we examined the expression of *Tox* (ba-pSN; C2) and *Gabrg1* (li-pSN; C3) in DRG of retrogradely labeled proprioceptors after cholera toxin B (CTB) injection into hindlimb (*gastrocnemius* (GS) and *tibialis anterior* (TA)) and back (*erector spinae* (ES)) muscles. First, to evaluate the injection specificity, we analyzed the position of labeled motor neurons. Only animals with correct labeled motor neurons (73) were used for further analysis of proprioceptors (Figure S5A). Second, we found that $\sim 82\%$ of ES proprioceptors (CTB⁺ and Pv⁺) express the ba-pSN marker *Tox* and $\sim 71\%$ of GS/TA proprioceptors show expression of the li-pSN marker *Gabrg1*

(Figures 15A and 15B), hence confirming the results of the anatomical defined single pSN transcriptome analysis.

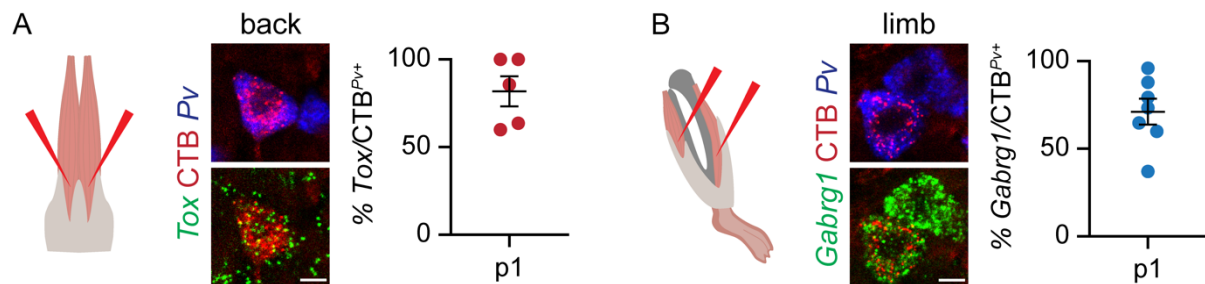


Figure 15. *Tox* and *Gabrg1* are specific for back and limb proprioceptors. (A) Expression of *Tox* and (B) *Gabrg1* in Pv^+ sensory neurons retrogradely labeled after cholera-toxin B (CTB) injection in back (*erector spinae* muscle, top) or hindlimb (*gastrocnemius* and *tibialis anterior* muscle, bottom) muscles of p4 wild-type mice (each point represents one animal, mean \pm SEM). Scale bar: 10 μ m.

5.4 Proprioceptor muscle-type identities emerge early in development

The presence of molecular signatures for ba-, ab-, and li-pSN at p1 led to the question of whether these genetic characteristics are already present earlier in development. We first performed a gene correlation analysis at p1. As expected, we could observe high correlation values defining each pSN muscle-type population (Figure 16A, left). The same analysis using our e15.5 dataset also shows the correlation of these gene signatures (Figure 16A, right), indicating the presence of molecular programs for proprioceptor muscle-type identities at early developmental stages. To evaluate these findings *in vivo*, we analyzed the gene expression of representative ba-pSN (*Tox*) and li-pSN (*Gabrg1*) in proprioceptors retrogradely labeled with Rhodamine-Dextran (RhD) from back or hindlimb muscles of e15.5 embryos (Figure 16B). Injection specificity was confirmed by the position of labeled MMC or LMC motor neurons (Figure S5B). In retrogradely labeled neurons from back muscles, *Tox* was found in ~87 % of ba-pSN. *Gabrg1* was expressed by ~67 % of RhD labeled li-pSN. These expression frequencies are comparable with those of early postnatal tracing experiments, which suggests that the expression of *Tox* and *Gabrg1* in proprioceptors is restricted according to their peripheral muscle-group target. In addition, these data indicate that particular genetic programs defining proprioceptor muscle-type identities arise early in development and remain active until early postnatal stages.

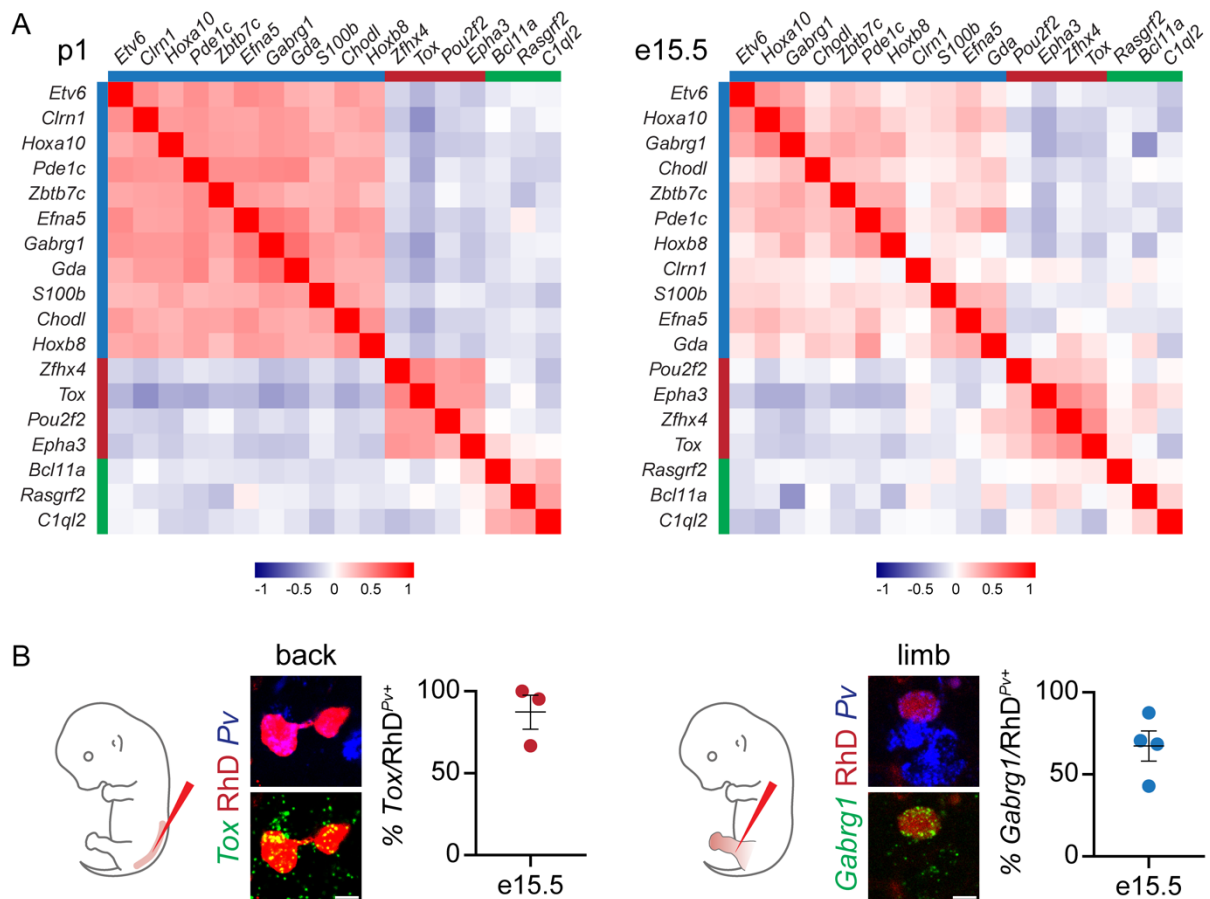


Figure 16. Signature genes of p1 back, abdominal, and limb proprioceptors are present at e15.5. (A) Heatmap representing pairwise gene-gene expression correlation values of li-pSN (blue bar), ba-pSN (red bar) and ab-pSN (green bar) signature genes at p1(left) and e15.5 (right). Scale: Pearson's r using log-counts. (B) Expression of *Tox* (ba-pSN) and *Gabrg1* (li-pSN) in Pv^+ sensory neurons after retrograde Rhodamine-Dextran labeling of e15.5 back (left) or hindlimb (right) muscles (each point represents one animal, mean \pm SEM). Scale bar: 10 μ m.

5.5 The presence of muscle spindle and Golgi-tendon organ signature genes

Recent studies published molecular markers for the three functional subtypes of proprioceptive sensory neurons - group Ia and II muscle spindles, as well as group Ib Golgi-tendon organs (38). We used these genes and performed correlation analyses to estimate their presence in our data sets, which could indicate whether muscle-type- or functional-signatures dominate at e15.5 and p1. At e15.5 we could not observe high correlation values and no clustering of marker genes representing one of the three subtypes (Figure 17, left). In contrast, we observed clusters of correlated genes representing group Ib and II proprioceptive sensory neurons in our p1 data set (Figure 17, right). For group II afferents, increased correlation values for *Camk4*, *Cdh13*, and *Heg1* could be detected. Elevated correlation values were also observed for *Itga2*, *Pou4f3*,

and *Pcdh17* representing group Ib afferents. Furthermore, a cluster comprising markers for group Ia and group II muscles spindles (*Hpse*, *Tpbgl*, *Calb1*, *Camk2n1*, *Nxph1*, *Tac1*) was detected in the p1 data set. The overall correlation values for pSN muscle-type markers were higher (Figure 16A) compared to receptor-type values (Figure 17) in our datasets. Together, this suggests that at embryonic and postnatal stages pSN muscle-type signatures are predominantly present compared to pSN receptor-type determinants.

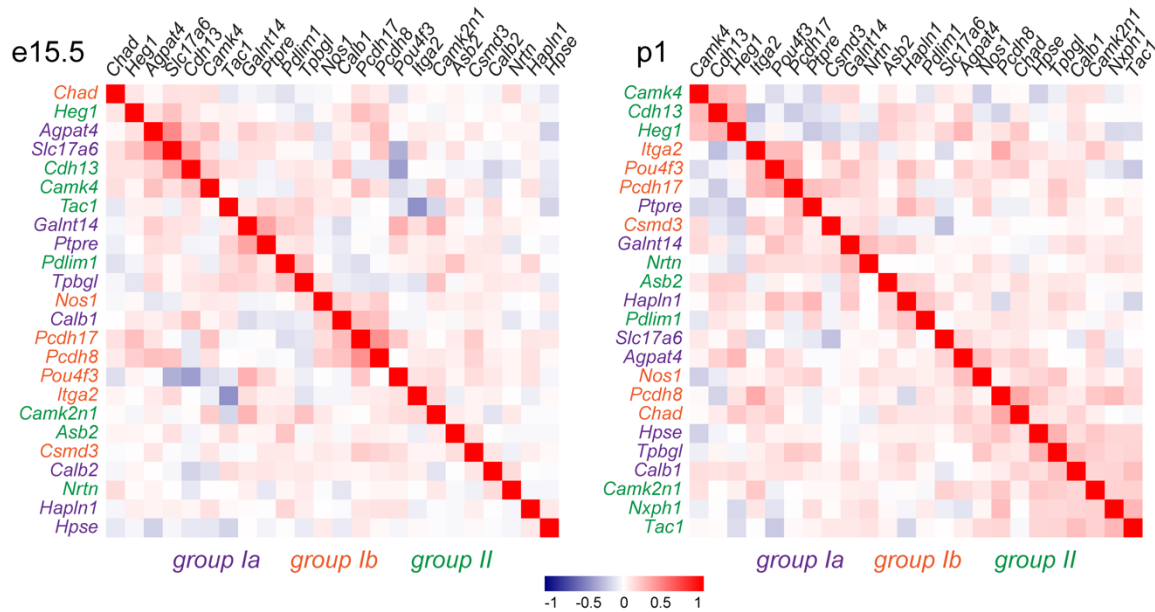


Figure 17. Presence of signature genes for group Ia, Ib, and II proprioceptor subtypes at e15.5 and p1. (A) Heatmap representing pairwise gene-gene expression correlation of recently published signature genes (38) for group Ia (violet), Ib (orange), and II (green) proprioceptive sensory neurons (functional subtypes) at p1(left) and e15.5 (right). Scale: Pearson's r using log-counts.

5.5 Distinct expression of ephrin/EphA in back and limb proprioceptors

The concept of proprioceptor muscle-type identities is based on their peripheral connectivity, which requires axon guidance processes directing pSN axons to their muscle targets early in development (91). Interestingly, we found several axon guidance molecules of the ephrin-A and EphA family expressed in distinct clusters at e15.5 and p1 (Figures 18A and 12J). In particular, the expression of *Efna5* and *Epha3* distinguishes li- and ba-pSN, respectively (Figure 18A). To validate these findings, we first performed *in situ* hybridizations by combining *Epha3* and *Efna5* probes in thoracic and lumbar DRG from *Pv^{Cre}; tdT* mice at e15.5 and p1. At both stages, *Epha3* was predominantly expressed in thoracic (e15.5 ~39 %, p1 ~60 %) and *Efna5* in lumbar (e15.5 ~40 %, p1 ~58 %) tdT⁺ neurons (Figure 18B).

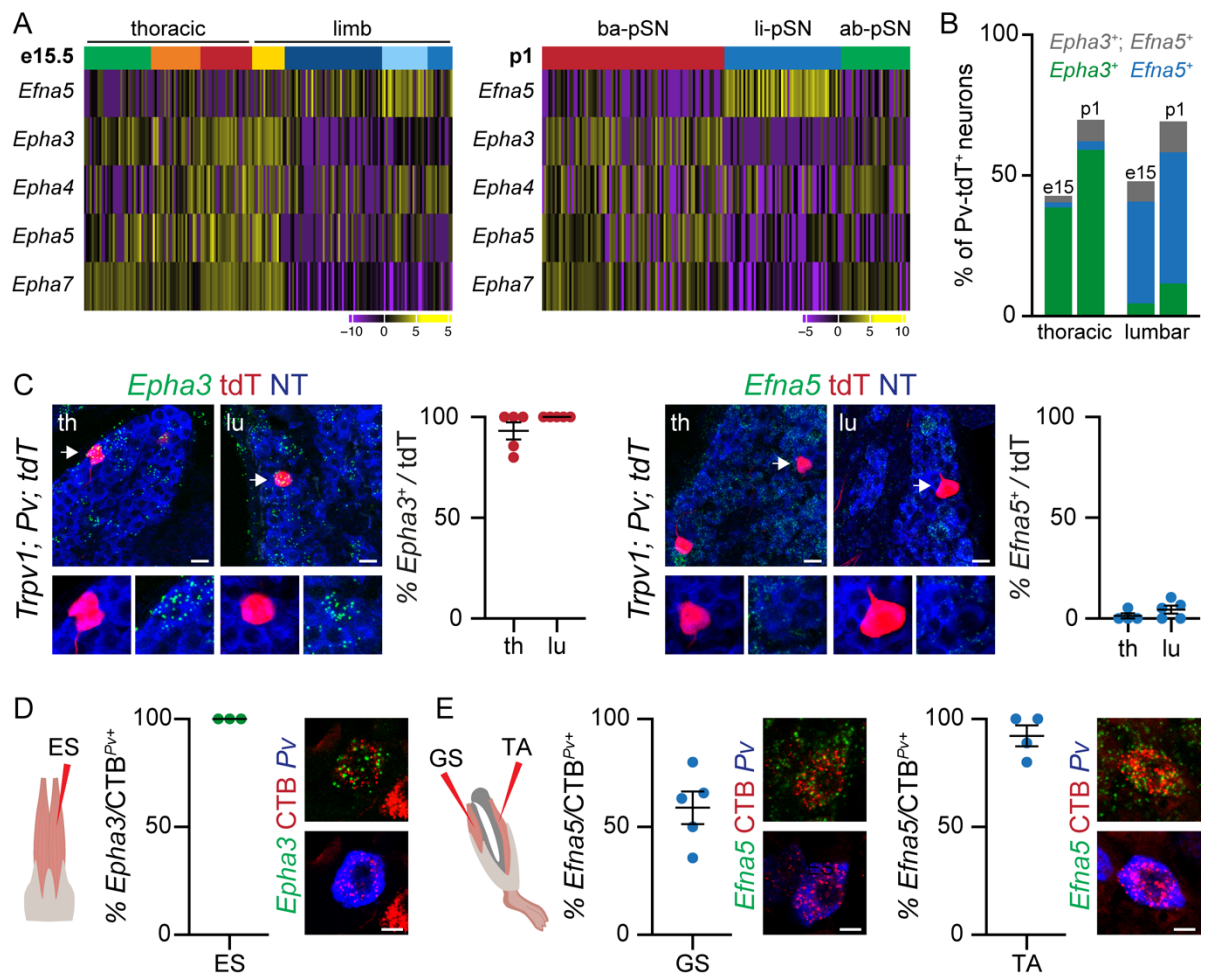


Figure 18. Distinct expression of EphA/ephrin-A in back and limb proprioceptors. (A) Heatmap representing differential expressed ephrin-A/EphA genes in e15.5 (left, clusters are arranged according to segmental origin) and p1 (right) proprioceptors. Scale: log-counts. (B) Percentage of *Epha3* (green), *Efna5* (blue) and *Epha3*, *Efna5* (gray) in tdT⁺ thoracic and lumbar DRG neurons of e15.5 and p1 *Pv^{Cre}; tdT* mice (n = DRG of 3 animals per age, mean). (C) Representative *in situ* hybridization images and quantification of *Epha3* (left) and *Efna5* (right) in tdT⁺ neurons labeling proprioceptors innervating back muscles in p1 *Trpv1^{Cre}; Pv^{Flp}; tdT* mice (each point represents one animal, mean ± SEM). Scale bar: 25 μm. (D) Expression of *Epha3* in Pv⁺ sensory neurons (*in situ* hybridization) retrogradely labeled after cholera-toxin B (CTB) injection into back (*erector spinae*) muscle and *Efna5* in CTB labeled pSN from (E) *gastrocnemius* (GS) and *tibialis anterior* (TA) muscle of p4 wild-type mice (each point represents one animal, mean ± SEM). Scale bar: 10 μm.

Additional expression analysis in ba-pSN using *Trpv1^{Cre}; Pv^{Flp}; tdT* mice showed expression of *Epha3* (thoracic ~93 %, lumbar ~100 %) in almost all tdT⁺ ba-pSN, whereas *Efna5* (thoracic ~1 %, lumbar ~4 %) was rarely found (Figure 18C). Lastly, we labeled retrogradely Pv⁺ sensory neurons by injecting CTB into ES, TA, and GS muscles and found *Epha3* expression in all CTB⁺/Pv⁺ ES-pSN while *Efna5* labeled ~59% of GS- and ~92% of TA-pSN (Figure 18D).

These data confirm *Epha3* and *Efna5* in addition to *Tox* and *Gabrg1* as molecular markers for ba-pSN and li-pSN, respectively.

Taken into account that ephrin-As and their receptors are involved in many axon guidance processes in the nervous systems (78), their presence in ba-pSN and li-pSN could imply that both molecules are involved in controlling the muscle target specificity of distinct proprioceptor subtypes. To test whether *Efna5* is involved in controlling li-pSN connectivity, we retrogradely labeled proprioceptors after CTB injections into TA and GS muscles of *Efna5*^{-/-} mice (Figures 19 and S6) (92).

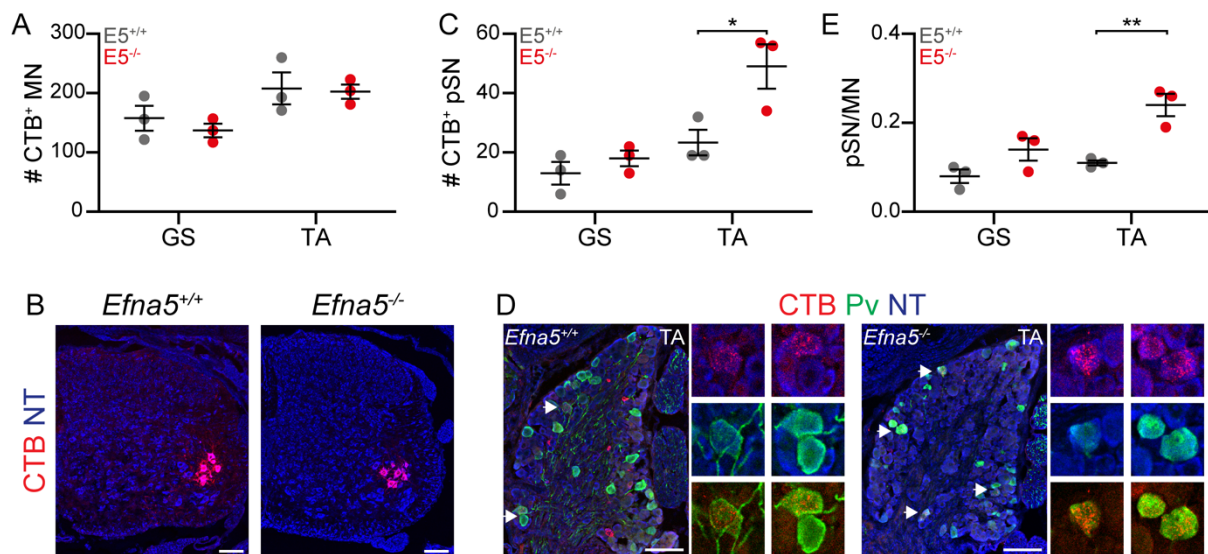


Figure 19. The absence of ephrin-A5 affects the targeting specificity of *Tibialis anterior* proprioceptors. (A) Quantification of retrogradely labeled motor neurons after CTB injection into the *gastrocnemius* (GS) and *tibialis anterior* (TA) muscle of p4 *Efna5*^{+/+} (gray) and *Efna5*^{-/-} (red) mice. (B) Representative images of motor neurons after retrograde CTB labeling from TA in of p4 *Efna5*^{+/+} (left) and *Efna5*^{-/-} (right) mice. Scale bar: 100 μ m. (C) Total number of retrogradely labeled Pv⁺/CTB⁺ proprioceptors after injection into GS and TA of p4 *Efna5*^{+/+} (gray) and *Efna5*^{-/-} (red) mice (each point represents one animal, mean \pm SEM, t-test, ns $p > 0.05$, * $p < 0.05$). (D) Representative images of Pv⁺/CTB⁺ pSN after retrograde CTB labeling from TA in p4 *Efna5*^{+/+} (left) and *Efna5*^{-/-} (right) mice. Scale bar: 100 μ m. (E) Ratio of Pv⁺/CTB⁺ labeled pSN per labeled motor neurons after CTB injection in GS and TA of p4 *Efna5*^{+/+} (gray) and *Efna5*^{-/-} (red) mice (each point represents one animal, mean \pm SEM, t-test, ns $p > 0.05$, ** $p < 0.01$).

To evaluate injection specificity and motor neuron connectivity, we analyzed the position (73, 93) and number of CTB labeled motor neurons in *Efna5*^{-/-} and *Efna5*^{+/+} mice and could not detect any differences (Figures 19A and 19B). We could observe a significant increase in proprioceptors innervating the TA, but not the GS muscle in *Efna5*^{-/-} mice (Figures 19C and 19D). Finally, we calculated the ratios of proprioceptors to motor neurons to account for

injection variability and could confirm the significant increase in TA proprioceptors (Figure 19E), which are characterized by *Efna5* expression (Figure 18E). In contrast, proprioceptors of the GS muscle are defined by partial expression of *Efna5* (Figure 18E) and show a minimal increase of pSN numbers in mice lacking *Efna5* (Figure 19E). Further analysis of central Pv^+ afferents at lumbar levels of *Efna5*^{-/-} and *Efna5*^{+/+} mice did not show differences in the overall projection patterns and afferent densities (Figure 20). Together, these data indicate a role of molecules belonging to the ephrin family in controlling the muscle connectivity of proprioceptors.

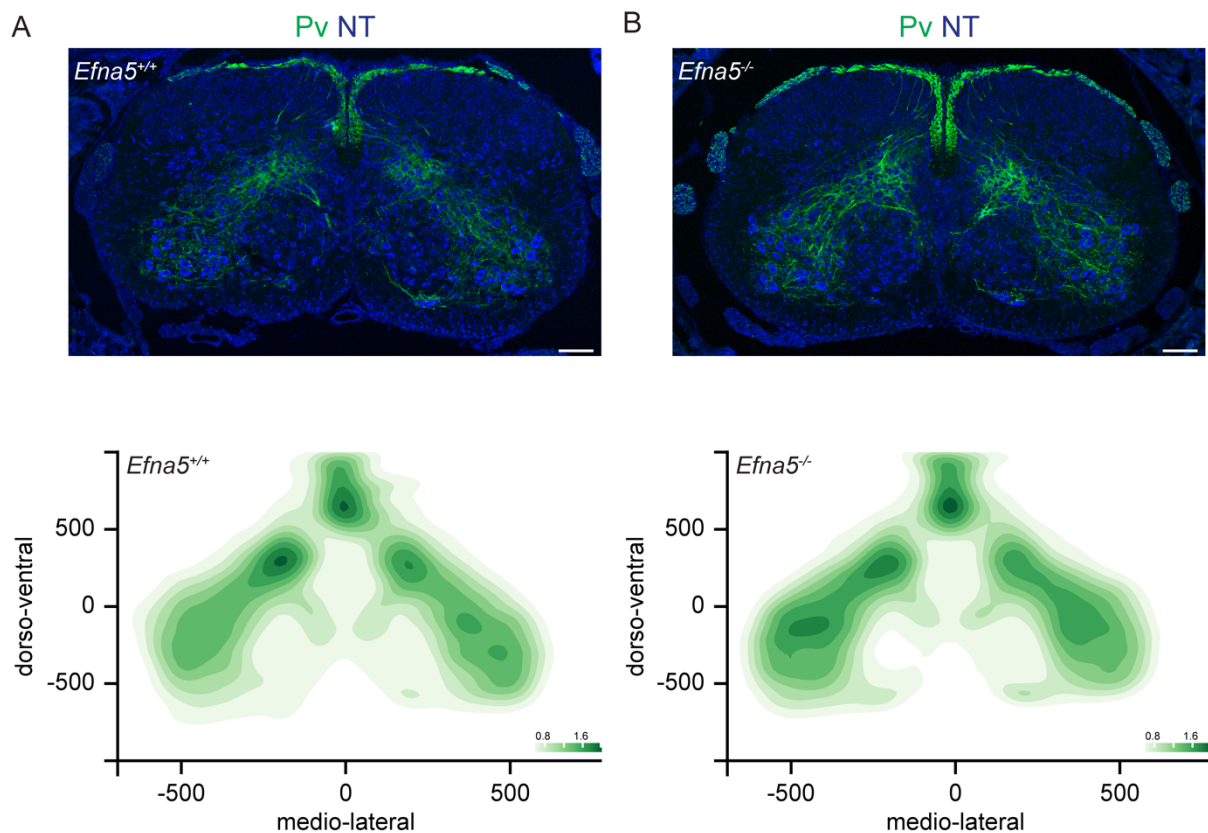


Figure 20. Density analysis of central parvalbumin⁺ afferents in *Efna5*^{+/+} and *Efna5*^{-/-} mice. (A) Representative images (top) and density plots (bottom) of central Pv^+ afferents at lumbar levels of p4 *Efna5*^{+/+} and (B) *Efna5*^{-/-} mice. For each density plot, 5 lumbar sections of 3 animals per genotype were analyzed using the Imaris spot function.

5.6 Expression of *Efna5* in the lumbar spinal cord

As sensory neurons track along motor neuron axons (91), we also examined the expression of *Efna5* in MMC and LMC motor neurons in lumbar spinal cord sections of wild-type p1 mice. Using *in situ* hybridization, we could detect different levels of *Efna5* expression within LMC

motor neurons (Figures 21A and 21A'). No expression of *Efna5* was observed in MMC motor neurons (Figure 21A'')

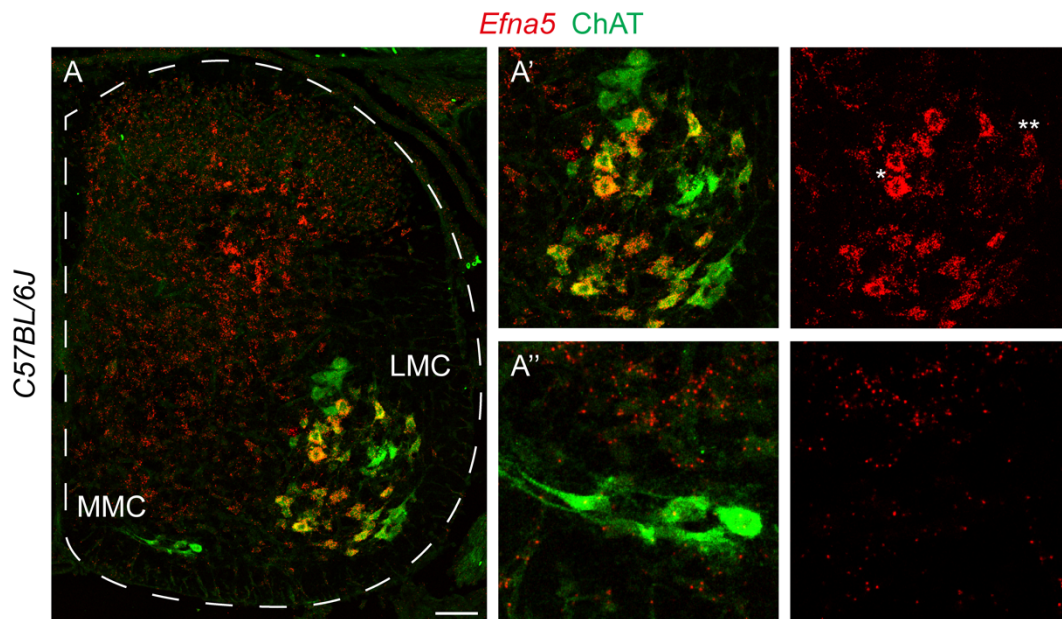


Figure 21. Expression of *Efna5* in lumbar motor neurons. (A) Representative images of a lumbar spinal cord section showing immunostained ChAT⁺ MMC and LMC motor neurons and the expression of *Efna5* (*in situ* hybridization) from a p1 wild-type mouse. (A') Lumbar MMC motor neurons do not show *Efna5* expression. (A'') LMC motor neurons show different levels (*high, **low) of *Efna5* expression. Scale bar: 100 μ m.

5.7 Expression of *Gabrg1* and *Efna5* in lumbar proprioceptors

The independent validation of *Gabrg1* and *Efna5* as li-pSN markers raised the question of to what extent both markers are expressed in lumbar Pv⁺ sensory neurons, which are mainly li-pSN, but also comprise ba-pSN and ~10-15% low-threshold mechanoreceptors (45). Therefore, we performed *in situ* hybridizations by combining *Gabrg1* and *Efna5* on lumbar (L3/L4) DRG sections of p1 *Pv^{Cre}; tdT* mice to estimate their expression patterns (Figure 22). *Gabrg1* expression was found in ~8 %, while *Efna5* was expressed in ~27 % of tdT⁺ neurons. Co-expression of *Gabrg1* and *Efna5* was found in ~38 % of tdT⁺ neurons. Together, the expression of both genes (single and double) covered ~74 % of lumbar tdT⁺ sensory neurons in p1 *Pv^{Cre}; tdT* mice (Figures 22A and 22B), suggesting that *Gabrg1* and *Efna5* could account for most of the hindlimb-proprioceptors.

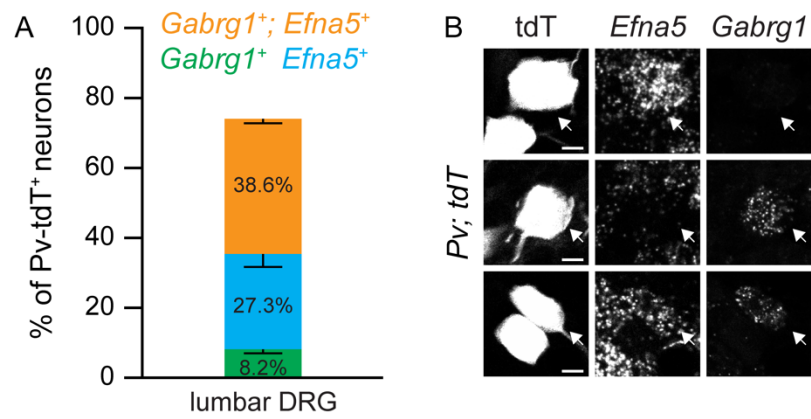


Figure 22. Combined expression of *Gabrg1* and *Efna5* in lumbar proprioceptors. (A) Percentage of *Gabrg1* (green), *Efna5* (blue), and *Gabrg1*; *Efna5* (orange) in tdT⁺ lumbar DRG neurons of p1 *Pv^{Cre}*; *tdT* mice (n = L3/L4 DRG from 4 animals, mean ± SEM). (B) Representative images of *Efna5*⁺; tdT⁺ (top), *Gabrg1*⁺; tdT⁺ (middle) and *Efna5*⁺; *Gabrg1*⁺; tdT⁺ (bottom) neurons from p1 *Pv^{Cre}*; *tdT* mice. Scale bar: 10 μm.

6. Discussion

Single-cell transcriptomic efforts have uncovered a great variety of molecular distinct somatosensory neuron subtypes (54, 94). Among these identified classes, proprioceptive sensory neurons represent a homogenous population, while their functional heterogeneity suggests at least three proprioceptor subtypes. Indeed, recent studies uncovered molecular correlates for the three major proprioceptor groups - Ia, Ib, and II, but the molecular diversity among them implies additional subgroups (38, 53). As proprioceptors innervate muscles with distinct anatomical identities (e.g., limb or axial muscles) and different biomechanical properties (e.g., flexor or extensor), they can be further partitioned into subsets according to the muscle they innervate. Nevertheless, very little is known about molecular determinants defining proprioceptor muscle-type identities. Therefore, in the present study, we devised a single-cell transcriptomic approach that takes advantage of the topographic organization of the proprioceptive system to reveal molecular profiles of proprioceptors defined by their connectivity to different muscle groups. We identified and validated signature genes for proprioceptor subtypes innervating back, abdominal, and hindlimb muscles and found that these molecular distinctions emerge at early developmental stages. Furthermore, we evaluated the role of the li-pSN marker *Efna5* in targeting hindlimb muscles and showed that its absence leads to an increased innervation of proprioceptors in the *Tibialis anterior* muscle.

6.1 Early expression of *Trpv1* labels a subset of back proprioceptors

Proprioceptive sensory neurons establish first connections with their muscle target in the periphery, which is achieved by embryonic day 15.5 and send later axon collaterals to their synaptic partners in the spinal cord. Based on the connectivity and topographic organization of proprioceptors and their putative cardinal muscle groups (back, abdominal, and hindlimb muscle), we separately analyzed the transcriptome of thoracic and lumbar proprioceptive sensory neurons at e15.5. By prediction we expected to identify clusters comprising neurons of lumbar origin as potential hindlimb-pSN, clusters consisting of lumbar and thoracic neurons as likely ba-pSN and clusters harboring only neurons from thoracic DRG as possible ab-pSN. To genetically label embryonic proprioceptors, we used a mouse line expressing tdT under the control of the parvalbumin promoter. The initial cluster analysis revealed not only proprioceptors but also mechanoreceptors. As a small population of low-threshold

mechanoreceptors expresses parvalbumin, it is likely that these neurons were also isolated, which could explain the appearance of mechanoreceptors in our analysis (27).

Next, with the focus on the proprioceptor clusters, we identified one cluster comprising neurons with an almost equal contribution from lumbar and thoracic proprioceptors, suggesting them as ba-pSN. Interestingly, these neurons specifically expressed *Trpv1*, a non-selective cation channel and a well-characterized marker for nociceptive/thermosensitive (heat) sensory neurons (86, 87, 95). Intrigued by this finding and the fact that *Trpv1* has not been reported as a marker of proprioceptive sensory neurons, we could confirm the expression of *Trpv1* in embryonic proprioceptors (*Runx3*⁺, *Pv*⁺) and that the expression of *Trpv1* and *Pv* in sensory neurons allows genetic labeling of proprioceptive sensory neurons whose central and peripheral connectivity is in agreement with ba-pSN identity. The interesting observation of *Trpv1* expression in *Pv*⁺ sensory neurons, although both are well-known markers for different classes of sensory neurons (14, 15, 27, 86), raises the question of what could be the potential role of *Trpv1* among proprioceptors. In this study, we detected *Trpv1* only at embryonic stages but not at early postnatal stages by scRNAseq (p1) and *in situ* hybridization (data not shown) in proprioceptive sensory neurons, implying a transient *Trpv1* expression in ba-pSN. In addition, the labeling efficiency of presynaptic puncta juxtaposed to MMC motor neurons as well as receptor-organs in the periphery by *tdT*⁺ indicate that *Trpv1* expression is restricted to a subset of ba-pSN. Recently, a single-cell transcriptomic study suggested that sensory neuron subclasses (including proprioceptors) transition from a transcriptionally unspecialized state to a transcriptionally distinct state depending on signaling cues from their intermediate or final peripheral target (54, 55). Although the *Trpv1* expression in proprioceptors would need to be characterized in more detail at different embryonic and postnatal stages, the current observations could be a consequence of transcriptional specification in ba-pSN when establishing their muscle connectivity.

Similar to our *Trpv1* observation, Oliver et al., 2021 (38) found *Tac1* (Tachykinin 1), a gene encoding the neuropeptides Neurokinin A and Substance P, which is a main characteristic of nociceptive sensory neurons identity, in group II pSN innervating muscle spindles (96). The biological role or function of both well-known nociceptive genes, *Trpv1* and *Tac1*, in proprioceptors remains unknown, but further molecular investigations of these markers could be helpful to gain more information on the development and/or function of proprioceptors.

6.2 Molecular signatures defining proprioceptor muscle-type identities

Intrigued by the unique opportunity to genetically label specifically ba-pSN, we devised another single-cell transcriptomic approach at p1. We identified three clusters, which could be defined as ba-pSN, ab-pSN, and li-pSN. Among many differentially expressed genes, we validated and characterized *Tox* and *Epha3* as signature genes of ba-pSN, *Efna5*, and *Gabrg1* as markers of li-pSN, and *C1ql2* for ab-pSN. Markers for back and abdominal pSN (*Tox* and *C1ql2*) together (~88 %) account for almost all thoracic proprioceptors, suggesting that our approach comprehensively captures neurons innervating trunk muscles. To prove this, a combined *in situ* hybridization with *Tox* and *C1ql2* needs to be performed, which was not possible due to the unavailability of both probes for distinct detection channels. The combined *in situ* hybridization of the li-pSN markers *Gabrg1* and *Efna5* revealed that both markers (single or co-expressed) cover together ~78 % of lumbar proprioceptors labeled by *Pv^{Cre}; tdT* mice. Taken into account the percentage of ba-pSN (~10 %, Figure 9) among lumbar proprioceptors and that a subset of low threshold mechanoreceptors (10-15 %, (45)) is also labeled by *Pv^{Cre}; tdT* mice in lumbar DRG, *Gabrg1* and *Efna5* together could be assumed to label almost all of li-pSN. However, to determine whether these combinations are expressed exclusively in proprioceptors and not by low-threshold mechanoreceptors, quadruple *in situ* hybridization for *Runx3*, *Pv*, *Efna5*, and *Gabrg1* is needed to ensure proprioceptor specificity. Our findings further imply that combinations of multiple molecules are required to represent proprioceptors of the whole hindlimb compartment, comprising 39 individual muscles (65). Therefore, it is feasible that our li-pSN markers already capture features of more fine-grained hindlimb proprioceptor identities, which could be of anatomical (e.g., dorsal vs. ventral, proximo vs. distal) and/or functional (e.g., synergist vs. antagonist, MS vs. GTO) nature.

The expression of *Gabrg1* in lumbar, but rarely if ever in thoracic proprioceptors, is in agreement with a recent study by Lee et al., 2012 (97) showing that *Gabrg1* is predominantly expressed in caudal cervical (C5-C8) and lumbar (L3-L5) DRG, spinal segments known to innervate distal limb muscles. Indeed, we could show that *Gabrg1* is expressed by proprioceptors innervating the distal hindlimb muscles *Tibialis anterior* and *Gastrocnemius*. The mechanisms controlling the difference in *Gabrg1* expression among proprioceptors along the rostro-caudal axis are unknown. Interestingly, Lee et al., 2012 (97) show differences in *Gabrg1* expression upon elimination or overexpression of NT3, suggesting that *Gabrg1* expression is regulated by NT3 signaling. Early proprioceptor survival and differentiation depend on TrkC/NT3 signaling, which induces the transcription factor Etv1, whose genetic

inactivation causes the termination of central pSN axons in ectopic dorsal positions in the intermediate spinal cord (24, 25). Investigating the precise role of *Etv1*, Nooij et al., 2013 (27) found that the survival of proprioceptors innervating abdominal and axial muscles depends almost entirely on *Etv1*, while hindlimb proprioceptors show a muscle-by-muscle *Etv1* dependency. Thereby and most strikingly, it was shown that the level of NT3 expression in individual muscles predicts the *Etv1* dependence of proprioceptors. Therefore, different expression levels of NT3 by individual hindlimb muscles could serve as a potential explanation for the expression of *Gabrg1* in subsets of hindlimb proprioceptors and differences in *Gabrg1* expression levels among them due to its NT3 sensitivity (Figures 13 and 15).

Animals perform skilled movements with exquisite specificity, which relies on the fact that inhibitory interneurons modulate the excitatory input to motor neurons, allowing precise spinal motor output (60). The majority of inhibitory interneurons form polysynaptic connections with motor or premotor neurons. In addition, a small subset of GABAergic interneurons synapse through axo-axonic interactions with sensory afferent terminals controlling sensory-motor drive through presynaptic inhibition, which in turn requires postsynaptic GABAA receptors (98). *Gabrg1* encodes for a GABAA receptors subunit. Considering that GABAA receptors are composed of different subunits influencing the channel properties of different dynamics and magnitude, *Gabrg1* might play a distinguished role in presynaptic inhibition in subsets of hindlimb innervating proprioceptors, allowing them to scale their sensory feedback. As genetic tools to access *Gabrg1* expressing neurons are lacking, it might be of interest to generate transgenic mouse lines to dissect central circuits connected with *Gabrg1*⁺ li-pSN and investigate the function of *Gabrg1* in li-pSN. This will also provide insights into the function of presynaptic inhibition in processing hindlimb specific sensory information (97, 99).

For proprioceptors innervating back muscles, we identified and validated *Tox* as a marker gene, which is a transcription factor belonging to the high mobility group box (HMG-box) superfamily (100). Although *Tox* is studied primarily in the context of the immune system, a recent single-cell transcriptomic study of proprioceptors by Wu et al., 2021 (53, 101) suggests *Tox* as a marker for a subset of group II proprioceptors. In agreement with our data, Wu et al., 2021 found *Tox* expression predominantly in proprioceptors at thoracic levels and with lower abundances at lumbar and cervical levels. In contrast to Wu et al., 2021 we found *Tox* expressed in proprioceptors innervating back muscles comprising group Ia, Ib, and II afferents using an intersectional mouse line *Trpv1*^{Cre}; *Pv*^{Flp}; *tdT* (Figure 10). This suggests *Tox* as a marker for a proprioceptor muscle-type population (ba-pSN), which includes functional

subtype aspects of group II afferents at later postnatal stages. As an additional interesting observation, we found *Tox2*, belonging to the same family of transcription factors as *Tox* (100), differentially expressed in a cluster with back proprioceptor identity (pC6, *Trpv1*⁺, Figure 8D). Although the functional roles of these transcription factors are not investigated in proprioceptors, a study by Artegiani et al., 2015 (102) could show that *Tox* plays a role in mammalian corticogenesis, whereby *Tox* expression was observed in neural stem cells during proliferation, down-regulated during differentiation and re-induced in subsets of newborn neurons. Further investigation of *Tox* downstream targets revealed enrichments in GO terms related to neurogenesis, axogenesis, CNS development, and transcription regulation. Experimental validation by overexpression of *Tox* in cortical progenitors caused inhibition of their differentiation and affected neural specification as well as neurite outgrowth. These interesting findings by Artegiani et al., 2015 (102) highlight the importance of *Tox* as a transcriptional regulator in neural development and raise the question of whether a similar function can be attributed to *Tox* in proprioceptors, especially in controlling the identity and connectivity of ba-pSN. Thereby it would be interesting to test whether the expression of *Tox* in non-ba-pSN during development can change their identity towards ba-pSN.

Furthermore, we validated *C1ql2* as a marker for the third identified cluster, which was defined as ab-pSN. To confirm that *C1ql2* is specific for ab-pSN, retrograde labeling from abdominal muscles and additional *in situ* hybridizations of *C1ql2* are needed. However, abdominal muscles are very thin, exacerbating the precise injection of retrograde tracers. In contrast to *Tox* and *Gabrg1*, which also showed expression in other DRG sensory neurons, *C1ql2* was found to be exclusively expressed in *Pv*⁺ and genetically labeled *Pv*⁺ DRG neurons. However, not much is known about the function of *C1ql2* in neurons. An early study proposes that *C1ql* proteins are involved in synapse formation and/or maintenance (103). More recently, Matsuda et al., 2016 (104) demonstrated that *C1ql2* and *C1ql3* are extracellular organizers in the hippocampus and needed to recruit functional postsynaptic kainite-type glutamate receptors to CA3 pyramidal neurons. As *C1ql2* is also differentially expressed at embryonic stage e15.5 (pC1) and is expressed specifically by *Pv*⁺ sensory neurons at later stages (p1) further research should be considered to first evaluate in more detail whether *C1ql2* is indeed specific for ab-pSN and second if it is involved in controlling their connectivity through synapse formation and/or maturation. Taken together, the validated markers for each subset of proprioceptors innervating distinct muscle groups provide a great entry point for further studies to unravel pSN subtype identities.

Aside from the single validated markers, our bioinformatical analysis implies that several genes are required to define a individual proprioceptor muscle-type population. The same was reported in single-cell transcriptomics studies to reveal molecular markers for the three pSN receptor-types (group Ia, Ib, II) (38, 53). Interestingly, Wu et al. 2021 (53) found markers defining subtypes for each of the three receptor-types and proposed, based on their segmental (cervical, thoracic, lumbar) expression patterns in proprioceptors, that they might correspond to different muscle groups (e.g., trunk and limb). Taken into account the revealed markers for group Ia, Ib, II proprioceptors by Wu et al. 2021 (53) and Oliver et al. 2021 (38) as well as the work by Poliak et al., 2016 (81) identifying markers for proprioceptors innervating the distal-dorsal (*Cdh13*) and distal-ventral (*Crtac1*) hindlimb compartments, further analysis will be required to resolve the molecular complexity of each pSN subtype and to identify molecules, which correlate with proprioceptor identity at a single muscle and/or functional level. Consequently, it will provide insights into biophysical, anatomical, and physiological features of proprioceptive sensory neurons.

6.3 Developmental emergence of proprioceptor subtypes

During development, proprioceptive sensory neurons acquire features defining their functional properties based on the muscle and nascent end-organ receptor they innervate. First, proprioceptive sensory neuron axons progress towards their peripheral target and generate mechanoreceptive end-organs with precise ratios and distributions according to the biomechanical requirements of the innervated muscle (105). Afterwards, proprioceptive afferents establish connections with multiple neural targets in the central nervous system to relay sensory feedback to motor circuits controlling the activity of relevant muscles (11, 17). Therefore, we ask whether the revealed early postnatal molecular signatures for each proprioceptor muscle-type population are already present at embryonic stage e15.5. We found high correlations of genes representing back, abdominal and limb pSN in our datasets at p1 and e15. In addition, we confirmed the expression of *Tox* in ba-pSN and *Gabrg1* in li-pSN after retrograde labeling from back and hindlimb muscles at e15.5. These findings suggest a model where distinct early embryonic programs control the peripheral and central connectivity of proprioceptive sensory neurons, followed by a postnatal refinement, which includes aspects of receptor-organ characteristics (MS and GTO). In support of this model, Oliver et al., 2021 (38) reported that transcriptional differences between MS and GTO could first be determined at early postnatal stages (p0 - p12), which was based on a correlation analysis of adult determined

signatures with dataset acquired at e14, p0 and p12. In addition, Wu et al., 2021 (53) found similar genes expressed at early postnatal and adult stages labeling MS and GTO and reported transcriptomic discrepancies compared to embryonic profiles. Both studies report the absence of transcriptomic lineage relationships of either MS and GTO between embryonic and postnatal stages, which is in agreement with our results (Figure 17). It remains to be investigated what concrete underlying programs control the muscle-type or receptor-type identity of proprioceptors during their development and maturation. To tackle this question, a metanalysis of already existing transcriptomic datasets of single proprioceptors from embryonic, early postnatal, and adult stages (38, 53, 54) could be used to analyze developmental trajectories of proprioceptors and to reveal molecular key features defining pSN muscle-type and receptor-type lineages. Thereby the knowledge of the already identified muscle-type (this study) marker genes can be used to investigate receptor-type features within a distinct pSN muscle-type population.

In addition to intrinsic determinants, previous research on proprioceptor survival and maturation provided evidence that signal cues from developing muscles also play an essential role in proprioceptor development. Poliak et al., 2016 (81) highlighted their importance by showing that *Cdh13*, a marker of proprioceptors innervating the dorsal limb mesenchyme, is no longer expressed when changing the dorsal limb mesenchyme identity into a ventral one. Work by Tourtellotte et al., 1998 and 2001 (15, 19) reported that the absence of *Egr3*, a transcription factor expressed in developing intrafusal muscle fibers, leads to an erosion of muscle spindles at postnatal stages. Therefore, an analysis taken in account known interactions of molecules present in pSN subtypes and muscles could be beneficial to understand how pSN subtypes achieve their distinct peripheral muscle connectivity and receptor (MS, GTO) emergence.

6.4 Ephrin-A signaling controls muscle-target specificity of proprioceptors

Spinal sensory-motor circuits rely on the exquisite connectivity of proprioceptors with distinct muscles in the periphery and respective synaptic partners in the central nervous system to execute coordinated movements. This target specificity requires precise navigation of axons. In our study, we found *Efna5* and four EphA receptors (*EphA3*, *EphA4*, *EphA5*, and *EphA7*), which are well-known axon guidance molecules in the nervous system (78, 79), differentially expressed by clusters assigned to either limb or axial projecting proprioceptors at embryonic and early postnatal stages. In particular, we validated *Epha3* as a ba-pSN marker and *Efna5* as

a marker for a subset of limb innervating proprioceptors. Interestingly, the absence of *Efna5* led to an increase in the innervation of proprioceptive sensory neurons in the *Tibialis anterior* muscle but did not affect the pSN innervation of the *Gastrocnemius*, suggesting that *Efna5* might play a role in distinct pSN-hindlimb muscle connectivity. This observation also implies that *Efna5* might be part of a repulsive mechanism that prevents aberrant innervation of limb muscles. In this study, we used a constitutive *Efna5* knock-out mouse model, which causes systemic loss of *Efna5*. Therefore, the absence of *Efna5* in other cells or tissues, especially motor neurons and the hindlimb mesenchyme, can also affect the observed targeting phenotype (91, 93).

Ephrin-A/EphA signaling plays an important role in navigating motor neuron axons either to the dorsal or ventral half of the limb mesenchyme and could influence the muscle by muscle dependence of proprioceptive sensory neuron axons innervation specificity (93, 106, 107). For example, elimination of *Efna2* and *Efna5* causes a partial misrouting of lateral LMC motor neuron axons into the ventral instead of the dorsal limb mesenchyme. Wang et al., 2012 (91) propose that nascent ephrin-A⁺ sensory axons track along EphA⁺ motor neuron axons en route to their peripheral target. Elimination of *Epha3/4* in motor neurons causes re-routing of dorsal projecting nerves towards ventral targets at thoracic levels. Furthermore, Wang et al. show that reducing *Efna2* and/or *Efna5* levels in double heterozygous *Epha3/4* mice triggers the loss of dorsal sensory nerves. Based on our experiments, neither MMC motor neurons nor ba-pSN express *Efna5*. In contrast, many li-pSN and LMC motor neurons do express *Efna5*. Considering that *Efna5* acts as a repulsive cue, the constitutive elimination of *Efna5* might abolish repulsive interactions and allow other proprioceptive sensory axons, for example, axial-pSN, to track along LMC motor neuron axons en route to their hindlimb muscle target, causing an increase of proprioceptors innervating the *Tibialis anterior* muscle. In addition, the unaffected pSN innervation of the *Gastrocnemius* in *Efna5*^{-/-} mice favors the hypothesis that misrouted axial proprioceptors are responsible for the observed TA-pSN phenotype and not other li-pSN. Our observation could also imply that different molecular programs are used to control the connectivity between proprioceptive sensory neurons and individual hindlimb muscles. Because of the intricacy of the ephrin-Eph signaling (78), future studies are needed to dissect its molecular logic controlling the guidance of proprioceptors to their specific muscle targets. Thereby conditional knock-out mouse lines should be used to specifically remove EphAs and/or ephrin-As from distinct neuronal populations.

7. Relevance and outlook

Proprioceptive sensory neurons play a critical role in controlling body posture and coordinated movements. Genetic perturbations of proprioceptors result in severe adaptive motor control deficits (49). However, it is still not well understood how proprioceptive feedback from distinct muscles and the three receptor subtypes is integrated into motor circuits to adjust motor output (60, 108). This is mainly due to the unavailability of genetic tools allowing access to concrete subtypes of proprioceptors based on the muscle or receptor they innervate. In this study, we identified distinct molecular markers for back, abdominal, and hindlimb proprioceptors. Those findings will allow the generation of a genetic toolbox that can be used to further dissect the diversity of proprioceptive sensory neurons. Furthermore, the ability to genetically label and manipulate distinct proprioceptor subtypes will allow us to study the function of proprioceptive feedback circuits in relation to the biomechanical properties of individual muscles in motor control.

In addition, we could show that molecular signatures of proprioceptors innervating specific muscle groups are present early in development and are maintained until early postnatal stages. In agreement with other studies, it implies that molecular programs defining group Ia, Ib, and II afferents arise at postnatal stages (38, 53). However, the exact underlying molecular mechanisms and their temporal activity are unknown. As most muscles contain all three receptor-types, future investigations of muscle specific proprioceptor subtypes will give insights into discrete molecular programs controlling the development of muscle spindles and Golgi-tendon organs.

8. References

1. S. C. Koch, D. Acton, M. Goulding, Spinal Circuits for Touch, Pain, and Itch. *Annu Rev Physiol.* 80, 189–217 (2018).
2. E. R. Kandel, J. H. Schwartz, T. M. Jessell, S. A. Siegelbaum, A. J. Hudspeth, *Principles of neural science* (McGraw-Hill, New York, 5th ed., 2013).
3. Principles of Neural Science, Fifth Edition | AccessNeurology | McGraw Hill Medical, (available at <https://neurology.mhmedical.com/book.aspx?bookID=1049>).
4. V. E. Abaira, D. D. Ginty, The Sensory Neurons of Touch. *Neuron.* 79, 618–639 (2013).
5. F. Lallemand, P. Ernfors, Molecular interactions underlying the specification of sensory neurons. *Trends in Neurosciences.* 35 (2012), pp. 373–381.
6. J. C. Tuthill, E. Azim, Proprioception. *Current Biology.* 28, R194–R203 (2018).
7. J. C. Kasemeier-Kulesa, P. M. Kulesa, F. Lefcort, Imaging neural crest cell dynamics during formation of dorsal root ganglia and sympathetic ganglia. *Development.* 132, 235–245 (2005).
8. Q. Ma, C. Fode, F. Guillemot, D. J. Anderson, NEUROGENIN1 and NEUROGENIN2 control two distinct waves of neurogenesis in developing dorsal root ganglia. *Genes Dev.* 13, 1717–1728 (1999).
9. S. Ventéo, S. Desiderio, P. Cabochette, A. Deslys, P. Carroll, A. Pattyn, Neurog2 Deficiency Uncovers a Critical Period of Cell Fate Plasticity and Vulnerability among Neural-Crest-Derived Somatosensory Progenitors. *Cell Reports.* 29, 2953-2960.e2 (2019).
10. F. Marmigère, P. Ernfors, Specification and connectivity of neuronal subtypes in the sensory lineage. *Nature Reviews Neuroscience.* 8, 114–127 (2007).
11. A. I. Chen, J. C. De Nooij, T. M. Jessell, Graded activity of transcription factor Runx3 specifies the laminar termination pattern of sensory axons in the developing spinal cord. *Neuron.* 49, 395–408 (2006).

12. I. Kramer, M. Sigrist, J. C. de Nooij, I. Taniuchi, T. M. Jessell, S. Arber, A Role for Runx Transcription Factor Signaling in Dorsal Root Ganglion Sensory Neuron Diversification. *Neuron*. 49, 379–393 (2006).
13. Y. Wang, H. Wu, P. Fontanet, S. Codeluppi, N. Akkuratova, C. Petitpré, Y. Xue-Franzén, K. Niederreither, A. Sharma, F. Da Silva, G. Comai, G. Agirman, D. Palumberi, S. Linnarsson, I. Adameyko, A. Moqrich, A. Schedl, G. La Manno, S. Hadjab, F. Lallemand, A cell fitness selection model for neuronal survival during development. *Nat Commun*. 10, 4137 (2019).
14. S. Hippenmeyer, N. A. Shneider, C. Birchmeier, S. J. Burden, T. M. Jessell, S. Arber, A Role for Neuregulin1 Signaling in Muscle Spindle Differentiation. *Neuron*. 36, 1035–1049 (2002).
15. W. G. Tourtellotte, J. Milbrandt, Sensory ataxia and muscle spindle agenesis in mice lacking the transcription factor Egr3. *Nature Genetics*. 20, 87–91 (1998).
16. J. C. V. M. Copray, I. J. Mantingh-Otter, N. Brouwer, Expression of calcium-binding proteins in the neurotrophin-3-dependent subpopulation of rat embryonic dorsal root ganglion cells in culture. *Developmental Brain Research*. 81, 57–65 (1994).
17. S. C. Mears, E. Frank, Formation of Specific Monosynaptic Connections between Muscle Spindle Afferents and Motoneurons in the Mouse. *J. Neurosci*. 17, 3128–3135 (1997).
18. I. Fariñas, G. A. Wilkinson, C. Backus, L. F. Reichardt, A. Patapoutian, Characterization of Neurotrophin and Trk Receptor Functions in Developing Sensory Ganglia: Direct NT-3 Activation of TrkB Neurons In Vivo. *Neuron*. 21, 325–334 (1998).
19. W. G. Tourtellotte, C. Keller-Peck, J. Milbrandt, J. Kucera, The Transcription Factor Egr3 Modulates Sensory Axon–Myotube Interactions during Muscle Spindle Morphogenesis. *Developmental Biology*. 232, 388–399 (2001).
20. S. Ozaki, W. D. Snider, Initial trajectories of sensory axons toward laminar targets in the developing mouse spinal cord. *J Comp Neurol*. 380, 215–229 (1997).
21. N. Zampieri, J. C. de Nooij, Regulating muscle spindle and Golgi tendon organ proprioceptor phenotypes. *Current Opinion in Physiology*. 19, 204–210 (2021).

22. J. L. Shadrach, J. Gomez-Frittelli, J. A. Kaltschmidt, Proprioception revisited: where do we stand? *Current Opinion in Physiology*. 21, 23–28 (2021).
23. Z. Wang, L. Y. Li, M. D. Taylor, D. E. Wright, E. Frank, Prenatal exposure to elevated NT3 disrupts synaptic selectivity in the spinal cord. *The Journal of neuroscience : the official journal of the Society for Neuroscience*. 27, 3686–94 (2007).
24. S. Arber, D. R. Ladle, J. H. Lin, E. Frank, T. M. Jessell, ETS Gene Er81 Controls the Formation of Functional Connections between Group Ia Sensory Afferents and Motor Neurons. *Cell*. 101, 485–498 (2000).
25. T. D. Patel, I. Kramer, J. Kucera, V. Niederkofler, T. M. Jessell, S. Arber, W. D. Snider, Peripheral NT3 Signaling Is Required for ETS Protein Expression and Central Patterning of Proprioceptive Sensory Afferents. *Neuron*. 38, 403–416 (2003).
26. B. Genç, P. H. Özdinler, A. E. Mendoza, R. S. Erzurumlu, A Chemoattractant Role for NT-3 in Proprioceptive Axon Guidance. *PLoS Biol*. 2, e403 (2004).
27. J. C. de Nooij, S. Doobar, T. M. Jessell, Etv1 Inactivation Reveals Proprioceptor Subclasses that Reflect the Level of NT3 Expression in Muscle Targets. *Neuron*. 77, 1055–1068 (2013).
28. F. Lallemand, U. Sterzenbach, S. Hadjab-Lallemand, J. B. Aquino, G. Castelo-Branco, I. Sinha, J. C. Villaescusa, D. Levanon, Y. Wang, M. C. M. Franck, O. Kharchenko, I. Adameyko, S. Linnarsson, Y. Groner, E. Turner, P. Ernfors, Positional differences of axon growth rates between sensory neurons encoded by runx3. *EMBO J*. 31, 3718–3729 (2012).
29. P. B. C. Matthews, “Mammalian muscle receptors and their central actions” (E. Arnold, 1972), (available at https://scholar.google.com/scholar_lookup?title=Mammalian+muscle+receptors+and+their+central+actions&author=Matthews%2C+Peter+B.+C.&publication_year=1972).
30. R. W. Banks, D. Barker, M. J. Stacey, J. Z. Young, Form and distribution of sensory terminals in cat hindlimb muscle spindles. *Philosophical Transactions of the Royal Society of London. B, Biological Sciences*. 299, 329–364 (1982).

31. T. Akay, W. G. Tourtellotte, S. Arber, T. M. Jessell, Degradation of mouse locomotor pattern in the absence of proprioceptive sensory feedback. *Proceedings of the National Academy of Sciences of the United States of America*. 111, 16877–16882 (2014).
32. M. O. Fernandes, W. G. Tourtellotte, Egr3-Dependent Muscle Spindle Stretch Receptor Intrafusal Muscle Fiber Differentiation and Fusimotor Innervation Homeostasis. *J. Neurosci*. 35, 5566–5578 (2015).
33. M. Leu, E. Bellmunt, M. Schwander, I. Fariñas, H. R. Brenner, U. Müller, Erbb2 regulates neuromuscular synapse formation and is essential for muscle spindle development. *Development*. 130, 2291–2301 (2003).
34. C. Cheret, M. Willem, F. R. Fricker, H. Wende, A. Wulf-Goldenberg, S. Tahirovic, K.-A. Nave, P. Saftig, C. Haass, A. N. Garratt, D. L. Bennett, C. Birchmeier, Bace1 and Neuregulin-1 cooperate to control formation and maintenance of muscle spindles. *EMBO J*. 32, 2015–2028 (2013).
35. M. C. Brown, I. Engberg, P. B. C. Matthews, The relative sensitivity to vibration of muscle receptors of the cat. *The Journal of Physiology*. 192, 773–800 (1967).
36. J. A. Vincent, H. M. Gabriel, A. S. Deardorff, P. Nardelli, R. E. W. Fyffe, T. Burkholder, T. C. Cope, Muscle proprioceptors in adult rat: mechanosensory signaling and synapse distribution in spinal cord. *Journal of Neurophysiology*. 118, 2687–2701 (2017).
37. A. Siegel, H. N. Saprú, H. E. Siegel, *Essential neuroscience* (Lippincott Williams & Wilkins, Philadelphia, 2006).
38. K. M. Oliver, D. M. Florez-Paz, T. C. Badea, G. Z. Mentis, V. Menon, J. C. de Nooij, Molecular correlates of muscle spindle and Golgi tendon organ afferents. *Nature Communications*. 12, 1451 (2021).
39. J. Houk, E. Henneman, Responses of Golgi tendon organs to active contractions of the soleus muscle of the cat. *Journal of Neurophysiology*. 30, 466–481 (1967).
40. P. Davies, J. Petit, J. J. A. Scott, The dynamic response of Golgi tendon organs to tetanic contraction of in-series motor units. *Brain Research*. 690, 82–91 (1995).

41. C. C. Hunt, R. S. Wilkinson, Y. Fukami, Ionic basis of the receptor potential in primary endings of mammalian muscle spindles. *Journal of General Physiology*. 71, 683–698 (1978).
42. G. S. Bewick, B. Reid, C. Richardson, R. W. Banks, Autogenic modulation of mechanoreceptor excitability by glutamate release from synaptic-like vesicles: evidence from the rat muscle spindle primary sensory ending. *The Journal of Physiology*. 562, 381–394 (2005).
43. G. S. Bewick, R. W. Banks, Mechanotransduction channels in proprioceptive sensory nerve terminals: still an open question? *Current Opinion in Physiology*. 20, 90–104 (2021).
44. V. G. Macefield, Physiological characteristics of low-threshold mechanoreceptors in joints, muscle and skin in human subjects. *Clinical and Experimental Pharmacology and Physiology*. 32, 135–144 (2005).
45. D. Wu, I. Schieren, Y. Qian, C. Zhang, T. M. Jessell, J. C. de Nooij, A Role for Sensory end Organ-Derived Signals in Regulating Muscle Spindle Proprioceptor Phenotype. *J. Neurosci*. 39, 4252–4267 (2019).
46. J. C. de Nooij, C. M. Simon, A. Simon, S. Doobar, K. P. Steel, R. W. Banks, G. Z. Mentis, G. S. Bewick, T. M. Jessell, The PDZ-Domain Protein Whirlin Facilitates Mechanosensory Signaling in Mammalian Proprioceptors. *J. Neurosci*. 35, 3073–3084 (2015).
47. S.-H. Woo, V. Lukacs, J. C. de Nooij, D. Zaytseva, C. R. Criddle, A. Francisco, T. M. Jessell, K. A. Wilkinson, A. Patapoutian, Piezo2 is the principal mechanotransduction channel for proprioception. *Nat. Neurosci*. 18, 1756–1762 (2015).
48. S.-H. Lin, Y.-R. Cheng, R. W. Banks, M.-Y. Min, G. S. Bewick, C.-C. Chen, Evidence for the involvement of ASIC3 in sensory mechanotransduction in proprioceptors. *Nat Commun*. 7, 11460 (2016).
49. A. T. Chesler, M. Szczot, D. Bharucha-Goebel, M. Čeko, S. Donkervoort, C. Laubacher, L. H. Hayes, K. Alter, C. Zampieri, C. Stanley, A. M. Innes, J. K. Mah, C. M. Grossmann, N. Bradley, D. Nguyen, A. R. Foley, C. E. Le Pichon, C. G. Bönnemann, The Role of

- PIEZO2 in Human Mechanosensation. *New England Journal of Medicine*. 375, 1355–1364 (2016).
50. G. Haliloglu, K. Becker, C. Temucin, B. Talim, N. Küçükşahin, M. Pergande, S. Motameny, P. Nürnberg, U. Aydingoz, H. Topaloglu, S. Cirak, Recessive PIEZO2 stop mutation causes distal arthrogryposis with distal muscle weakness, scoliosis and proprioception defects. *J Hum Genet*. 62, 497–501 (2017).
 51. A. a. Mahmud, N. a. Nahid, C. Nassif, M. s. b. Sayeed, M. u. Ahmed, M. Parveen, M. i. Khalil, M. m. Islam, Z. Nahar, F. Rypens, F. f. Hamdan, G. a. Rouleau, A. Hasnat, J. I. Michaud, Loss of the proprioception and touch sensation channel PIEZO2 in siblings with a progressive form of contractures. *Clinical Genetics*. 91, 470–475 (2017).
 52. E. Assaraf, R. Blecher, L. Heinemann-Yerushalmi, S. Krief, R. Carmel Vinestock, I. E. Biton, V. Brumfeld, R. Rotkopf, E. Avisar, G. Agar, E. Zelzer, Piezo2 expressed in proprioceptive neurons is essential for skeletal integrity. *Nat Commun*. 11, 3168 (2020).
 53. H. Wu, C. Petitpré, P. Fontanet, A. Sharma, C. Bellardita, R. M. Quadros, P. R. Jannig, Y. Wang, J. A. Heimel, K. K. Y. Cheung, S. Wanderoy, Y. Xuan, K. Meletis, J. Ruas, C. B. Gurumurthy, O. Kiehn, S. Hadjab, F. Lallemand, Distinct subtypes of proprioceptive dorsal root ganglion neurons regulate adaptive proprioception in mice. *Nature Communications*, 1–13 (2021).
 54. N. Sharma, K. Flaherty, K. Lezgiyeva, D. E. Wagner, A. M. Klein, D. D. Ginty, The emergence of transcriptional identity in somatosensory neurons. *Nature*, 1–7 (2020).
 55. S. Meltzer, C. Santiago, N. Sharma, D. D. Ginty, The cellular and molecular basis of somatosensory neuron development. *Neuron*. 109, 3736–3757 (2021).
 56. F. Imai, Y. Yoshida, Molecular mechanisms underlying monosynaptic sensory-motor circuit development in the spinal cord. *Dev Dyn*. 247, 581–587 (2018).
 57. N. Balaskas, D. Ng, N. Zampieri, The Positional Logic of Sensory-Motor Reflex Circuit Assembly. *Neuroscience*. 450, 142–150 (2020).

58. J. C. Eccles, R. M. Eccles, A. Lundberg, The convergence of monosynaptic excitatory afferents on to many different species of alpha motoneurons. *J Physiol.* 137, 22–50 (1957).
59. T. R. Nichols, A Biomechanical Perspective on Spinal Mechanisms of Coordinated Muscular Action: An Architecture Principle. *CTO.* 151, 1–1 (1994).
60. U. Windhorst, Muscle proprioceptive feedback and spinal networks. *Brain Res Bull.* 73, 155–202 (2007).
61. A. G. Brown, R. E. Fyffe, Direct observations on the contacts made between Ia afferent fibres and alpha-motoneurons in the cat's lumbosacral spinal cord. (1981), (available at <https://www.ncbi.nlm.nih.gov/pmc/articles/PMC1274440/>).
62. N. Kudo, T. Yamada, Morphological and physiological studies of development of the monosynaptic reflex pathway in the rat lumbar spinal cord. *The Journal of Physiology.* 389, 441–459 (1987).
63. A. I. Mendelsohn, C. M. Simon, L. F. Abbott, G. Z. Mentis, T. M. Jessell, Activity Regulates the Incidence of Heteronymous Sensory-Motor Connections. *Neuron.* 87, 111–123 (2015).
64. B. Mendelson, E. Frank, Specific monosynaptic sensory-motor connections form in the absence of patterned neural activity and motoneuronal cell death. *The Journal of neuroscience : the official journal of the Society for Neuroscience.* 11, 1390–403 (1991).
65. J. P. Charles, O. Cappellari, A. J. Spence, J. R. Hutchinson, D. J. Wells, Musculoskeletal Geometry, Muscle Architecture and Functional Specialisations of the Mouse Hindlimb. *PLOS ONE.* 11, e0147669 (2016).
66. J. S. Dasen, T. M. Jessell, in *Current Topics in Developmental Biology* (Academic Press, 2009; <https://www.sciencedirect.com/science/article/pii/S007021530988006X>), vol. 88 of *Genes*, pp. 169–200.
67. G. J. Romanes, in *Progress in Brain Research*, J. C. Eccles, J. P. Schadé, Eds. (Elsevier, 1964; <https://www.sciencedirect.com/science/article/pii/S0079612308640455>), vol. 11 of *Organization of the Spinal Cord*, pp. 93–119.

68. V. G. Vanderhorst, G. Holstege, Organization of lumbosacral motoneuronal cell groups innervating hindlimb, pelvic floor, and axial muscles in the cat. *J Comp Neurol.* 382, 46–76 (1997).
69. S. McHanwellt, T. J. Biscoe, D. R. Wilkie, The localization of the motoneurons supplying the hindlimb muscles of the mouse. *Philosophical Transactions of the Royal Society of London. B, Biological Sciences.* 293, 477–508 (1981).
70. T. M. Jessell, Neuronal specification in the spinal cord: inductive signals and transcriptional codes. *Nature Reviews Genetics.* 1, 20–29 (2000).
71. J. S. Dasen, B. C. Tice, S. Brenner-Morton, T. M. Jessell, A Hox Regulatory Network Establishes Motor Neuron Pool Identity and Target-Muscle Connectivity. *Cell.* 123, 477–491 (2005).
72. J. S. Dasen, A. De Camilli, B. Wang, P. W. Tucker, T. M. Jessell, Hox Repertoires for Motor Neuron Diversity and Connectivity Gated by a Single Accessory Factor, FoxP1. *Cell.* 134, 304–316 (2008).
73. G. Sürmeli, T. Akay, G. Ippolito, P. W. Tucker, T. M. Jessell, Patterns of Spinal Sensory-Motor Connectivity Prescribed by a Dorsoventral Positional Template. *Cell.* 147, 653–665 (2011).
74. E. Vrieseling, S. Arber, Target-Induced Transcriptional Control of Dendritic Patterning and Connectivity in Motor Neurons by the ETS Gene Pea3. *Cell.* 127, 1439–1452 (2006).
75. N. Balaskas, L. F. Abbott, T. M. Jessell, D. Ng, Positional Strategies for Connection Specificity and Synaptic Organization in Spinal Sensory-Motor Circuits. *Neuron.* 102, 1143-1156.e4 (2019).
76. E. Pecho-Vrieseling, M. Sigrist, Y. Yoshida, T. M. Jessell, S. Arber, Specificity of sensory–motor connections encoded by Sema3e–Plxnd1 recognition. *Nature.* 459, 842–846 (2009).

77. K. Fukuhara, F. Imai, D. R. Ladle, K. Katayama, J. R. Leslie, S. Arber, T. M. Jessell, Y. Yoshida, Specificity of Monosynaptic Sensory-Motor Connections Imposed by Repellent Sema3E-PlexinD1 Signaling. *Cell Reports*. 5, 748–758 (2013).
78. A. Kania, R. Klein, Mechanisms of ephrin–Eph signalling in development, physiology and disease. *Nature Reviews Molecular Cell Biology*. 17, 240–256 (2016).
79. N. Stifani, Motor neurons and the generation of spinal motor neurons diversity. *Front. Cell. Neurosci.* 8 (2014), doi:10.3389/fncel.2014.00293.
80. D. Bonanomi, S. L. Pfaff, Motor Axon Pathfinding. *Cold Spring Harb Perspect Biol.* 2 (2010), doi:10.1101/cshperspect.a001735.
81. S. Poliak, A. L. Norovich, M. Yamagata, J. R. Sanes, T. M. Jessell, Muscle-type Identity of Proprioceptors Specified by Spatially Restricted Signals from Limb Mesenchyme. *Cell*. 164, 512–525 (2016).
82. T. Hashimshony, N. Senderovich, G. Avital, A. Klochendler, Y. de Leeuw, L. Anavy, D. Gennert, S. Li, K. J. Livak, O. Rozenblatt-Rosen, Y. Dor, A. Regev, I. Yanai, CEL-Seq2: sensitive highly-multiplexed single-cell RNA-Seq. *Genome Biol.* 17 (2016), doi:10.1186/s13059-016-0938-8.
83. E. A. Susaki, K. Tainaka, D. Perrin, H. Yukinaga, A. Kuno, H. R. Ueda, Advanced CUBIC protocols for whole-brain and whole-body clearing and imaging. *Nat Protoc.* 10, 1709–1727 (2015).
84. T. Kaiser, J. T. Ting, P. Monteiro, G. Feng, Transgenic labeling of parvalbumin-expressing neurons with tdTomato. *Neuroscience*. 321, 236–245 (2016).
85. P. Philippidou, J. S. Dasen, Hox genes: choreographers in neural development, architects of circuit organization. *Neuron*. 80, 12–34 (2013).
86. S. K. Mishra, S. M. Tisel, P. Orestes, S. K. Bhangoo, M. A. Hoon, TRPV1-lineage neurons are required for thermal sensation. *The EMBO Journal*. 30, 582–593 (2011).
87. D. J. Cavanaugh, A. T. Chesler, A. C. Jackson, Y. M. Sigal, H. Yamanaka, R. Grant, D. O’Donnell, R. a Nicoll, N. M. Shah, D. Julius, A. I. Basbaum, Trpv1 Reporter Mice

- Reveal Highly Restricted Brain Distribution and Functional Expression in Arteriolar Smooth Muscle Cells. *Journal of Neuroscience*. 31, 5067–5077 (2011).
88. L. Madisen, T. A. Zwingman, S. M. Sunkin, S. W. Oh, H. A. Zariwala, H. Gu, L. L. Ng, R. D. Palmiter, M. J. Hawrylycz, A. R. Jones, E. S. Lein, H. Zeng, A. Hatim, H. Gu, L. L. Ng, R. D. Palmiter, M. J. Hawrylycz, R. Allan, E. S. Lein, H. Zeng, H. A. Zariwala, H. Gu, L. L. Ng, R. D. Palmiter, M. J. Hawrylycz, A. R. Jones, E. S. Lein, H. Zeng, A. Hatim, H. Gu, L. L. Ng, R. D. Palmiter, M. J. Hawrylycz, R. Allan, E. S. Lein, H. Zeng, A robust and high-throughput Cre Repointing and characterization. *Nat Neurosci*. 13, 133–140 (2010).
 89. L. Madisen, A. R. Garner, D. Shimaoka, A. S. Chuong, N. C. Klapoetke, L. Li, A. van der Bourg, Y. Niino, L. Egolf, C. Monetti, H. Gu, M. Mills, A. Cheng, B. Tasic, T. N. Nguyen, S. M. Sunkin, A. Benucci, A. Nagy, A. Miyawaki, F. Helmchen, R. M. Empson, T. Knöpfel, E. S. Boyden, R. C. Reid, M. Carandini, H. Zeng, Transgenic Mice for Intersectional Targeting of Neural Sensors and Effectors with High Specificity and Performance. *Neuron*. 85, 942–958 (2015).
 90. A. J. Loutit, J. R. Potas, Restoring Somatosensation: Advantages and Current Limitations of Targeting the Brainstem Dorsal Column Nuclei Complex. *Frontiers in Neuroscience*. 14 (2020) (available at <https://www.frontiersin.org/article/10.3389/fnins.2020.00156>).
 91. L. Wang, R. Klein, B. Zheng, T. Marquardt, Anatomical Coupling of Sensory and Motor Nerve Trajectory via Axon Tracking. *Neuron*. 71, 263–277 (2011).
 92. J. Frisé, P. A. Yates, T. McLaughlin, G. C. Friedman, D. D. M. O’Leary, M. Barbacid, Ephrin-A5 (AL-1/RAGS) Is Essential for Proper Retinal Axon Guidance and Topographic Mapping in the Mammalian Visual System. *Neuron*. 20, 235–243 (1998).
 93. D. Bonanomi, O. Chivatakarn, G. Bai, H. Abdesslem, K. Lettieri, T. Marquardt, B. A. Pierchala, S. L. Pfaff, Ret is a multifunctional co-receptor that integrates diffusible- and contact-axon guidance signals. *Cell*. 148, 568–582 (2012).
 94. D. Usoskin, A. Furlan, S. Islam, H. Abdo, P. Lönnerberg, D. Lou, J. Hjerling-Leffler, J. Haeggström, O. Kharchenko, P. V. Kharchenko, S. Linnarsson, P. Ernfors, Unbiased

- classification of sensory neuron types by large-scale single-cell RNA sequencing. *Nature Neuroscience*. 18, 145–153 (2015).
95. M. J. Caterina, M. A. Schumacher, M. Tominaga, T. A. Rosen, J. D. Levine, D. Julius, The capsaicin receptor: a heat-activated ion channel in the pain pathway. *Nature*. 389, 816–824 (1997).
 96. Y. Q. Cao, P. W. Mantyh, E. J. Carlson, A.-M. Gillespie, C. J. Epstein, A. I. Basbaum, Primary afferent tachykinins are required to experience moderate to intense pain. *Nature*. 392, 390–394 (1998).
 97. J. Lee, A. Friese, M. Mielich, M. Sigrist, S. Arber, Scaling Proprioceptor Gene Transcription by Retrograde NT3 Signaling. *PLOS ONE*. 7, e45551 (2012).
 98. J. C. Eccles, R. M. Eccles, F. Magni, Central inhibitory action attributable to presynaptic depolarization produced by muscle afferent volleys. *J Physiol*. 159, 147–166 (1961).
 99. A. J. P. Fink, K. R. Croce, Z. J. Huang, L. F. Abbott, T. M. Jessell, E. Azim, Presynaptic inhibition of spinal sensory feedback ensures smooth movement. *Nature*. 509, 43–48 (2014).
 100. C. Liang, S. Huang, Y. Zhao, S. Chen, Y. Li, TOX as a potential target for immunotherapy in lymphocytic malignancies. *Biomarker Research*. 9, 20 (2021).
 101. P. Aliahmad, A. Seksenyan, J. Kaye, The many roles of TOX in the immune system. *Curr Opin Immunol*. 24, 173–177 (2012).
 102. B. Artigiani, A. M. Jesus Domingues, S. Bragado Alonso, E. Brandl, S. Massalini, A. Dahl, F. Calegari, Tox: a multifunctional transcription factor and novel regulator of mammalian corticogenesis. *EMBO J*. 34, 896–910 (2015).
 103. M. F. Bolliger, D. C. Martinelli, T. C. Südhof, The cell-adhesion G protein-coupled receptor BAI3 is a high-affinity receptor for C1q-like proteins. *Proceedings of the National Academy of Sciences*. 108, 2534–2539 (2011).
 104. K. Matsuda, T. Budisantoso, N. Mitakidis, Y. Sugaya, E. Miura, W. Kakegawa, M. Yamasaki, K. Konno, M. Uchigashima, M. Abe, I. Watanabe, M. Kano, M. Watanabe,

- K. Sakimura, A. R. Aricescu, M. Yuzaki, Transsynaptic Modulation of Kainate Receptor Functions by C1q-like Proteins. *Neuron*. 90, 752–767 (2016).
105. R. W. Banks, M. Hulliger, H. H. Saed, M. J. Stacey, A comparative analysis of the encapsulated end-organs of mammalian skeletal muscles and of their sensory nerve endings. *Journal of anatomy*. 214, 859–87 (2009).
106. F. Helmbacher, S. Schneider-Maunoury, P. Topilko, L. Tiret, P. Charnay, Targeting of the EphA4 tyrosine kinase receptor affects dorsal/ventral pathfinding of limb motor axons. *Development (Cambridge, England)*. 127, 3313–24 (2000).
107. A. Kania, T. M. Jessell, Topographic motor projections in the limb imposed by LIM homeodomain protein regulation of ephrin-A:EphA interactions. *Neuron*. 38, 581–96 (2003).
108. K. G. Pearson, Generating the walking gait: role of sensory feedback. *Prog Brain Res*. 143, 123–129 (2004).

9. Appendix

9.1. Supplemental figures

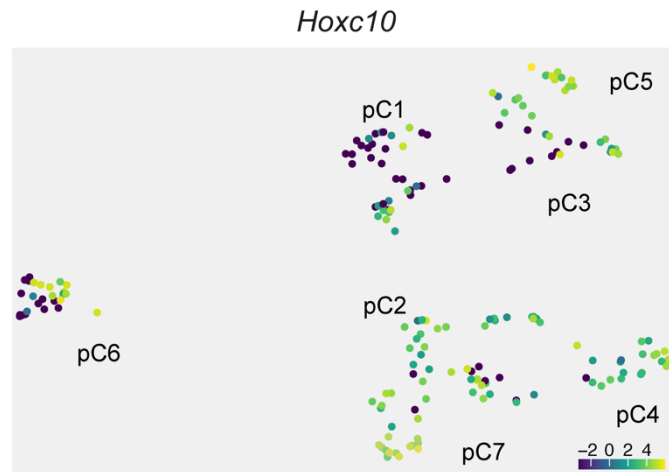


Figure S1. *Hoxc10* expression of thoracic and lumbar parvalbumin⁺ sensory neurons at e15.5. UMAP representation showing the expression values of the lumbar marker gene *Hoxc10* among clusters. Scale: log-counts.

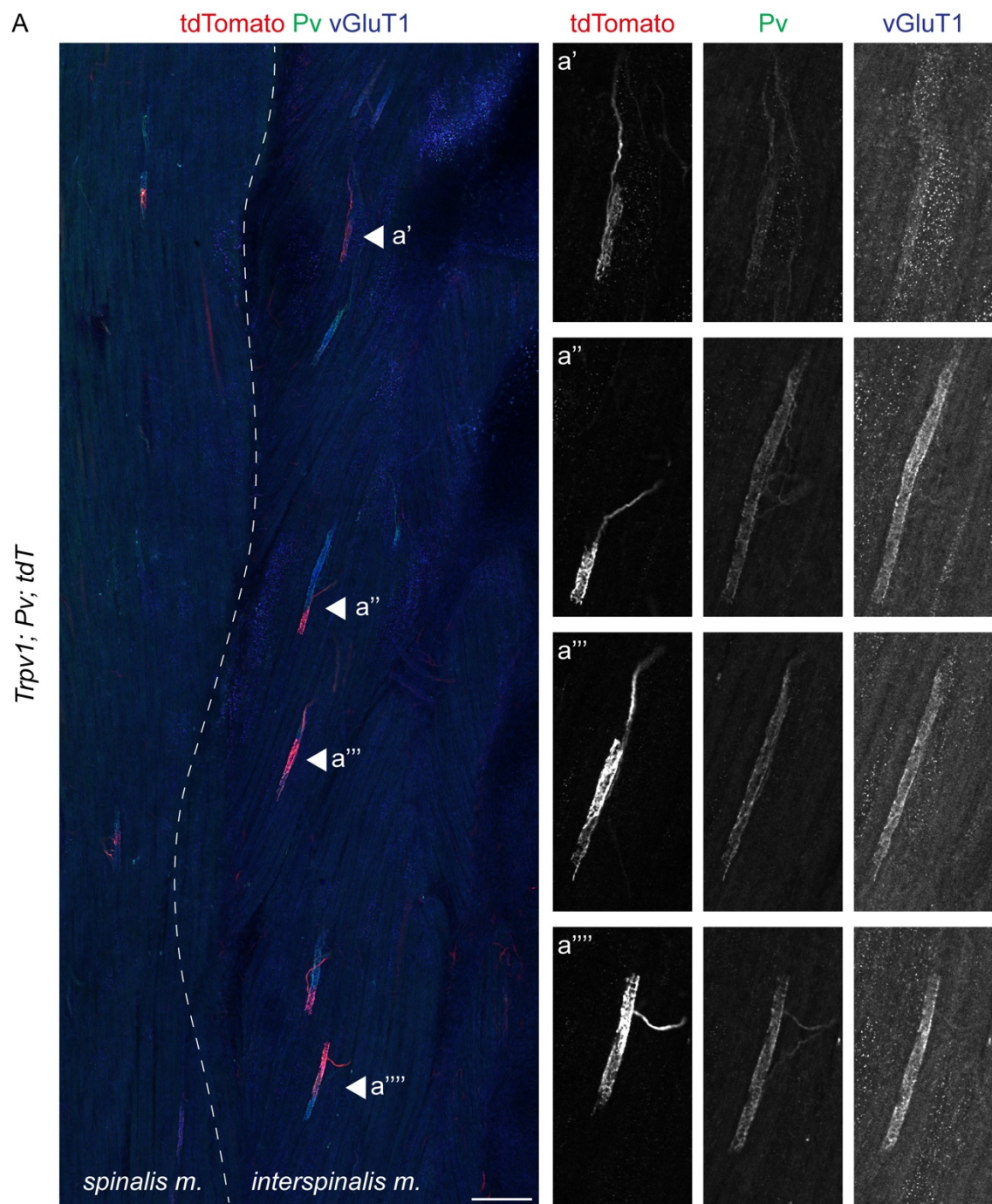


Figure S2. Muscle spindles in back muscles. (A) Representative images of tdT^+ , Pv^+ , $vGluT1^+$ labeled muscle spindles in back muscles (spinalis and interspinalis) from a p7 *Trpv1^{Cre}; Pv^{Flp}; tdT* mouse. Scale bar: 150 μ m.

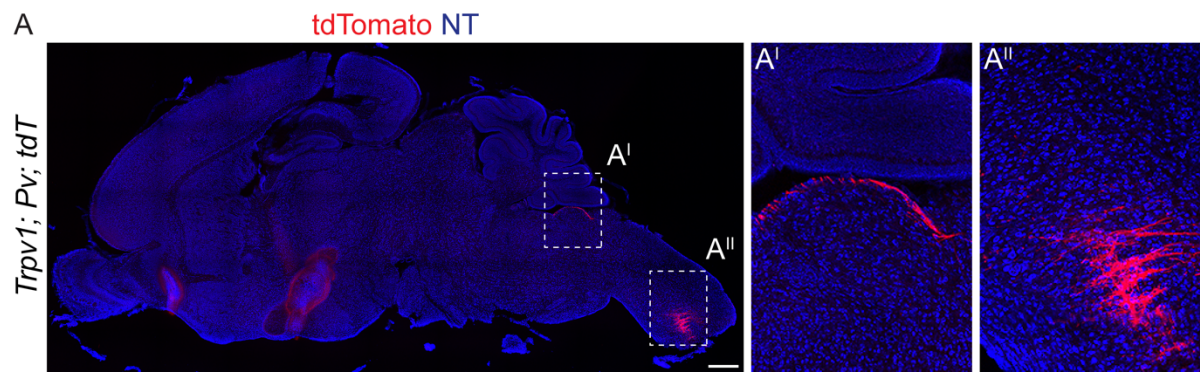


Figure S3. Genetic labeling of back-pSN afferents. (A) Representative sagittal brain section of tdT⁺ afferents of proprioceptive sensory neurons in the dorsal brain stem (A') and cervical spinal cord (A'') of p7 *Trpv1*^{Cre}; *Pv*^{Flp}; *tdT* mice. Scale bar: 500 μm.

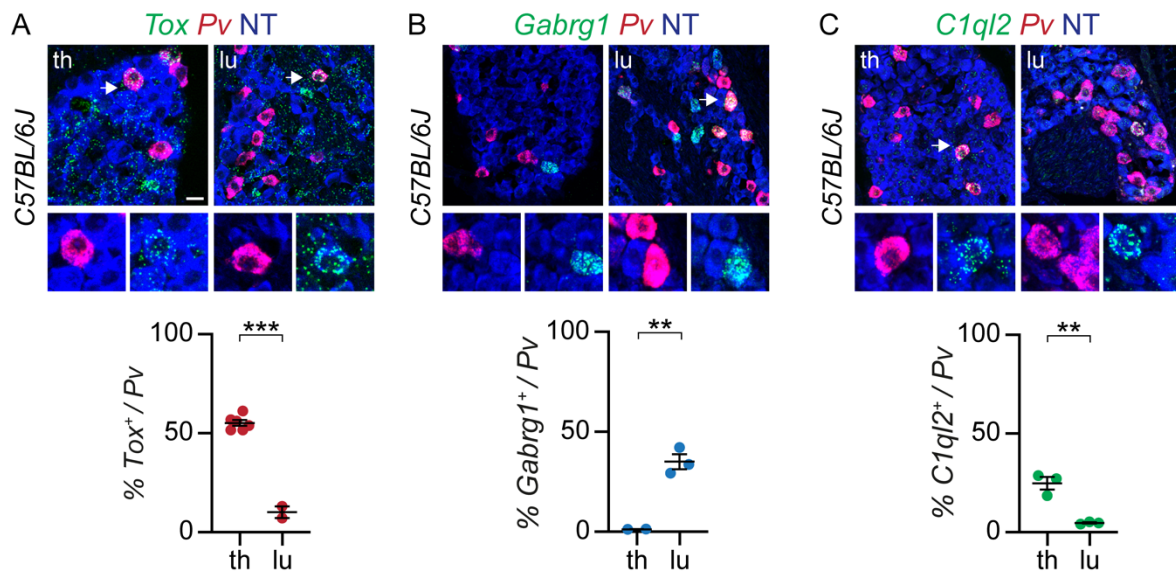


Figure S4. Expression of marker genes for back, limb, and abdominal proprioceptors in *Pv*⁺ sensory neurons. Expression analysis using *in situ* hybridization of *Tox* (A), *Gabrg1* (B), and *C1ql2* (C) in *Pv*⁺ sensory neurons of thoracic and lumbar DRG from p1 wild type mice (each point represents one animal, mean ± SEM, t-test, ** p < 0.01, *** p < 0.001). Scale bar: 25 μm.

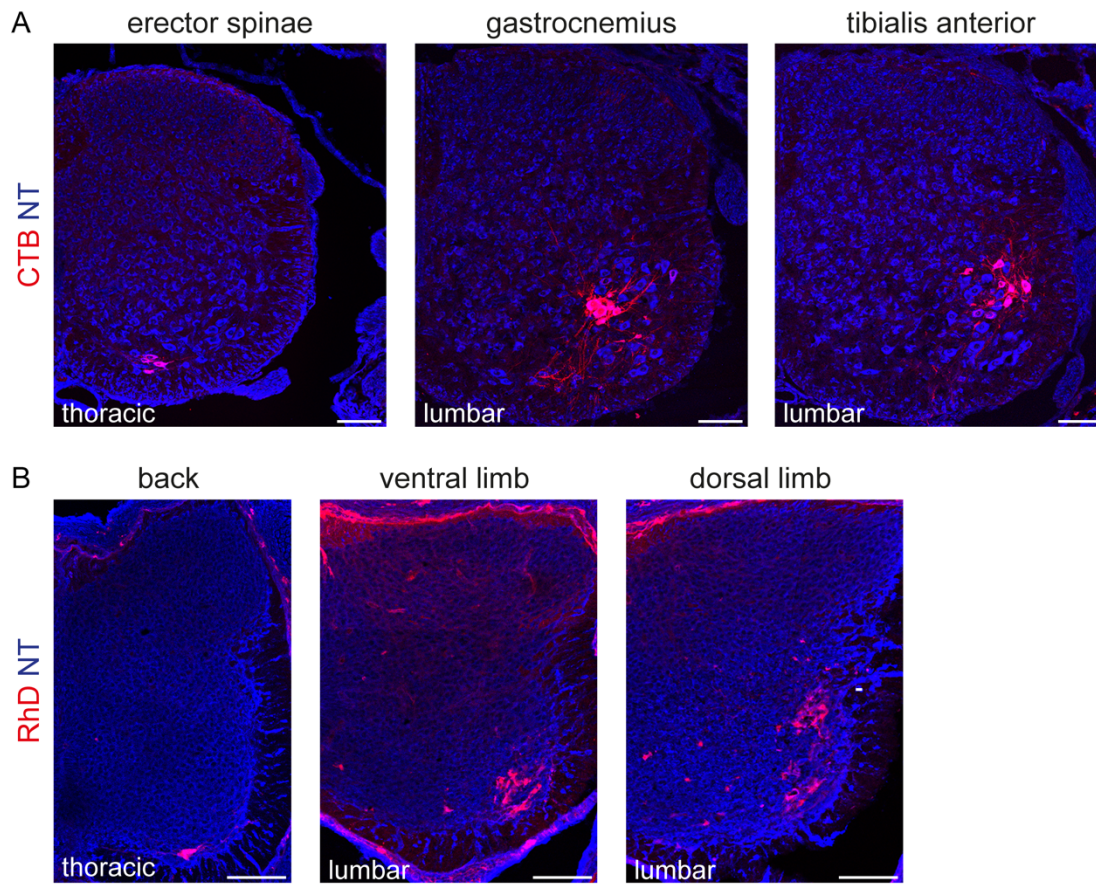


Figure S5. Retrograde labeling of back and hindlimb innervating motor neurons. (A) Representative images of retrogradely labeled motor neurons after CTB⁵⁵⁵ injection into back (*Erector spinae*) and hindlimb (*Gastrocnemius* and *Tibialis anterior*) muscles of p4 wild-type mice. Scale bar: 100 μ m. (B) Representative images of retrogradely labeled motor neurons after RhD injection into back muscles (back muscles) as well as ventral and dorsal hindlimb muscles of e15.5 wild-type embryos. Scale bar: 100 μ m.

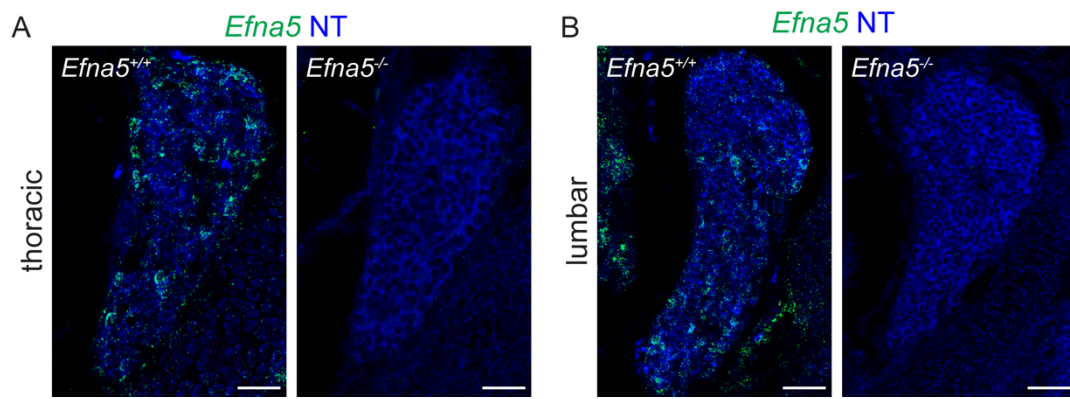


Figure S6. Expression of *EfnA5* in DRG of *EfnA5*^{+/+} and *EfnA5*^{-/-} mice. (A) Representative images of *EfnA5* expression (*in situ* hybridization) in thoracic and (B) lumbar DRG of e15.5 *EfnA5*^{+/+} (WT) and *EfnA5*^{-/-} (KO). Scale bar: 50 μ m.

9.2 List of publications

Dietrich S, Company C, Song K, Lowenstein ED, Riedel L, Birchmeier C, Gargiulo G, Zampieri N. The molecular foundation of proprioceptor muscle-type identity. Under consideration.

Pimpinella S, Sauve I, **Dietrich S**, Zampieri N. Rabies anterograde monosynaptic tracing allows identification of postsynaptic circuits receiving distinct somatosensory input. *Neuroscience* (2022).